Elucidating the Structures and Catalytic Properties *of* Metallic Nanoparticles

by

Jack B. A. Davis

A thesis submitted to the

University of Birmingham

for the degree of

Doctor of Philosophy

School of Chemistry
University of Birmingham
August 2015

Abstract

The publications contained within this thesis present the application and development of computational methods for the study of metallic nanoparticles and nanoalloys. Principally these studies are dedicated to their structural characterisation and their interactions with small molecules; vital first steps toward understanding their role in key catalytic processes. Publications have also assessed the applicability of statistical mechanical methods and dispersion corrected DFT to these studies.

Palladium-iridium nanoalloys, which are under current investigation for their catalytic properties, are studied extensively using a range of computational methods. Their interactions with hydrogen and benzene are probed in order to better understand their role in tetralin hydroconversion and the preferential oxidation of CO. Structures are revealed to reflect the strongly demixing behaviour of the bulk alloy, with nanosize effects seen in their interactions with hydrogen.

The Birmingham Parallel Genetic Algorithm is presented and applied to the direct density functional theory global optimisation of Iridium and both gas-phase and surface supported gold-iridium nanoparticles. The program is shown to be capable of overcoming previous size restrictions while characterising quantum size effects in the iridium and gold-iridium structures. Significant differences are seen between the surface-supported and gas-phase gold-iridium structures.

Acknowledgements

This body of work would not have been possible without the support and guidance of my supervisor Prof. Roy Johnston. Roy has provided me with endless opportunities for training and collaboration, both nationally and internationally, and guided me through often challenging projects. I am also indebted to my second supervisor Dr Sarah Horswell, who has taught me not to split my infinitives. I have benefited immeasurably from their experience and academic insight.

I have had the pleasure of meeting and collaborating with Micha Polak, Leonid Rubinovich, Armin Shayeghi, Francesca Baletto and Laurent Piccolo. Much of the work presented in this thesis is a result of projects completed because of their contributions and, in cases, hospitality at their respective institutions.

I must also thank the Johnston and Chakrabarti groups for providing me with a stimulating work environment throughout my PhD. My time in Birmingham would have been far less enjoyable without Lewis Smeeton, Daniel Morphew, Sridhar Neelamraju, Ilker Demiroglu and Paul Jennings.

Publications

1. Jack B. A. Davis, Sarah L. Horswell and Roy L. Johnston, *'Global Optimization of 8-10 Atom Palladium-Iridium Nanoalloys at the DFT Level'*, The Journal of Physical Chemistry A, 2014, **118 (1)**, 208-214.

2. Jack B. A. Davis, Roy L. Johnston, Leonid Rubinovich, Micha Polak, *'Comparative Modelling of Chemical Ordering in Palladium-Iridium Nanoalloys'*. The Journal of Chemical Physics, 2014, **141**, 224307.

3. Jack B. A. Davis, Sarah L. Horswell, Laurent Piccolo and Roy L. Johnston, *Computational Study of the Adsorption of Benzene and Hydrogen on Palladium-Iridium Nanoalloys*, Journal of Organometallic Chemistry, 2015, **792**, 190-193.

4. Jack B. A. Davis, Francesca Baletto and Roy L. Johnston, *'The Effect of Dispersion Correction on the Adsorption of CO on Metallic Nanoparticles'*, The Journal of Physical Chemistry A, 2015 **119 (37)**, 9703-9709.

5. Armin Shayeghi, Daniel Götz, Jack B. A. Davis, Rolf Schäfer and and Roy L. Johnston, *'Pool-BCGA: A Parallelised Generation-Free Genetic Algorithm for the Ab Initio Global Optimisation of Nanoalloy Clusters'*, Physical Chemistry Chemical Physics, 2014, **17**, 2104-2112.

6. Jack B. A. Davis, Armin Shayeghi, Sarah L. Horswell and Roy L. Johnston, *'The Birmingham Parallel Genetic Algorithm and its Application to the Direct DFT Global Optimisation of Ir_N $(N = 10 - 20)$ Clusters'*, Nanoscale, 2015, **7**, 14032-14038.

7. Jack B. A. Davis, Sarah L. Horswell and Roy L. Johnston, *'The Application of a Parallel Genetic Algorithm to the Global Optimisation of Gas-Phase and Supported Gold-Iridium Nanoalloys'*, **In Prep**.

Abbreviations

NA Nanoalloy

NP Nanoparticle

BCGA Birmingham Cluster Genetic Algorithm

BPGA Birmingham Parallel Genetic Algorithm

DFT Density Functional Theory

FCEM Free Energy Concentration Expansion Method

CBEV Coordination Dependent Bond Energy Variations

Contents

1 | Introduction

1.1 Metallic Nanoparticles

Nanoparticles (NPs) are aggregates of atoms, ions or molecules whose size can be anywhere between 1 and 100 nm.[1,2] There is considerable interest in NPs as their properties often differ from those of their constituent atoms or molecules or of their corresponding bulk materials.[3,4] These properties often depend on the NP size and, as such, can be tuned by altering NP size and shape. The stability of NPs can also be affected by their size, with certain "magic-number" size NPs, with closed electron shells or complete geometric shells, displaying increased stability.[5,6]

Metallic NPs are clusters of metallic elements. Those made up of two or more elements are known as nanoalloys (NAs). Metallic NAs and NPs have a range of potential optical, magnetic and catalytic applications.[7] The combination of metallic elements in a NA mean a system's properties are no longer only dependent on the size and shape of the cluster but also on the composition and ordering of the elements. This can produce materials with well-defined, tunable properties.[7,8].

The presence of more than one element in a NA enables the formation of a new set of isomers, known as homotops.[9] These are structures of the same size, geometry and composition which differ only in the ordering of their constituent elements. The number of possible homotops N_{H} for a particular N-atom cluster structure is calculated as follows:

$$N_{\mathrm{H}} = \frac{N!}{N_{\mathrm{A}}!N_{\mathrm{B}}!} \tag{1.1}$$

where N_A and N_B are the numbers of atoms of elements A and B. N_H rises combinatorially with system size and is greatest for 50/50 compositions. This is without symmetry considerations which can reduce the actual total number of inequivalent homotops, depending on the order of the point group.

The ordering of elements found in NAs give rise to a set of common mixing patterns, shown in figure 1.1. The core-shell arrangement, where a core of atom type A is surrounded by a layer of atom type B, is commonly seen in nanoalloy systems.

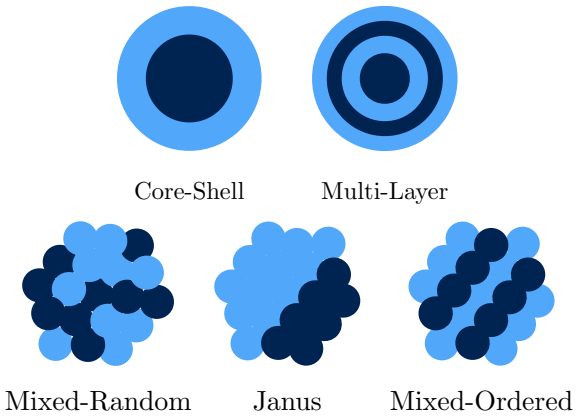

Figure 1.1: Common mixing patterns seen in NAs.

The mixing pattern seen in a NA is a often as a result of a combination of factors which include:

1. The relative strengths of the homo- and heterometallic bonds.
2. The surface energies of the bulk elements.
3. The relative sizes of the constituent elements.
4. The presence of substrates or ligands.
5. Charge transfer.
6. Magnetic effects.

The structural characterisation of nanoalloys is a vital first step toward understanding their properties. It is possible to characterise the structures and ordering of NAs using both experimental and computational methods. Electron microscopy techniques, such as transmission electron microscopy (TEM) and scanning transmission electron microscopy (STEM) allow atomic resolution. If STEM is combined with high angle angular dark field (HAADF) imaging, it becomes possible to distinguish between atom types based on their differing atomic numbers, and therefore to characterise the chemical ordering in a NA.[7]

Computationally, a range of methods exist to characterise NAs, including basin-hopping,[10] genetic algorithm[11] and statistical mechanical methods, such as the Free Energy Concentration Expansion Method.[12]

1.2 Genetic Algorithms

A genetic algorithm (GA) is a search method based on the principles of natural selection.[13–15] GAs have been developed and applied extensively to the global optimisation of cluster geometries. When first applied to atomic clusters GAs utilised binary strings to represent geometries, which were operated on bitwise.[16,17] The representation of geometries in Cartesian coordinates was introduced by Zeiri,[18–20] which removed the need for conversion between the binary strings and Cartesian coordinates. Deaven and Ho later combined the energetic evaluation of each cluster geometry with a local minimisation of the coordinates with respect to the coordinates.[21] This transforms the energy landscape of the cluster into a stepped surface, greatly reducing the search space the GA has to explore to find the global minimum.

This energetic evaluation of a potential cluster geometry can be performed at varying levels of theory, depending on the system and its size. The structures of larger clusters can be modelled accurately using emperical potentials parametrised on the properties of the bulk material. These include Lennard-Jones,[22] Born-Mayer,[23] Sutton-Chen,[24] Murrell-Mottram[25] potentials and those based on the second moment approximation of the tight-binding schemeCleri1991.

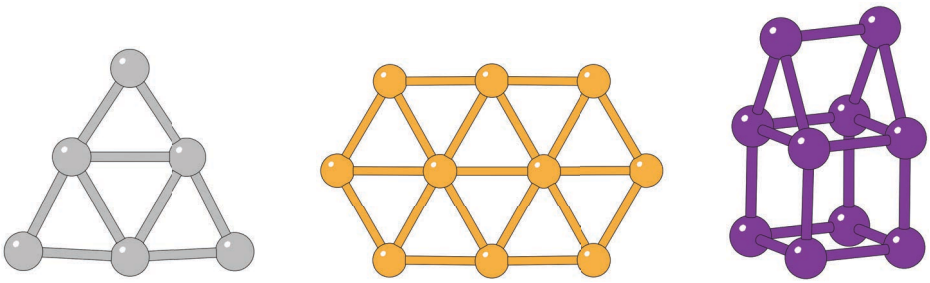

Figure 1.2: The 2D structures of Pt_6^+ and Au_{10} and the cubic structure of Ir_{10}.

For some subnanometre clusters empirical potentials fitted to the bulk are no longer capable of accurately describing the energy landscape of the system.[26] System such as, Pt_n, Au_n and Ir_n require a quantum mechanical description of their landscape in order to characterise the 2D structures seen for Au_n and Pt_n and the cubic structures seen for Ir_n (figure 1.2).[27,28]

Au requires such a quantum mechanical description because of relativistic effects which promote s-d hybridisation. Relativistic effects are prevalent throughout 3rd row elements due to the size of the respective nuclei and it is therefore to be expected that most will require such a quantum mechanical description.

Numerous GAs have been developed and applied to the global optimisation of clusters at various levels of theory.[29–34] However, a quantum mechanical description of the landscape greatly increases the computational cost of global optimisation. This limits the possible size of the system it is possible to study with these methods.

1.3 Palladium-Iridium

Pd clusters have been studied and applied in a range of catalytic processes, including methanol decomposition and the oxidation of cyclohexane.[35–40] Ir clusters are currently used as catalysts for a range of organic reactions. These include olefin hydrogenation, oligomerization, and ring-opening of cycloalkanes.[41] Larger Ir nanoparticles have been shown to be active in C-C bond hydrogenolysis.[42] Selective molecular recognition has also been seen in supported Ir cluster-based catalysts.[43]

It is widely known that alloying metals can result in increased catalytic activity

and efficiency.[44,45] In NA systems it is normally hoped that combining metals will either result in a lower cost catalyst or in increased efficiency through the combination of the catalytic properties of the constituent metals.This can result in synergistic catalytic properties which are better than either metal alone.

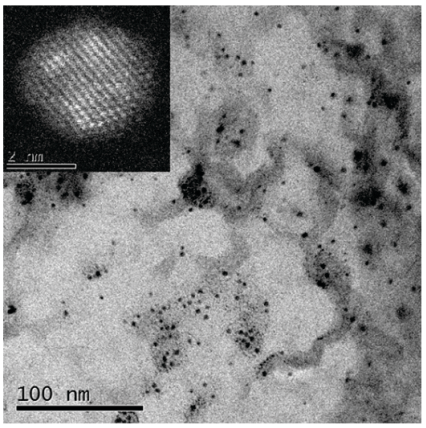

Figure 1.3: STEM images of PdIr NA clusters, with a HAADF image shown top right.[46]

Palladium-Iridium is a strongly demixing alloy system,[47–49] the properties of which are reflected in those of the corresponding NAs. Pd-Ir nanoalloys have been investigated both theoretically[50–52] and experimentally.[53–59] for their catalytic properties and their potential application to key catalytic processes. These studies have included applications to tetralin hydroconversion and the preferential oxidation of CO (PROX).[53–55,58,60] A scanning transition electron microscopy (STEM) image of PdIr clusters used in these studies is shown in figure 1.3.

Tetralin hydroconversion (Figure 1.4) is a model process used to study the effectiveness of a catalyst in the removal of polyaromatic hydrocarbons from diesel fuel. This is a particularly important process as the combustion of polyaromatic hydrocarbons produces particulate which, according to current legislation, must be reduced in emissions.[55] Studies have also been conducted on the application of Pd-Ir to the preferential oxidation of CO (PROX), a process for the removal of CO from H_2 streams used in proton-exchange membrane fuel cells.[54] In both processes it was hoped that the combination of Pd and Ir would impart the catalytic properties of each metal into the resulting catalyst and give an increased efficiency in the

nanoalloy catalyst.

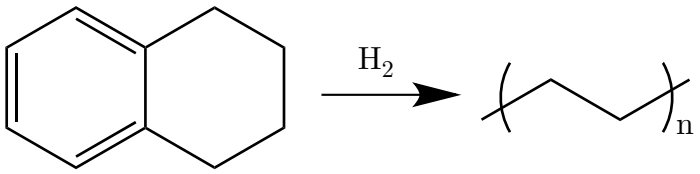

Figure 1.4: Tetralin hydroconversion.

Supported Ir catalysts have been shown to be active in C-C bond hydrogenolysis and successfully applied to tetralin hydroconversion.[61] Pd exhibits increased thioresistance and improved hydrogen activation properties when compared with other noble metals. Depending on the relative proportions of the metals, the addition of Pd to Ir has shown that increased activity and selectivity could be obtained from the catalyst.[55]

In PROX it has been shown the addition of Ir to Pd inhibits the formation of hydrides, which would otherwise poison the catalyst and result in reduced performance. This decrease in the overall sorption (adsorption and absorption) properties of the Pd-Ir catalyst results in increased performance.[53]

2 | Methodology

2.1 Global Optimisation

The potential energy surface (PES) of a system is a representation of its potential energy with respect to its atomic or molecular coordinates.[62] The PES, $V(\mathbf{r})$, of an N-atom system is a $(3N + 1)$ dimensional object based on $3N$ spatial coordinates, represented by the vector $\mathbf{r}$, and the potential energy V of the system. The PES has several key features: these include points at which $\nabla V(\mathbf{r}) = 0$, which correspond to local minimum structures, and saddle points corresponding to transition states. The local minimum with the lowest V is known as the global minimum.

The location of the global minimum on a PES is known as global optimisation and is a common problem throughout the sciences. Global optimisation is a computational demanding task as the number of local minima on the PES tends to grow exponentially with system size. Global optimisation is an 'NP-hard' problem, as no known algorithm exists to guarantee the location of the global minimum within a time that scales with the system size.

A variety of methods are available specifically tailored for the global optimisation of cluster geometries. These include basin-hopping[10] and genetic algorithms.[11] These methods have been widely applied and demonstrated to capable of accurately and completely sampling the PES of a cluster to determine its global minimum structure.

2.1.1 Birmingham Cluster Genetic Algorithm

The Birmingham Cluster Genetic Algorithm (BCGA) is a genetic algorithm for structural characterisation of metallic nanoparticles and nanoalloys.[11]

The BCGA is a generation based genetic algorithm and a run begins with a initial generation of a fixed number of cluster geometries, generated with random x, y and z coordinates. These coordinates are scaled to ensure that the volume of the cluster's scales correctly with the number of atoms. The clusters are then evaluated with either an empirical potential, such as the Gupta potential (BCGA-Gupta), or through a DFT calculation (BCGA-DFT) *via* interfaces to common DFT programs.

The choice of whether to evaluate a clusters' potential energy with an empirical potential or DFT depends on the size and type of system being studied. Direct DFT global optimisation is extremely computationally expensive and limits calculations to around 10 atoms. This, however, is a highly interesting size range where quantum size and relativistic effects, such as spin-orbit coupling, tend to determine structures and the use of DFT is required to describe these interactions.[26,63–65]

This evaluation is combined with a local minimisation of a cluster's potential energy with respect to its atomic coordinates. This is performed using either an internal L-BFGS routine or the in-built minimisation routine of the interfaced DFT program.[66] This transforms the complex energy landscape of the cluster into a simpler stepped surface, as shown in figure 2.1. The clusters are assigned a fitness based on their energy, with a higher fitness representing a lower energy.

A second generation, made up of offspring and mutants, is produced. The number of offspring and mutants in this new generation is fixed, with the number of mutants normally set to be around 10% of the total generation.

Offspring are a product of crossover which is carried according to the Deaven and Ho cut and splice method.[21] Crossover requires two parent clusters to be selected. This selection is based on the clusters' fitness and performed through roulette wheel selection. Clusters with a higher fitness have a higher probability of being selected and passing on their structural characteristics to the next generation. Mutation is

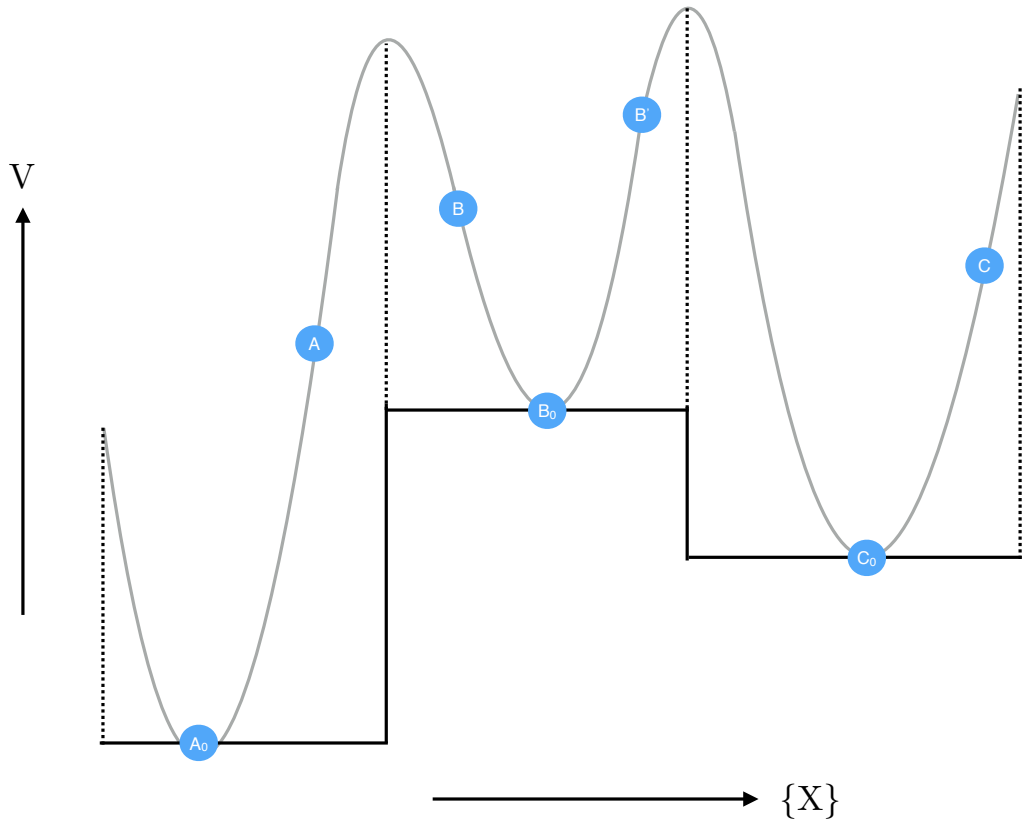

Figure 2.1: The transformation of the landscape of reaction coordinate X into a stepped surface after local minimisation with repect to energy V.

carried out according to a variety of mutation schemes, including atom-displacement, homotop-swapping and the introduction of a new random geometry to the generation.

The program will go on creating and evaluating new generations of clusters through crossover and mutation until convergence is achieved. This is defined as being when the energies of the generation do not change for a set number of generations.

2.2 Empirical Potentials

2.2.1 Gupta Potential

The Gupta potential is based on the second moment approximation to tight-binding theory and is constructed from an attractive many-body term, V^m, and a repulsive pair term, V^r, summed over all N atoms.[67]

$$V_{clus} = \sum_{i}^{N} [V^r(i) - V^m(i)] \tag{2.1}$$

where, for element types a and b and bond length r_{ij},

$$V^r(i) = \sum_{j \neq i}^{N} A(a,b) e^{(-p(a,b)(r_{ij}/r_0(a,b)-1))} \tag{2.2}$$

and

$$V^m(i) = \left[\sum_{j \neq i}^{N} \zeta^2(a,b) e^{(-2q(a,b)(r_{ij}/r_0(a,b)-1))} \right]^{1/2}. \tag{2.3}$$

where A, ζ, p and q are parameters fitted to experimental values of the lattice parameters, experimental cohesive energies and elastic constants, respectively, at 0 K.[68]

2.3 Molecular Quantum Mechanics

2.3.1 Quantum Chemistry

The aim of quantum chemistry is solution of the non-relativistic, time-independent Schrödinger equation.

$$\hat{H}\Psi = E\Psi \tag{2.4}$$

The Hamiltonian operator, $\hat{H}$, is the differential operator for the energy of a molecular system.

$$\hat{H} = -\frac{1}{2}\sum_{i=1}^{N}\nabla_i^2 - \frac{1}{2}\sum_{A=1}^{M}\frac{1}{M_A}\nabla_A^2 - \sum_{i=1}^{N}\sum_{A=1}^{M}\frac{Z_a}{r_{iA}} + \sum_{i=1}^{N}\sum_{j>i}^{N}\frac{1}{r_{ij}} + \sum_{A=1}^{M}\sum_{B>A}^{M}\frac{Z_A Z_B}{R_{AB}} \tag{2.5}$$

The M nuclei in the system are represented by A and B, with i and j representing the N electrons.Here M_A is the mass of nucleus A and r_{pq} is distance between particles p and q

Terms 1 and 2 of $\hat{H}$ describe the kinetic energy of the electrons and nuclei. Term 3 represents the effective electrostatic interactions between the nuclei and the electrons. Terms 4 and 5 are the repulsive potentials due to electron-electron and nucleus-nucleus interactions, respectively.

The Hamiltonian operator in equation 2.5 is shown in atomic units, where physical quantities are expressed as multiples of physical constants. The mass of nucleus A, M_A, is given as a multiple of the mass of an electron.

The Laplacian operator ∇_q^2 is the sum of differential operators in cartesian coordinates.

$$\nabla_q^2 = \frac{\partial^2}{\partial x_q^2} + \frac{\partial^2}{\partial y_q^2} + \frac{\partial^2}{\partial z_q^2} \tag{2.6}$$

The wave function, Ψ_i, represents the i'th state of the system.

$$\Psi_i \left(\mathbf{x}_1, \mathbf{x}_2, ..., \mathbf{x}_N, \mathbf{R}_1, \mathbf{R}_2, ..., \mathbf{R}_M\right) \tag{2.7}$$

The system depends on the $3N$ spatial coordinates $\{\mathbf{r}_i\}$ and N spin coordinates $\{s_i\}$, collectively termed $\{\mathbf{x}_i\}$, of the electrons and the 3M spatial coordinates of the nuclei $\{r_i\}$. The wave function Ψ_i contains all quantum information for a system. In equation 2.4, E is the energy of the state described by Ψ_i.

The Born-Oppenheimer approximation assumes that because the mass of a nucleus is far greater than that of an electron it is possible to make an approximation that the electrons of a system will be moving in a field of fixed nuclei. As the nuclei are clamped their kinetic energies become zero and the nucleus-nucleus repulsion becomes a constant. The Hamiltonian in equation 2.5 now reduces to the electronic Hamiltonian shown in 2.8

$$\hat{H}_{elec} = -\frac{1}{2}\sum_{i=1}^{N}\nabla_i^2 - \sum_{i=1}^{N}\sum_{A=1}^{M}\frac{Z_a}{r_{iA}} + \sum_{i=1}^{N}\sum_{j>i}^{N}\frac{1}{r_{ij}} = \hat{T} + \hat{V}_{Ne} + \hat{V}_{ee} \tag{2.8}$$

This makes the solution of Schrödinger equation with $\hat{H}_{elec}$ the electronic wave function Ψ_{elec}, and the electronic energy E_{elec}. The total energy E_{tot} becomes the sum of E_{elec} and a constant nuclear repulsion term, shown in 2.9.

$$E_{nuc} = \sum_{A=1}^{M}\sum_{B<A}^{M}\frac{Z_a Z_b}{r_{AB}} \tag{2.9}$$

$$E_{tot} = E_{elec} + E_{nuc} \tag{2.10}$$

The square of Ψ is the electron density $\rho(\mathbf{r})$, or the probability that electrons 1,2,...N are found simultaneously in volume elements $d\mathbf{x}_1, d\mathbf{x}_2, ..., d\mathbf{x}_N$. The electron density is defined as the multiple integral over all spin coordinates and all but one spatial coordinate.

$$\rho(\mathbf{r}) = N\int ... \int \left|\Psi\left(\mathbf{x}_1, \mathbf{x}_2, ..., \mathbf{x}_N\right)\right|^2 ds_1, d\mathbf{x}_2, ..., d\mathbf{x}_N \tag{2.11}$$

2.3.2 Density Functional Theory

At the heart of density functional theory is the use of electron density to replace the complicated N-electron wave function. The electron density, unlike the wave function, is an experimentally observable quantity.

For the electron density to replace the wave function it must be possible to construct the Hamiltonian from it. The Hamiltonian of a system is defined by three variables, the number of electrons N, the nuclear charges Z_a and the position of the nuclei in space R_A. The electron density has cusps corresponding to R_A. The positions of the nuclei are also related to the charges of the nuclei through equation 2.12. The total number of electrons can also be obtained by integrating the electron density (equation 2.13).

$$\lim_{r_{ia}\to 0}\left[\frac{\partial}{\partial r}+2Z_a\right]\bar{\rho}(\mathbf{r})=0 \tag{2.12}$$

$$\int \rho(\mathbf{r}_1)d\mathbf{r}_1 = N \tag{2.13}$$

The first proof that the Hamiltonian of a molecular system could be constructed from the electron density was formulated by Hohenberg and Kohn in 1964.[69] Their first theorem states that *'the external potential, $V_{ext}(\mathbf{r})$ is a unique functional of $\rho(\mathbf{r})$; since, in turn V_{ext} fixes $\hat{H}$ we see that the full many particle ground state is a unique functional of $\rho(\mathbf{r})$'*.[69] The ground state energy of a system, defined by an external potential V_{ext}, is therefore available through a functional of the ground state electron density ρ_0, $E_0[\rho_0]$, as are its underlying components.

Their second theorem states that the ground state energy of a system E_0 is obtained from the true ground state electron density ρ_0.

Kohn-Sham showed that the exact ground state energy E_0 of an N-electron system can be obtained from equation 2.14.[70]

$$E[\rho] = -\frac{\hbar}{2m_e}\sum_{i=1}^{n}\int \psi_i^*(\mathbf{r}_1)\nabla_1^2\psi_i(\mathbf{r}_1)d\mathbf{r}_1 - \sum_{I=1}^{N}\int \frac{Z_I e^2}{4\pi\epsilon_0 r_{I1}}\rho(\mathbf{r}_1)d\mathbf{r}_1 + \frac{1}{2}\int \frac{\rho(\mathbf{r_1})\rho(\mathbf{r_2})e^2}{4\pi\epsilon_0 r_{I2}}d\mathbf{r_1}d\mathbf{r_2} + E_{XC}[\rho] \tag{2.14}$$

The terms in 2.14 represent the kinetic energy of the electrons, the electron-nuclei interactions, the coulombic interactions between all orbitals and the exchange-correlation energy E_{XC}, respectively. The exchange correlation energy is a functional of the electron density representing all non-classical electron-electron interactions but, its analytical expression is unknown and therefore requires approximation.

The Kohn-Sham orbitals ψ_i $(i = 1, 2, ..., n)$ are one-electron spatial orbitals through which it is possible to obtain the exact ground state electron density ρ_0 at a given position $\mathbf{r}$. This is achieved by summing over all occupied Kohn-Sham orbitals, as shown in equation 2.15.

$$\rho(\mathbf{r}) = \sum_{i=1}^{n} |\psi_i(\mathbf{r})|^2 \tag{2.15}$$

The Kohn-Sham orbitals may be obtained through solving the Kohn-Sham equations shown in equation 2.16, where ϵ_i are the Kohn-Sham orbital energies and V_{XC} is the exchange-correlation potential.

$$\left\{-\frac{\hbar^2}{2m_e}\nabla_i^2 - \sum_{I=1}^{N}\frac{Z_I e^2}{4\pi\epsilon_0 r_{I1}}d\mathbf{r}_2 + \int \frac{\rho(\mathbf{r}_2)e^2}{4\pi\epsilon_0 r_{I2}} + V_{XC}(\mathbf{r}_1)\right\}\psi_i(\mathbf{r}_1) = \epsilon_i\psi_i(\mathbf{r}_1) \tag{2.16}$$

To solve the Kohn-Sham equations an initial guess is made for the electron density. The equations are then solved self-consistently by first computing V_{XC} as a function of $\mathbf{r}$. An initial set of orbitals is obtained by solving the Kohn-Sham equations and is used to compute an improved density using 2.15. This process is repeated until the density and exchange-correlation energy converge, from which point the ground state energy is obtained using 2.14.

2.3.3 Exchange-Correlation Functionals

Several approximations are available for the exchange-correlation functional of the Kohn-Sham equations, most of which are based on the Local Density Approximation (equation 2.17).

$$E_{XC}^{LDA}[\rho] = \int \rho(\mathbf{r})\, \epsilon_{XC}(\rho(\mathbf{r}))\, d\mathbf{r} \tag{2.17}$$

The Local Density Approximation (LDA) is based on the properties of the uniform electron gas, which is a hypothetical system of electrons against a positive background charge distribution, whose form for its exchange and correlation energies is known. In equation 2.14 $\epsilon_{XC}(\rho(\mathbf{r}))$ is the exchange-correlation energy of a particle in this uniform electron gas.

Open-shell systems, have a differing number of spin-up, α, and spin-down, β, electrons. These systems greatly benefit from the use of unrestricted exchange-correlation functionals where two spin densities, ρ_α and ρ_β, are used instead of one. The LDA functional can be extended to depend on these two spin densities, becoming the Local Spin Density Approximation (LSDA), with equation 2.17 becoming 2.18.

$$E_{XC}^{LSDA}[\rho_\alpha, \rho_\beta] = \int \rho(\mathbf{r})\, \epsilon_{XC}(\rho_\alpha(\mathbf{r}), \rho_\beta(\mathbf{r}))\, d\mathbf{r} \tag{2.18}$$

Applications of LDA and LSDA functionals are limited to solid-state applications. For molecular systems a variety of functionals, based on the Generalised Gradient Approximation (GGA) are utilised. These include the gradient of the density and are generally of the form given in equation 2.19.

$$E_{XC}^{GGA}[\rho_\alpha, \rho_\beta] = \int f(\rho_\alpha, \rho_\beta, \nabla\rho_\alpha, \nabla\rho_\beta]\, dr \tag{2.19}$$

Dispersion Correction

Van-der-Waals forces comprise three main interactions found within a molecular system. These include the attractive or repulsive forces between two permanent dipoles (Keesom force), the force due to the induction of an induced dipole due to permanent dipoles (Debye forces) and the force between two instantaneously induced dipoles (London dispersion forces). The London forces arise from the response of electrons to instantaneous charge density fluctuations elsewhere in a system.

Exchange-correlation functionals fail to describe the London dispersion component of the vdW forces. There are a range of methodologies available for the inclusion of these forces within a DFT calculation, ranging in accuracy and additional computational cost. The simplest of these is Grimme's DFT+D2 correction. In the DFT+D2 approach,[71] the total energy is described by a sum of the Kohn-Sham energy, E_{DFT} and a vdW semi-empirical pair correction $E^{(2)}_{disp}$, to account for missing vdW forces.

$$E_{DFT-D} = E_{KS-DFT} + E^{(2)}_{disp} \tag{2.20}$$

$E^{(2)}_{disp}$ is given by

$$E^{(2)}_{disp} = -s_6 \sum_{i=1}^{N_{at-1}} \sum_{j=i+1}^{N_{at}} \frac{C^6_{ij}}{R^6_{ij}} f_{dmp}\left(R_{ij}\right) \tag{2.21}$$

where N_{at} is the total number of atoms, C^6_{ij} is the dispersion coefficient, R_{ij} is the bond distance for atom pair ij and s_6 is the global scaling factor, dependent on the choice of exchange-correlation functional. A damping factor, f_{dmp}, is used to prevent singularities at small distances.

Several methods building on Grimme's method seek to achieve higher accuracy while maintaining the low computational cost. These methods seek to improve the accuracy of the C^{ij}_6 terms by introducing some environmental dependence to the term.. Methods of this type include those of Tkatchenko and Scheffler, Becke-Johnson and Grimme's DFT+D3 approach.[72–74]

The DFT+D3 approach seeks to improve on the accuracy of DFT+D2 through on-the-fly calculation of dispersion coefficients during the DFT calculations and the inclusion of a three-body component to the E_{disp} term,

$$E_{disp} = E_{disp}^{(2)} + E_{disp}^{(3)} \tag{2.22}$$

where $E_{disp}^{(3)}$ is given by

$$E_{disp}^{(3)} = \sum_{ABC} f_{f(3)}\left(\bar{r}_{ABC}\right) E^{ABC} \tag{2.23}$$

and the sum is over all triples ABC. Geometrically averaged radii $\bar{r}^{ABC}$ are used in the damping function, $f_{f(3)}$. The inclusion of three-body terms increases the scaling of the computational cost from $O(N_{atoms}^2)$ to $O(N_{atoms}^3)$ but the cost of the inclusion of the D3 correction is still negligible when compared with the overall cost of a DFT calculation.

The optPBE functional is an example of the vdW-DF approach,[75–78] which requires no external input and instead seeks to treat dispersion interactions directly using the electron density. The exchange-correlation energy is given by

$$E_{XC} = E_x^{GGA} + E_c^{LDA} + E_c^{nl}, \tag{2.24}$$

where E_x^{GGA} is the exchange energy for a given GGA functional and E_c^{LDA} is the LDA correlation energy. Dispersion is included directly using a non-local correlation, E_c^{nl}, which is calculated using a double space integral of the form

$$E_c^{nl} = \iint \mathrm{d}\mathbf{r}_1 \mathrm{d}\mathbf{r}_2 \; n\left(\mathbf{r}_1\right) \varphi\left(\mathbf{r}_1, \mathbf{r}_2\right) n\left(\mathbf{r}_2\right), \tag{2.25}$$

where $n(\mathbf{r})$ is electron density and φ is an integration kernel. The choice of exchange functional important, as Dion's original revPBE approach was shown to produce intermolecular binding distances which were too large.[78] The optPBE functional seeks to overcome these problems by using a less repulsive exchange functional.

2.3.4 Plane-Wave DFT

It is possible to solve the Schrödinger equation for a periodic system, defined by lattice vectors $\mathbf{a_1}$, $\mathbf{a_2}$ and $\mathbf{a_3}$ using Bloch's theorem. The solution is a sum of terms given in equation 2.26.

$$\psi_{\mathbf{k}}(\mathbf{r}) = e^{i\mathbf{k}\cdot\mathbf{r}} u_{\mathbf{k}}(\mathbf{r}), \tag{2.26}$$

The functions $e^{i\mathbf{k}\cdot\mathbf{r}}$ are known as plane-waves and make it possible to solve the Schrödinger equation in terms of $\mathbf{k}$, rather than $\mathbf{r}$. While the vectors $\mathbf{r}$ exist in real space the $\mathbf{k}$ exist in reciprocal space, or k-space, and are defined by their reciprocal lattice vectors, $\mathbf{b}_1$, $\mathbf{b}_2$ and $\mathbf{b}_3$. Reciprocal space is such that a larger real vector is represented by a shorter reciprocal vector.

A primitive cell in k-space is known as the Brillouin zone. There are several important points in the Brillouin zone, the most significant of which is the point at which $\mathbf{k} = 0$, or the Γ-point.

It is possible to expand $u_{\mathbf{k}}(r)$, where $u_{\mathbf{k}}(r)$ is a periodic function with the same periodicity of the cell, in terms of plane waves,

$$u_{\mathbf{k}}(r) = \sum_{\mathbf{G}} c_{\mathbf{G}} e^{[i\mathbf{G}\cdot\mathbf{r}]}, \tag{2.27}$$

where the vectors defined by $\mathbf{G}$ are in reciprocal space. The combination of equations 2.26 and 2.27 gives

$$\psi_{\mathbf{k}}(\mathbf{r}) = \sum_{|\mathbf{G}+\mathbf{k}|<G_{cut}} c_{\mathbf{k}+\mathbf{G}} e^{[i(\mathbf{k}+\mathbf{G})\mathbf{r}]}. \tag{2.28}$$

The summation in 2.28 is truncated to only include solutions with a kinetic energy less than G_{cut}, otherwise the solution would require an infinite summation over all possible values of $\mathbf{G}$.

Large cut-offs are required for plane waves oscillating on short length scales, which is exactly the behaviour of the wave functions of core electrons. These core

electrons, however, are normally not involved in bonding and can instead be replaced with pseudopotentials. This approximation reduces the number of plane waves required in a calculation and reduces the overall computational cost. Commonly used pseudopotentials are ultrasoft pseudopotentials and projector augmented-wave pseudopotentials.

2.4 Statistical Mechanical Methods

2.4.1 Free Energy Concentration Expansion Method

The free energy concentration expansion method (FCEM) is a statistical mechanical approximation for the prediction of chemical ordering in NAs of up to 1000 atoms.[12,79]

FCEM expressions for binary alloys are obtained using the Ising model Hamiltonian and an expansion of the partition function and free energy in terms of solute concentration. The free energy of a multicomponent alloy consisting of distinct arrays of N_p $(p = 1, 2...)$ geometrically identical atomic sites, characterised by concentrations, c_p^I of constituents I, is given by[12]

$$\begin{aligned} F &= kT \sum_p \left(N_p \sum_I c_p^I \ln c_q^I \right) \\ &+ \sum_{p \leq q} \left(N_{pq} \frac{1}{2} \sum_I w_{pq}^{II} (c_p^I + c_q^I) \right) \\ &- \sum_{\{IJ\}} \left[V_{pq}^{IJ} \left(c_p^I c_q^J + c_p^J c_q^I \right) + kT c_p^I c_p^J c_q^I c_q^J \frac{1}{b} \ln \left(\cosh \left(b \frac{2V_{pq}^{IJ}}{kT} \right) \right) \right]. \end{aligned} \tag{2.29}$$

Clusters are treated as a series of symmetry inequivalent shells belonging to the different layers of a cluster.[80] Numerical minimisation of F gives all I-constituent equilibrium concentrations for shell number p, c_p^I. The model requires the input of the number of atoms in each shell, N_p, and the number of nearest-neighbour (NN) broken-bonds belonging to p and q shells.

The first term in the expression is the configurational entropy of the system, the second term contributes the homoatomic interactions, w_{pq}^{II}, the third term the effective heteroatomic interactions, V_{pq}^{IJ}, between constituents I and J. The last term is the short range order contribution (b is obtained by fitting FCEM predictions to Monte Carlo simulations).[79]

Homoatomic interactions, w_{pq}^{II}, can be derived using several methods. It can be estimated using site energies derived from experimental dimer bond energies, surface energies and cohesive energies, using the Naval Research Laboratory tight-binding (NRL-TB) method or through the coordination dependent bond energy variation method (CBEV).[79,81,82] The effective heteroatomic interactions, V_{pq}^{IJ} are estimated using the ΔH_{mix} of a system.

Using FCEM it is also possible to minimise the free energy for a series of temperatures, giving the temperature dependence of site concentrations. This can be used to characterise phase separation in alloy systems.

2.4.2 Coordination Dependent Bond Energy Variations

In order to understand fully the role bond energy variations, δw_{pq}, play in systems with small atomic mismatches, or similar heteroatomic interactions, more reliable energetic data is required. One such method for obtaining more accurate δw_{pq} is the use of coordination-dependent bond energy variations (CBEV), extracted from DFT-computed surface energies.[82]

The surface energy of a system can be written in terms of NN pair-bond-energy variations, δw_{pq}, relative to that of the bulk value, w_b, and the number of broken bonds, ΔZ_p as

$$E_s = \sum_p \frac{1}{2} \left(\sum_{q(q \neq p} \delta w_{pq}^{II} - \Delta Z_p w_b \right). \tag{2.30}$$

The functional dependence of CBEV is approximated by a polynomial function. The coefficients of the polynomial are fitted to the DFT computed energies for six

surfaces (111), (100), (110), (311), (331) and (210).

For a $p-q$ pair-bond with ΔZ_p and ΔZ_q NN broken bonds, the variation, δw_{pq}, is considered as a polynomial of two coordination variables: one symmetric, $x_{pq} = \Delta Z_p + \Delta Z_q$, for the total number of broken bonds and one anti-symmetric, $y_{pq} = \Delta Z_p - \Delta Z_q$, which takes into account the possible non-equivalence of two sites.

DFT-calculated surface energies are mapped into the six-coefficients of a polynomial $(a_{(1,0)}, a_{(2,0)}, a_{(0,2)}, a_{(3,0)}, a_{(1,2)}, a_{(4,0)})$ and odd powers of y are omitted due to symmetry considerations ($\delta w_{pq} = \delta w_{qp}$)

$$\delta w_{pq} = a_{1,0}x_{pq} + a_{2,0}x_{pq}^2 + a_{0,2}y_{pq}^2 + a_{3,0}x_{pq}^3 + a_{1,2}x_{pq}y_{pq}^2 + a_{4,0}x_{pq}^4. \tag{2.31}$$

The use of a polynomial allows energy variations to be treated as coordination-dependent functions, rather than numerical values. This ensures transferability between different geometries without the need to refit interactions.

2.5 Energetics

2.5.1 Binding Energy

The binding energies E_b were calculated using the following expression

$$\mathrm{E}_b = \frac{\mathrm{E}_{A_nB_m} - (n\mathrm{E}_A + m\mathrm{E}_B)}{N} \tag{2.32}$$

where $\mathrm{E}_{A_nB_m}$ is the total energy of the cluster and E_{A_N} and E_{B_N} are the spin-polarised atom of type A and B.

3 | The Structural Characterisation of Palladium-Iridium Nanoalloys

3.1 Introduction

PdIr NAs are currently under investigation for their application in a wide-range of catalytic processes. A vital first step in rationalising these catalytic properties is their structural characterisation. In the following studies of PdIr nanoalloys three methods were utilised to achieve this; direct DFT global optimisation with the BCGA-DFT method, a hybrid approach utilising the BCGA-Gupta method and subsequent DFT calculations and the FCEM/CBEV statistical mechanical method.

In publication 1 the direct DFT global optimisation of $N = 8 - 10$ Pd_nIr_{N-n} clusters is performed using the BCGA-DFT method.[63] Significant quantum-size effects are revealed in the system. Cubic structures are seen for Ir and Ir-rich clusters, including Pd_2Ir_6, Pd_3Ir_6 and Pd_4Ir_6 as shown in figure 3.1. The mixing energies of clusters were in many cases found to be positive, an indication of the preference for the monometallic structures over the bimetallic.[83] The spin of these clusters was further investigated through a series of reoptimisations at various fixed multiplicities.

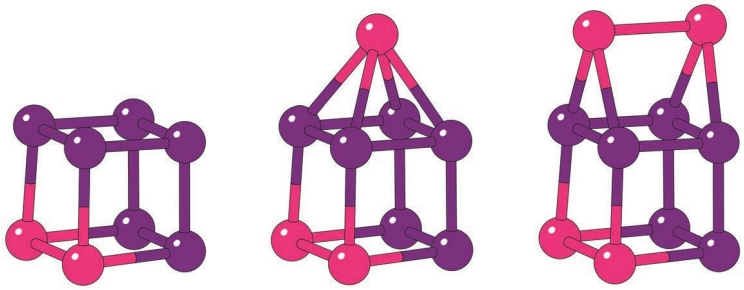

Figure 3.1: Cubic structures of Pd_2Ir_6, Pd_3Ir_6 and Pd_4Ir_6 from BCGA-DFT calculations.

Publication 2 is a comparative study of two methods used for the characterisation of structure and chemical ordering in NA systems. The first, more commonly used method, was a hybrid approach whereby low energy minima are produced using the BCGA-Gupta method. A selection of the minima are taken and their ordering refined using DFT local minimisation.[84] The global minima produced from this hybrid approach were compared with those produced by the FCEM/CBEV method.

Statistical mechanical methods are less commonly used for the structural characterisation of nanoalloys but offer some distinct advantages.[85,86] The FCEM is such a method, which is capable of predicting the chemical ordering of a fixed NA geometry. This approach has a very low computational cost when compared with other global optimisation and DFT-based methods and is capable of characterising the compositional ordering of NPs of thousands of atoms.[12] These methods rely on the accuracy of the input energetics. FCEM utilises accurate bond energy variations derived from the CBEV method,[87] which itself relies on the input of surface energies calculated using DFT.[88]

In this study surface energies were calculated for Pd and Ir for the (111), (110), (100), (311), (331) and (210) surface orientations. These were then used, in combination with the corrected cohesive energies of Pd and Ir,[89] in the parametrisation of the CBEV parameters used in the FCEM calculations that followed.

FCEM calculations were performed on the 38-atom Pd_4Ir_{34}, Pd_8Ir_{30} and $Pd_{20}Ir_{18}$ and 79-atom Pd_4Ir_{75} and Pd_8Ir_{70} truncated octahedra. Local minimisations were performed on the resulting structures and compared with the results of the hybrid

BCGA-Gupta/DFT method. The results of the FCEM/CBEV calculations were shown to be accurate, especially in the case of the 79-atom cluster.

3.2 Publication 1

Title

Global Optimization of 8-10 Atom Palladium-Iridium Nanoalloys at the DFT Level

Authors

Jack B. A. Davis, Sarah L. Horswell and Roy L. Johnston

Journal The Journal of Physical Chemistry A

Volume 118

Pages 208-214

DOI 10.1021/jp408519z

Submitted

26th August 2013

Accepted

13th December 2013

THE JOURNAL OF PHYSICAL CHEMISTRY A

Article

pubs.acs.org/JPCA

Global Optimization of 8−10 Atom Palladium−Iridium Nanoalloys at the DFT Level

Jack B. A. Davis, Sarah L. Horswell, and Roy L. Johnston*

School of Chemistry, University of Birmingham, Edgbaston, B15 2TT, Birmingham, United Kingdom

Supporting Information

ABSTRACT: The global optimization of $Pd_nIr_{(N-n)}$ $N = 8-10$ clusters has been performed using the Birmingham Cluster Genetic Algorithm (BCGA). Structures were evaluated directly using density functional theory (DFT), which has allowed the identification of Ir and Ir-rich PdIr cubic global minima, displaying a strong tendency to segregate. The ability of the searches to find the putative global minimum has been assessed using a homotop search method, which shows a high degree of success. The role of spin in the system has been considered through a series of spin-restricted reoptimizations of BCGA-DFT minima. The preferred spin of the clusters is found to vary widely with composition, showing no overall trend in lowest-energy multiplicities.

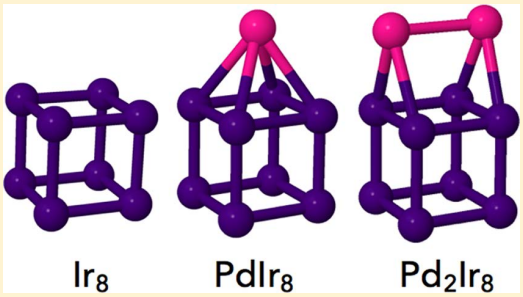

3.3 Publication 2

Title

Comparative Modelling of Chemical Ordering in Palladium-Iridium Nanoalloys

Authors

Jack B. A. Davis, Sarah L. Horswell and Roy L. Johnston

Journal The Journal of Chemical Physics

Volume 141

Pages 224307

DOI 10.1063/1.4903188

Submitted

1st October 2014

Accepted

18th November 2014

3.3.1 Author Contribution

The author contribution to publication 2 is the calculation of the surface energies from which Leonid Rubinovich (Ben-Gurion University) produced the CBEV energetics. These parameters were then used by the author for the FCEM calculations on the 38, 79 and 201-atom NAs. The author also performed the BCGA-Gupta calculations and the DFT calculations on the low energy minima which were used for the comparison.

THE JOURNAL OF CHEMICAL PHYSICS **141**, 224307 (2014)

Comparative modelling of chemical ordering in palladium-iridium nanoalloys

Jack B. A. Davis,[1] Roy L. Johnston,[1,a)] Leonid Rubinovich,[2] and Micha Polak[2,b)]
[1]*School of Chemistry, University of Birmingham, Birmingham B15 2TT, United Kingdom*
[2]*Department of Chemistry, Ben-Gurion University of the Negev, Beer-Sheva 84105, Israel*

(Received 1 October 2014; accepted 18 November 2014; published online 9 December 2014)

Chemical ordering in "magic-number" palladium-iridium nanoalloys has been studied by means of density functional theory (DFT) computations, and compared to those obtained by the Free Energy Concentration Expansion Method (FCEM) using derived coordination dependent bond energy variations (CBEV), and by the Birmingham Cluster Genetic Algorithm using the Gupta potential. Several compositions have been studied for 38- and 79-atom particles as well as the site preference for a single Ir dopant atom in the 201-atom truncated octahedron (TO). The 79- and 38-atom nanoalloy homotops predicted for the TO by the FCEM/CBEV are shown to be, respectively, the global minima and competitive low energy minima. Significant reordering of minima predicted by the Gupta potential is seen after reoptimisation at the DFT level. [http://dx.doi.org/10.1063/1.4903188]

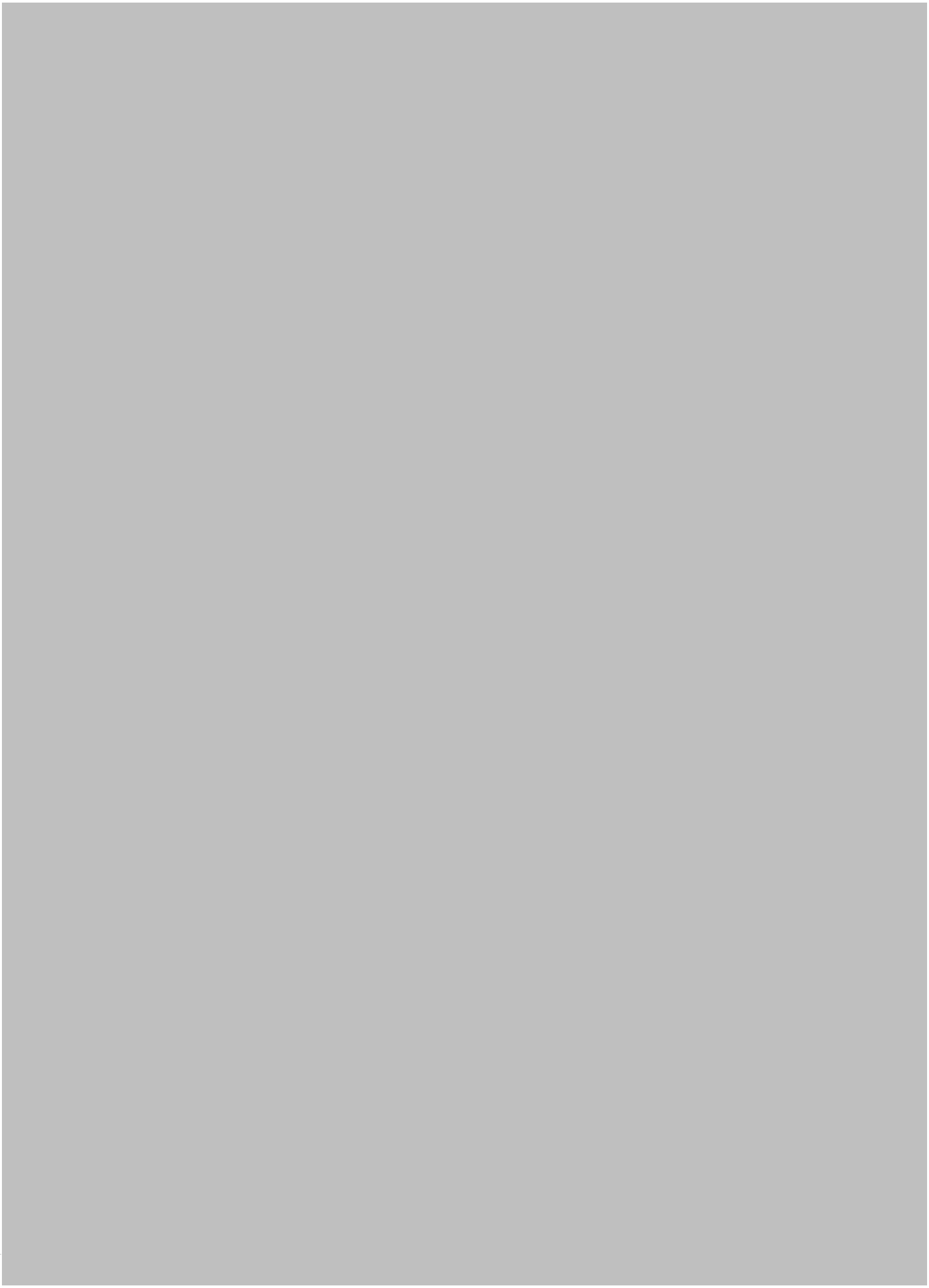

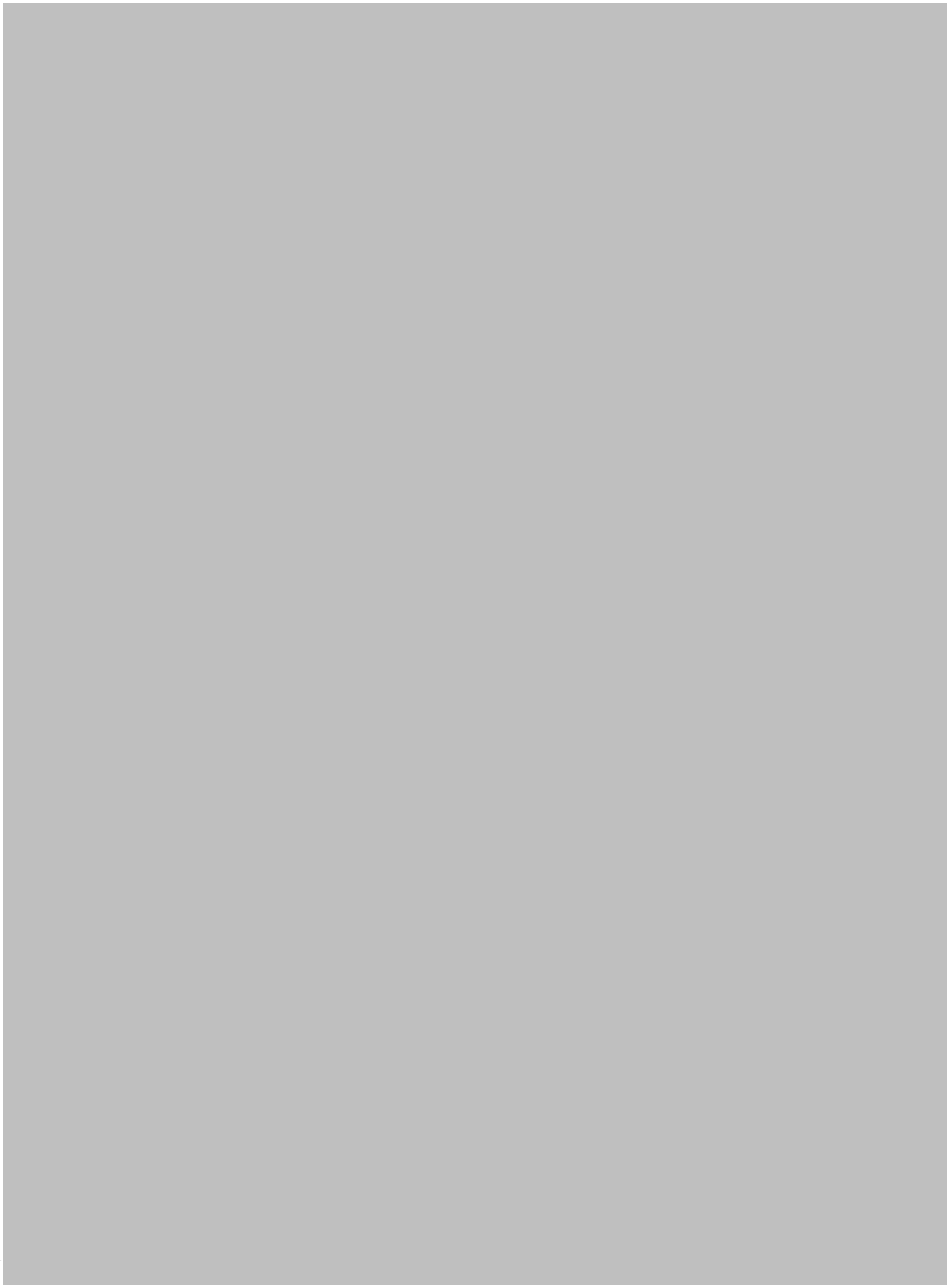

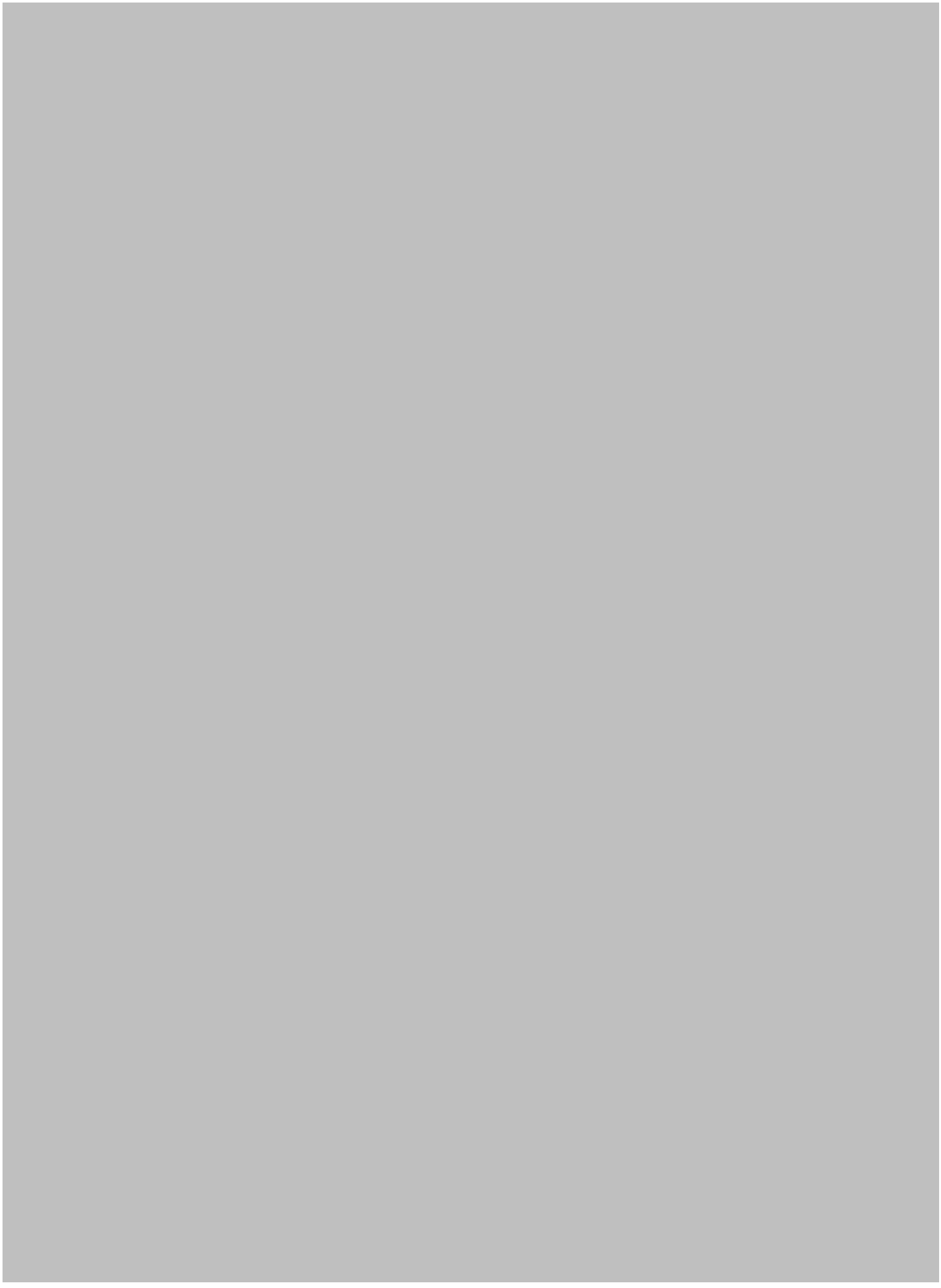

4 | Small Molecule Adsorption and the Effect of Dispersion Correction

4.1 Introduction

The following publications set out to determine the most favourable adsorption sites on a variety of mono- and bimetallic NAs, which after structural characterisation, is the next step in rationalising the catalytic properties of a NA.

In Publication 3 random search global optimisation method is used to determine the most favourable, or lowest energy, adsorption site.[90] This is a relatively simple method whereby a predetermined NA structure is placed adjacent to a ligand molecule. The NA is then rotated randomly while the ligand molecule remains fixed. The system is then locally minimised using VASP. This procedure is repeated for a fixed number of steps and the lowest energy adsorption site is then taken. This program is available through Bitbucket.[91]

This method was applied to the 38-atom PdIr truncated octahedra (TO) obtained using the FCEM/CBEV methodology. These were ideal structures to study the effect of the composition on the adsorption properties of a NA system. The lowest energy adsorption site were determined for H_2 and benzene for three compositions, Pd_4Ir_{34}, Pd_8Ir_{30} and $Pd_{20}Ir_{18}$, and the monometallic TO structures. Significant quantum-size effects in adsorption of H_2 were seen in the Ir and Ir-rich system.

Publication 4 is a study of the effect of a variety of dispersion corrections on the adsorption of CO on monometallic Pt, Au, Pd and Ir 38-atom TO and 55-atom Icosahedral (Ico) structures. The effect of dispersion corrections is of significant current interest and has not been previously investigated for NPs.[92,93] The effect of Grimme's D2 and D3 corrections and the optPBE vdW exchange-correlation functional are compared with results using the standard PBE exchange-correlation functional. Significant effects are seen in the Pt and Au systems, with limited effects seen for the Ir and Pd clusters. Some differences are also seen when comparing the TO and Ico geometries.

While other higher-level methods which accurately describe dispersion are available,[94,95] the choice of the D2 and the D3 dispersion corrections was based on their current application in a wide range of computational studies and their low computational cost.[71,74,96] The choice of optPBE was based on a comparison of a range of vdW exchange-correlation functionals. These seek to calculate the dispersion forces directly from the electron density, not from pre-computed coefficients such as D2 and D3. Five exchange-correlation functionals were tested, vdW-DF, vdW-DF2, optPBE, optB86 and optB88.[75,77,78,97,98] The binding energy E_b was calculated for Pt, Au, Pd and Ir 38-atom TOs (table 4.1) and compared with the standard PBE results. The opt functionals are all optimised for metallic systems. The optPBE functional was chosen for our study because it gives E_b values similar to the PBE exchange-correlation functional. The gaps in table 4.1 are due to convergence issues with the optB88 functionals.

	Pt	Au	Pd	Ir
	E_b / eV	E_b / eV	E_b / eV	E_b / eV
PBE	-4.391	-2.415	-2.824	-5.698
optB86	-4.782	-2.741	-3.102	-6.476
optB88	-	-2.619	-	-4.343
optPBE	-4.418	-2.455	-2.777	-5.989
vdW-DF	-3.947	-1.752	-2.390	-5.441
vdW-DF2	-4.086	-2.102	-2.433	-5.138

Table 4.1: Binding energies E_b, per atoms, for the 38-atom Pt, Au, Pd and Ir TOs for PBE and vdW exchange-correlation-functionals.

4.2 Publication 3

Title

Computational Study of the Adsorption of Benzene and Hydrogen on Palladium-Iridium Nanoalloys

Authors

Jack B. A. Davis, Sarah L. Horswell, Laurent Piccolo and Roy L. Johnston

Journal Journal of Organometallic Chemistry

Volume 792

Pages 190-193

DOI 10.1016/j.jorganchem.2015.04.033

Submitted

30th January 2015

Accepted

12th April 2015

Journal of Organometallic Chemistry 792 (2015) 190–193

Contents lists available at ScienceDirect

Journal of Organometallic Chemistry

journal homepage: www.elsevier.com/locate/jorganchem

Computational study of the adsorption of benzene and hydrogen on palladium–iridium nanoalloys

Jack B.A. Davis [a], Sarah L. Horswell [a], Laurent Piccolo [b], Roy L. Johnston [a, *]

[a] School of Chemistry, University of Birmingham, B15 2TT, United Kingdom
[b] Institut de Recherches sur la Catalyse et l'Environnement de Lyon (IRCELYON), UMR 5256 CNRS & Université Lyon 1, 2 avenue Albert Einstein, F-69626 Villeurbanne Cedex, France

ARTICLE INFO

Article history:
Received 30 January 2015
Received in revised form
12 April 2015
Accepted 21 April 2015
Available online 30 April 2015

Keywords:
Palladium
Iridium
Nanoalloy
Catalysis
Benzene
Hydrogen

ABSTRACT

The preferred chemisorption sites on a variety of palladium–iridium nanoalloys are determined for benzene and hydrogen molecules. Available sites on the surface of the nanoalloys are explored using a random-search method, directly at the density functional level of theory. These searches successfully reveal the site preference for benzene and significant nanosize effects in the chemisorption of hydrogen. It is hoped that through the study of the chemisorption properties of Pd–Ir nanoalloys, complex catalytic processes, such as tetralin hydroconversion and the preferential oxidation of CO, can be better understood.

http://dx.doi.org/10.1016/j.jorganchem.2015.04.033
0022-328X/

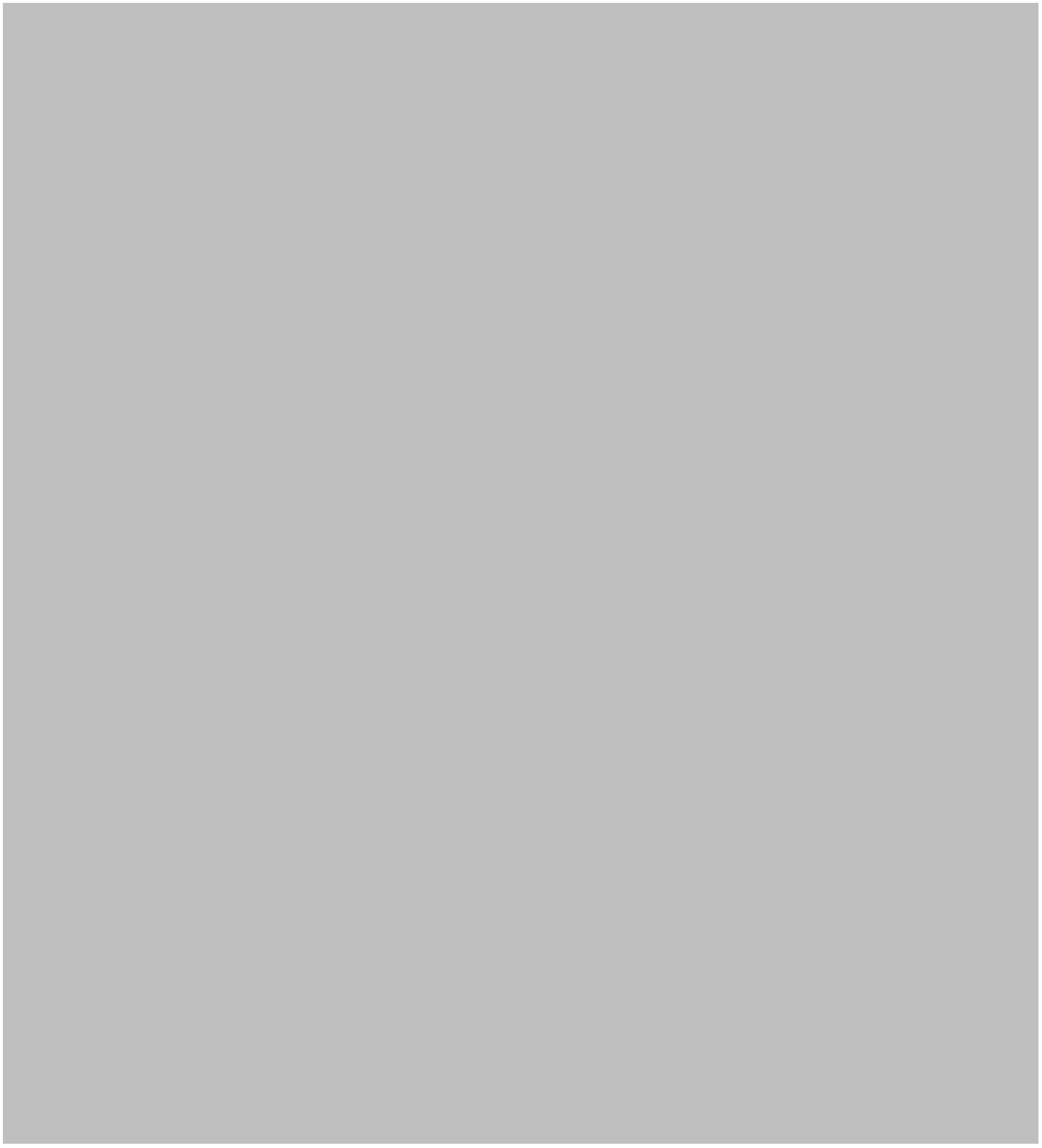

4.3 Publication 4

Title

The Effect of Dispersion Correction on the Adsorption of CO on Metallic Nanoparticles

Authors

Jack B. A. Davis, Francesca Baletto and Roy L. Johnston

Journal The Journal of Physical Chemistry A

Volume 119 (37)

Pages 9703-9709

DOI 10.1021/acs.jpca.5b05710

Submitted

15th June 2015

Accepted

31st August 2015

THE JOURNAL OF PHYSICAL CHEMISTRY A

Article

pubs.acs.org/JPCA

The Effect of Dispersion Correction on the Adsorption of CO on Metallic Nanoparticles

Jack B. A. Davis,[†] Francesca Baletto,[‡] and Roy L. Johnston*[,†]

[†]School of Chemistry, University of Birmingham, Birmingham, West Midlands B15 2TT, United Kingdom

[‡]Department of Physics, Kings College London, London WC2R 2LS, United Kingdom

ABSTRACT: The effect of dispersion corrections at a range of theory levels on the chemisorption properties of metallic nanoparticles is presented. The site preference for CO on Pt, Au, Pd, and Ir nanoparticles is determined for two geometries, the 38-atom truncated octahedron and the 55-atom icosahedron using density functional theory (DFT). The effects of Grimme's DFT-D2 and DFT-D3 corrections and the optPBE vdW-DF on the site preference of CO is then compared to the "standard" DFT results. Functional behavior is shown to depend not only on the metal but also on the geometry of the nanoparticle with significant effects seen for Pt and Au. There are both qualitative and quantitative differences between the functionals, with significant energetic differences in the chemical ordering of inequivalent sites and adsorption energies varying by up to 1.6 eV.

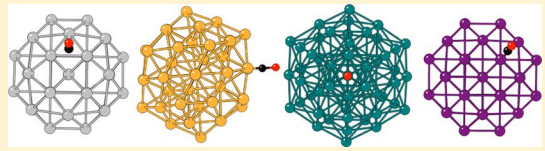

5 | The Development of Parallel Genetic Algorithms

5.1 Introduction

The following publications outline the development of a parallel methodology for the DFT global optimisation of metallic NPs and NAs and its application to small monometallic Au and Ir clusters and AuIr NAs, both in the gas-phase and supported on a MgO(100) surface.

In publication 5 the parallel pool methodology is presented and implemented within the BCGA. This new scheme was benchmarked through its application to the global optimisation of Au_5Ag_5, using the Gupta potential, and Au_{10}, at the DFT level. Further testing was performed on Au_{20}, which allowed the parallelism of the method to be assessed.

The successful application of the methodology was followed by the development of the Birmingham Parallel Genetic Algorithm (BPGA),[99] a new object-oriented Python-based program. The BPGA was developed specifically for the direct DFT global optimisation of clusters, utilising an interface to the Vienna Ab-initio Simulation Package (VASP).[100–103] The choice of both an object-oriented design and the Python programming language was to ensure a highly-transferable, modifiable and easily maintainable code.

In publication 7 the BPGA was applied to the global optimisation of Ir_N $N = 10 - 20$ clusters, a system under investigation for its catalytic properties.[43,104] Per-

forming the global optimisation at the DFT level of theory revealed the cubic structures seen in Ir clusters of this size.[28,105–107] The structures of several sizes were revealed for the first time.

The draft publication demonstrates the application of the BPGA to the global optimisation of gas-phase and supported $N = 4-6$ Au_nIr_{N-n} NAs. There is a large computational cost associated with performing a global optimisation in the presence of a surface MgO(100) slab and therefore these calculations benefited from the parallelism of BPGA. This study revealed significant differences in the surface-absorbed and gas-phase global minimum structures, including differences in structure and chemical ordering.

5.2 Publication 5

Title

Pool-BCGA: A Parallelised Generation-Free Genetic Algorithm for the Ab-Initio Global Optimisation of Nanoalloy Clusters

Authors

Armin Shayeghi, Daniel Götz, Jack B. A. Davis, Rolf Schäfer and Roy L. Johnston

Journal Physical Chemistry Chemical Physics

Volume 17

Pages 2104-2112

DOI 10.1039/C4CP04323E

Submitted

25th September 2014

Accepted

1st December 2014

5.2.1 Author Contribution

The development of the pool genetic algorithm and its implementation within the BCGA was performed by Armin Shayeghi and Daniel Götz ((T.U. Darmstadt). The author's contribution to this work was the testing of the pool methodology and its application to the Au_{20}. The application to Au_{20} allowed the parallelism of the methodology to be tested on a large system whose gas-phase structure is widely known.[27]

PCCP

PAPER

Cite this: *Phys. Chem. Chem. Phys.*, 2015, **17**, 2104

Pool-BCGA: a parallelised generation-free genetic algorithm for the *ab initio* global optimisation of nanoalloy clusters

A. Shayeghi,*[a] D. Götz,[b] J. B. A. Davis,[c] R. Schäfer[a] and R. L. Johnston*[c]

Received 25th September 2014,
Accepted 1st December 2014

DOI: 10.1039/c4cp04323e

www.rsc.org/pccp

The Birmingham cluster genetic algorithm is a package that performs global optimisations for homo- and bimetallic clusters based on either first principles methods or empirical potentials. Here, we present a new parallel implementation of the code which employs a pool strategy in order to eliminate sequential steps and significantly improve performance. The new approach meets all requirements of an evolutionary algorithm and contains the main features of the previous implementation. The performance of the pool genetic algorithm is tested using the Gupta potential for the global optimisation of the $Au_{10}Pd_{10}$ cluster, which demonstrates the high efficiency of the method. The new implementation is also used for the global optimisation of the Au_{10} and Au_{20} clusters directly at the density functional theory level.

1 Introduction

Modern nanoscience involves the study of promising nanoscale materials, which exhibit a wide variety of interesting physical and chemical properties. Nanoparticles composed of atoms and molecules lie between the atomic and bulk regimes with strongly size and composition dependent properties.[1] It remains desirable to close the gap between well-understood bulk properties and our knowledge of atomic behaviour in nanoscale research.

A detailed structural characterisation of this transition regime is therefore of high interest in order to rationalise the exceptional characteristics of nanoscale materials. Generating geometric structure candidates for a comparison with experimental observations is laborious for large systems and eventually becomes infeasible. From a theoretical view it is useful to carry out a global optimisation of the potential energy surface (PES) as a function of all coordinates, while the level of theory needed has to adequately represent the system being studied.

Since the electronic structure of large nanoparticles is expected to resemble the bulk phase, tailored model or empirical potentials (EPs) such as Gupta,[2] Sutton–Chen,[3] and Murrell–Mottram,[4] fitted to properties of the solid phase, enable a reasonable description of the PES. For smaller nanoparticles, *i.e.* nanoclusters, a quantum chemical treatment becomes necessary for which the computational costs are greater than in the case of using EPs. But unbiased global optimisation at this higher level of theory therefore requires the development of an efficient algorithm.

Nanoalloys (nanoparticles composed of more than one metal) are of considerable interest for their catalytic, optical and magnetic properties.[5] Their global optimisation is further complicated by the presence of a large number of homotops – inequivalent permutational isomers.[6,8] For this reason, the strategy was developed of optimising selected structures with DFT after searching by means of atomistic models using the second-moment approximation to the tight-binding model (SMATB).[7] Evolutionary algorithms such as the Lamarckian Birmingham cluster genetic algorithm (BCGA),[9] which combines local minimisation with a genetic algorithm (GA), are useful tools for searching the conformational space for the global minimum (GM) structure and lowest-energy local minima, especially when combined with first principles methods in the density functional theory (DFT) based BCGA approach.[10] This procedure notably enables the theoretical investigation of elaborate mono- and bimetallic clusters using a GA with results consistent with experiments.[11–16] For details on global optimisation algorithms, especially focused on genetic algorithms and basin hopping techniques, the reader is referred to the literature.[17,18]

The first use of GAs for global geometry optimisation of molecular clusters was reported by Hartke,[19] and Xiao and Williams,[20] using binary encoded geometries and bitwise acting genetic operators on binary strings.[21–23] Later a GA approach that operated on cartesian coordinates of the atoms was introduced by Zeiri,[24] which removed the requirement for encoding and decoding binary genes.[9] This was followed by the development of GAs for cluster optimisation by Deaven and Ho,[25] who

[a] *Eduard-Zintl-Institut, Technische Universität Darmstadt, Alarich-Weiss-Straße 8, 64287 Darmstadt, Germany. E-mail: shayeghi@cluster.pc.chemie.tu-darmstadt.de*
[b] *Ernst-Berl-Institut, Technische Universität Darmstadt, Alarich-Weiss-Straße 8, 64287 Darmstadt, Germany*
[c] *School of Chemistry, University of Birmingham, Edgbaston, Birmingham B15 2TT, UK. E-mail: r.l.johnston@bham.ac.uk*

performed gradient driven local minimisations for newly generated cluster structures. Further, Doye and Wales established how local minimisations effectively transform a multidimensional PES into a staircase-like surface, where the steps represent basins of attraction.[26] This coarse-grained representation of the PES reduces the conformational space and therefore simplifies the PES that the GA has to search. The local minimisations generally correspond to a Lamarckian evolution, since individuals pass on a proportion of their characteristics to their offspring. This procedure has been found to improve the efficiency of global optimisations and is implemented within the BCGA program, following the approach of Zeiri using real-valued cartesian coordinates.[9,24] Recent GA implementations are the OGOLEM code for arbitrary mixtures of flexible molecules of Dieterich and Hartke,[27] the hybrid *ab initio* genetic algorithm (HAGA), for surface and gas-phase structures,[28,29] and the gradient embedded genetic algorithm program (GEGA) for the global optimisation of mixed clusters formed by molecules and atoms.[30,31] Very recently the surface BCGA (S-BCGA)[32] and the first principles based GA of Vilhelmsen and Hammer[33] for the global optimisation of supported clusters have been reported. Also very recently the perturbation theory re-assignment extended GA for mixed-metallic clusters has proven to be very useful.[34]

The traditional generation based BCGA program is a sequential code where local optimisations of individuals are not independent from one-another. In fact, a limitation on treatable cluster sizes or rather the level of computational sophistication arises due to the sequentially performed geometry optimisations acting as a bottleneck.[35] Newly created individuals of a given population are geometrically relaxed with respect to their total energy. The best population members, with respect to their fitness (determined by a fitness function which depends on the total energy), are then selected for mating and mutation in order to create novel structures and to form the next generation. This cycle is then repeated until the energy of the lowest-lying isomers changes by less than a specified threshold within a certain number of generations. Thus, if more than the optimum number of processors is used in a first principles based global optimisation, the overall CPU time plateaus and the cores are used inefficiently due to the imperfect parallelisation of the local optimisations. In order to improve the efficiency of this approach, the goal must be to enable the independent relaxation of several geometries at the same time as schematically shown in Fig. 1, where several GA processes simultaneously optimise geometries managed by a global database (pool). This, however, cannot be implemented efficiently within the generation-based BCGA program.

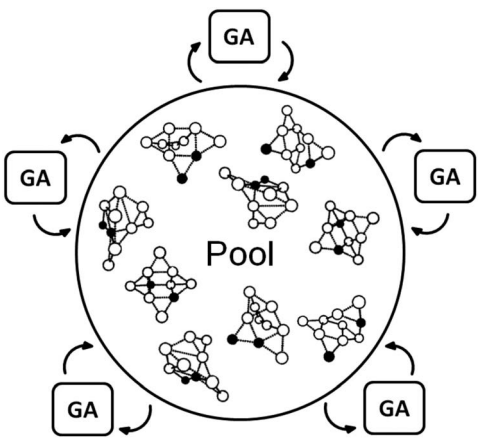

Fig. 1 Scheme of a global database (containing structural information) organizing slaves which independently apply genetic operators to the n individuals of the database. The population is held by a master acting as a pool of constant size.

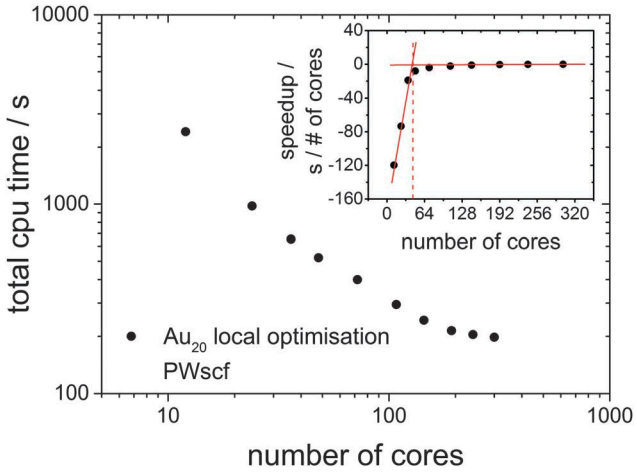

Fig. 2 Logarithmic benchmark plot of a local relaxation for the T_d isomer of Au_{20} starting from a random atom displaced version of the already optimised structure at the PBE/PWscf level of theory. It is shown, that the optimum number of processors is below 100 cores in this case as using a larger number of cores would not scale efficiently. The inset shows the derivative of the total CPU time *versus* the number of processors. The optimal number of processors for the global optimisation is in the range 36–64.

Since the DFT-BCGA code employed here makes use of a plane-wave self-consistent field (PWscf) pseudopotential approach, a benchmark calculation of a geometry optimisation for the predicted GM structure of Au_{20} (T_d symmetry)[36–38] has been performed in order to demonstrate the importance of an improved GA parallelisation to counter the imperfect DFT parallelisation. The total CPU time in these minimisations, starting from a random atom displaced version of the already optimised structure is shown in Fig. 2. The Au_{20} cluster was chosen for the benchmark calculations since, especially for such a large system, local optimisations lead to a slowdown in the global optimisation. The corresponding benchmark calculations indicate that the optimum number of processors should be below 100 cores (the best price-performance ratio should be for 36–64, as shown in the inset of Fig. 2) since a larger number of cores would not speed up the calculations efficiently. The total CPU time can be reduced by one order of magnitude going from 10 cores to 100 but does not improve significantly when using up to 300 cores. Benchmark calculations for a local optimisation of the Au_{10} cluster show the same tendency, with lower absolute CPU time, and are therefore not shown here. This indicates the importance of developing a parallelised GA

code which uses several GA subprocesses performing local minimisations on an efficient and ideal number of processors (48 cores in this case) at the same time, managed by a global database (see Fig. 1).

In this work, we present a significantly improved GA implementation which incorporates the BCGA and eliminates serial bottlenecks by replacing the generation based GA approach by a flexible pool model,[35] here denoted as pool-BCGA. Within this pool strategy individual subprocesses share the entire work leading to a parallelisation of the algorithm. This procedure allows several geometry optimisations to be run at the same time. The gain in speed is obvious as local optimisations are the bottlenecks in a global optimisation, especially when using *ab initio* methods in local relaxations. In principle, one could also think about running parallel geometry optimisation tasks in the generation based BCGA. But, several ongoing optimisations would have different time demands and therefore each generation would have to wait for the slowest population members leading to processor idle times.

The development of parallel GA implementations has previously been reported for both atomic and molecular clusters,[27,33,35,40,41] Global geometry optimisation at the DFT[42] or *ab initio*[43] level is generally found to be very expensive and not suitable for larger clusters, for which global optimisation at a lower level of theory would be appropriate. This leads to the commonly found two-stage procedure of performing the global search at *e.g.* the force-field or semi-empirical level, followed by a DFT or *ab initio* refinement of the best candidates.[44] In the DFT-BCGA code used in this work, the global optimisation is performed at the relatively cheap pseudopotential PWscf level, which enables larger systems to be treated at the DFT level, while the best candidates can still be refined using a higher level of theory. However, the direct GA method is easily implemented with higher level approaches such as MP2 and CC calculations. The flexible concept replaces the generation based algorithm by using a global database consisting of geometric and energetic information about a specified number of individuals. Several independent subprocesses make use of this database by applying mating and mutation operators to the pool members and form new individuals. These new individuals compete with current members of the pool and are immediately added to the pool if they are lower in energy.

We first test the method for the global optimisation of the $Au_{10}Pd_{10}$ cluster, using the Gupta potential, for an extensive statistical analysis of the new implementation. The 20-atom cluster is also interesting from a catalytic point of view,[45] and offers an ideal test system, especially due to the large number of homotops $N = (N_{Au} + N_{Pd})!/N_{Au}!N_{Pd}! \approx 185\,000$ for a given geometry.[8] The resulting knowledge from these investigations, in terms of mating and mutation, is further used for the DFT based global optimisation of the Au_{10} cluster. It represents a suitable test system for the DFT case in order to compare the efficiency of both implementations, as it has been well studied in the past.[38,46,47] Finally, the parallelisation of the code is tested by carrying out the global optimisation of Au_{20} at the DFT level, a system previously well studied experimentally[36,37] while geometries have been found by genetic algorithms[38,48] and the basin-hopping approach[39] based on DFT.

2 Methodology

2.1 Computational details

In the benchmark calculations, employing the Gupta empirical potential in geometry optimisation steps, many-body scaling parameters are chosen according to values for Au–Pd nanoclusters with 34-/38-atoms[49] and 98-atoms[13] from the literature.

In the DFT calculations, the Perdew–Berke–Ernzerhof (PBE) xc functional,[50] and ultrasoft pseudopotentials of the Rabe–Rappe–Kaxiras–Joannopoulos type,[51] with nonlinear core corrections are employed. For the calculation of electronic energies, a kinetic energy cutoff of 40 Ry and an electronic self consistency criterion of 10^{-5} eV are used. The efficiency of electronic convergence for metallic states is improved using the Methfessel–Paxton smearing scheme.[52] Local relaxations are performed with total energy and force convergence threshold values of 10^{-3} eV and 10^{-2} eV Å^{-1}, respectively. All DFT calculations are performed within the Quantum Espresso (QE) package.[53]

2.2 Pool-BCGA

To make use of the flexible parallelisation possibilities associated with a pool configuration, the application of mating and mutation operators to given geometries and their local optimisation and fitness assignment is managed by independently working pool-BCGA subprocesses synchronizing with a global database. As well as handling the atom coordinates and total energy of all structures currently in the pool, the global database is also needed to coordinate the individual subprocesses during runtime. The general workflow of the pool strategy is depicted in Fig. 3. The first step (''initial-mode'') consists of constructing an initial pool of individuals by

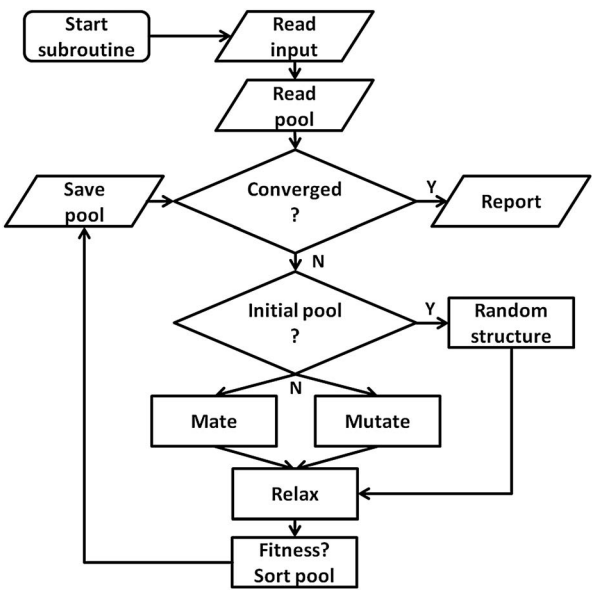

Fig. 3 The genetic operators are applied by the subprocesses on the members of this pool. The flowchart shows how a single pool subprocess works independently from other instances, while all subprocesses communicate with the global database.

generating random structures within a spherical or cubic simulation cell, which is set to be larger than the dimensions of the random cluster. This continues until the desired pool size is reached followed by the second step (“pool-mode”). In the pool-mode, mating and mutation operators are employed on clusters chosen according to either a roulette selection condition, where a random selection is weighted by the assigned fitness, or a tournament selection, and adopt the Deaven–Ho crossover method using a cut and splice crossover operator.[25] Random rotations are performed on parent clusters which are then cut horizontally about one (1-point) or two (2-point) positions parallel to the *xy* plane. Complementary fragments are then spliced together. For 1-point crossover, the cutting plane can be chosen at random or weighted according to the relative fitnesses of the two parents, while in the 2-point case the cutting planes are chosen at random.

In contrast to the default settings of the generation based GA, where the number of offspring grows with an increasing mutation rate, in a pool-GA calculation mutation and mating are performed with a certain probability as the pool size is kept fixed. This must be taken into account when setting the parameters in a typical pool-GA run. The offspring structures compete with the structures present in the pool according to their total energy after their local optimisation. Offspring with a better fitness (lower total energy) replace higher lying pool members. After checking for repeated optimised structures using a moments of inertia selection routine, the pool is sorted by ascending total energy. Finally, convergence is achieved when the minimum energy in the pool changes by less than a pre-defined energy difference (typically 10^{-3} eV) within a specified total number of optimised geometries. This ensures an elitist behaviour of the GA in combination with good diversity in the pool. If convergence is not reached, the subprocesses start a new cycle, repeating the steps described above.

When executing the pool-GA, general runtime configuration settings are read from input files before the GA initially synchronises with the global database. The GA then enters the pool convergence loop. If the convergence criterion is not reached, the GA continues with a check for the current mode (“initial-” or “pool-mode”). As mentioned above, initial-mode means that new structures are created by randomly choosing atom coordinates inside the simulation cell while the pool-mode uses either mating or mutation operators in order to form new individuals. The new structures are then locally optimised by either passing the atom coordinates to an external *ab initio* quantum chemistry program (*e.g.* QE[53] or NWChem[54]) or one of the empirical potentials (*e.g.* Gupta) embedded in the code. This pool-based approach allows the code to be easily restarted if it runs out of CPU time. The user is left free to restart as many subprocesses as preferred, depending on the available computational resources. However, aborted local optimisations are not restarted. Instead, new subprocesses are initiated, starting with new geometries which are generated from the current pool configuration by the evolutionary principles mentioned above.

3 Results and discussion

3.1 Assessment with the Gupta potential: $Au_{10}Pd_{10}$

Here the a single pool-GA subprocess and the previous generation based GA are applied to the global optimisation of the $Au_{10}Pd_{10}$ cluster using the Gupta potential. This procedure serves as a test of the implementation before the GA is extended to the DFT-based version. Using a less expensive calculation also allows the parameter space for using the pool-GA to be classified and to show the equivalence of both implementations. However, only the parameters in which the two implementations differ substantially are tested here. For a detailed description of the BCGA code in general its functionality and settings, the reader is directed to the literature.[9]

Fig. 4 compares the pool-GA, for different pool sizes, to a random structure search. The same mutation rate is used in all calculations, with an atom exchange mutation rate of 0.5 because of homotops, beside the cluster replacement mutation adding new random structures. By applying the atom exchange mutation operator to the replacement mutation, the GA becomes considerably more efficient.[17,55] The solid lines represent averaged evolutionary progress plots from 1000 GA runs for each case. Evolutionary progress plots describe the evolution of the globally lowest-lying structure with the number of generations or optimised structures, respectively. The runs are averaged in order to test reproducibility and permit a meaningful statistical statement. Increasing the population size tends to reduce the efficiency of finding the GM. This is due to the increasing number of individuals in the pool and taking into consideration the same roulette selection scheme and parameters used in all calculations, a higher probability for selecting bad parents is to be expected when the pool size is increased. The optimum population size should be large

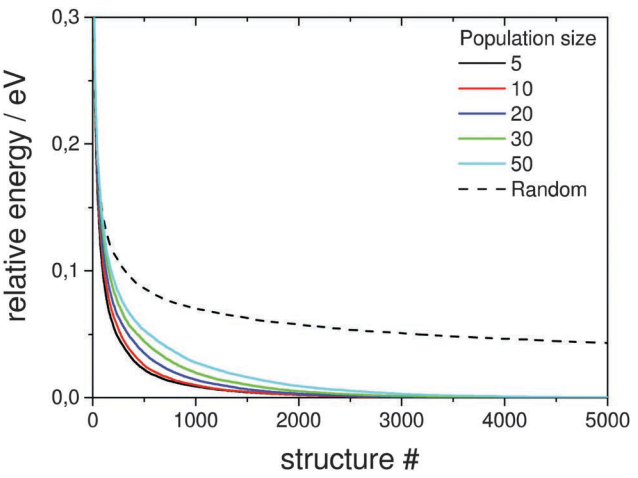

Fig. 4 Comparison of averaged evolutionary progress plots for different population sizes for a single pool-GA subprocess. A constant mutation rate of 0.2 with an atom exchange rate of 0.5 is employed. Each solid line represents the evolution of the global energetically lowest-lying structure *versus* the number of optimised structures averaged over 1000 GA runs to demonstrate reproducibility. The implementation is also compared to a random structure search as internal standard for probing the general efficiency and comparability.

enough to accommodate a high structural diversity, but small enough to remain largely elitist. A comparison to the generation-based GA, in the same way as mentioned above, shows the same behaviour and is therefore not depicted here. The random structure search, which in both cases acts as an internal standard, illustrates the high efficiency of both GA implementations in general and shows that a single pool-GA subprocess has a comparable efficiency to the generation-based GA. The pool-GA and the generation based approach compare well, as shown in Fig. 5, where both implementations are compared to a random structure search. Typically, the random search is not able to find the GM. Fig. 6 shows lognormal fits to probability densities of finding the GM after a certain number of optimised structures within the 1000 GA runs for several pool sizes. An additional plot, embedded in this figure, describes the linear scale up of the maximum number of optimisations needed *versus* the pool size. The good comparability of both GA approaches makes the pool-BCGA implementation a powerful tool for the prediction of cluster structures since many subprocesses can be run at the same time, while the convergence of the pool, using a single subprocess, compares well to the generation based code. This allows a much higher efficiency through communication of several subprocesses *via* the global database.

In order to test how the mutation rate influences both a single pool-GA subprocess and the generation based code, Fig. 7 shows averaged evolutionary progress plots where both GAs are compared for different mutation rates while using a population size of 10. The general trend is that mutation reduces the efficiency of finding the GM structure which means that mutation on average produces higher lying structures. While the pool-GA, shown in Fig. 7(a) rapidly loses efficiency with increasing mutation rate, the generational GA (Fig. 7(b)) is less influenced, which initially might appear as an unexpected result. It becomes clearer, however, if one considers, that in the pool implementation the population size is kept fixed. In the traditional BCGA the number of offspring

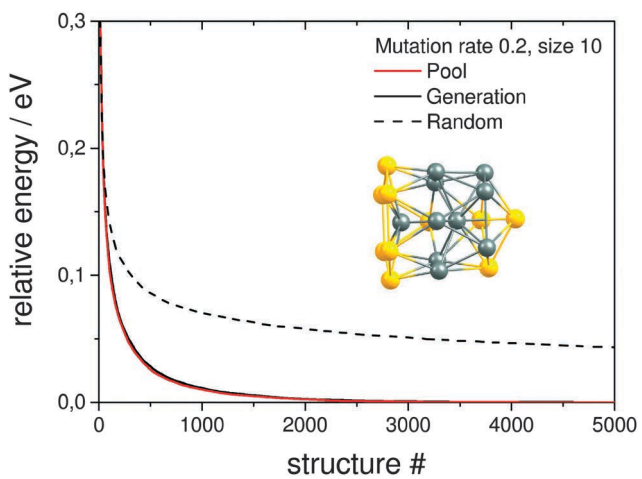

Fig. 5 Comparison of averaged evolutionary progress plots for the generation based GA and the single pool-GA for a population size of 10 using a mutation rate of 0.2 and an exchange rate of 0.5. Also included is the result of a random structure search. The GM structure of the $Au_{10}Pd_{10}$ cluster at the Gupta potential level is embedded.

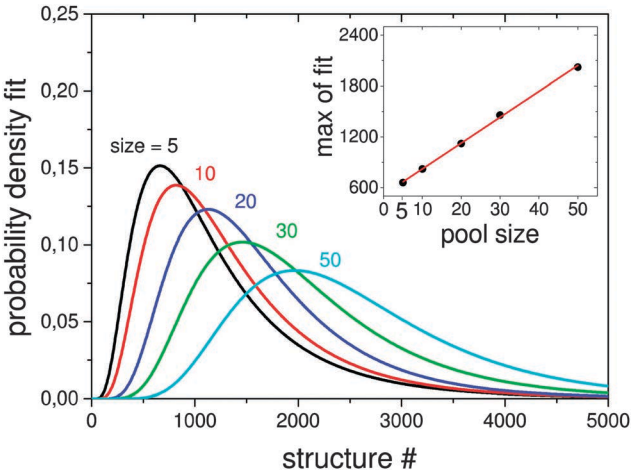

Fig. 6 Lognormal fits to probability densities of finding the GM in 1000 GA runs depending on the population size. The number of optimisations needed to find the GM scales linearly with the size as can be seen in the inset.

is, by default, 0.8 times the generation size. The mutation rate is then multiplied by the sum of the generation size and the number of offspring. For a population size of 10 and a mutation rate of 0.2, this means 8 offspring are generated from mating and 3.6 mutants on average since $(10 + 8) \times 0.2 = 3.6$. For the pool-GA, therefore, the efficiency seems to be lowered with increasing mutation rate due to the reduced mating rate which makes the implementation less elitist. However, the structural diversity in a given population can be increased by using a low mutation rate and, therefore, it should not be completely neglected. Again lognormal fits to probability densities of finding the GM after a certain number of optimised structures within 1000 GA runs, depending on the mutation rate, are shown in Fig. 8. The plot embedded in this figure shows an exponential scale up of the maximum number of optimisations needed *versus* the mutation rate. The probability densities for mutation rates larger than 0.8 could not be well fitted due to the very small efficiency of finding the GM.

3.2 Assessment with plane wave DFT

3.2.1 Au_{10}. Since the systematic global optimisation of neutral Au_n (n = 2–20) cluster structures has been reported previously using GAs coupled with DFT,[38,48] we employ this system in order to test the efficiency of the DFT based pool-GA. First, global optimisation is performed for the Au_{10} cluster using the sequential generation based DFT-BCGA program with a mutation rate of 0.1 and a population size of 10. The pool-GA is further used to perform a global optimisation of the same cluster with a pool size of 10 and a mutation rate of 0.1 in order to test whether both implementations find the GM and the same local minima. Additionally, the total number of optimised structures is compared for both cases in order to explicitly prove the parallelisation efficiency for a given example. The benchmark calculations illustrated in Fig. 9 show the total number of optimised structures for a limit of 12 hours walltime for up to 5 pool subprocesses each ideally running on 48 processors, showing

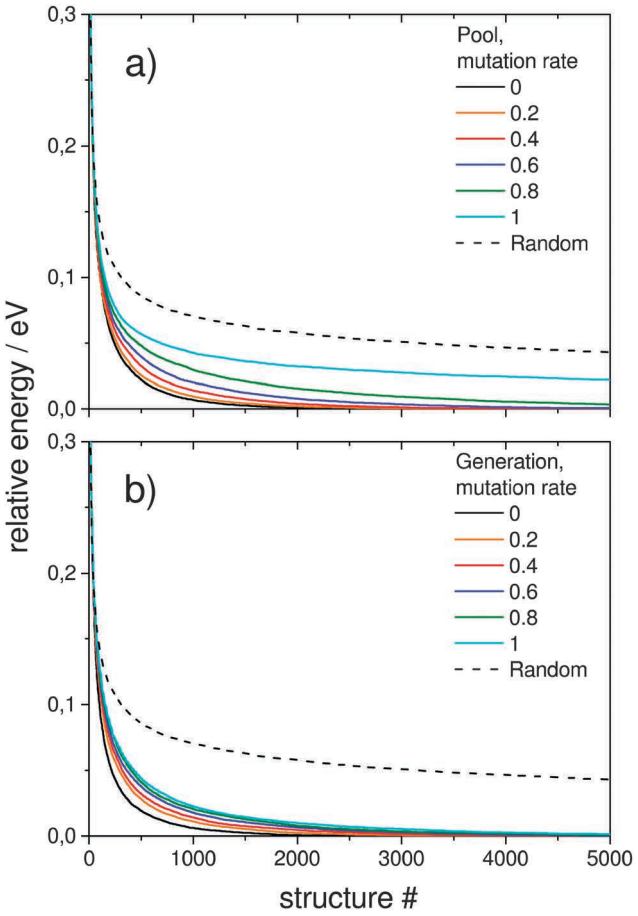

Fig. 7 Influence of the mutation rate on the averaged evolutionary progress plots averaged over 1000 GA runs for of (a) a single pool-GA subprocess and (b) the generation based GA for a constant size of 10 compared to a random structure search as an internal standard. Mutation reduces the efficiency of finding the GM.

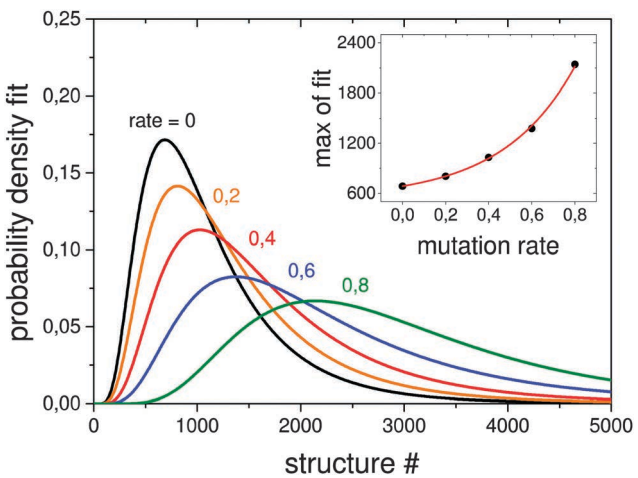

Fig. 8 Lognormal fits to probability densities of finding the GM in 1000 GA runs depending on the mutation rate. The number of optimisations needed to find the GM scales exponentially with the mutation rate as can be seen in the inset. The probability density for higher mutation rates or a random structure search cannot be well fitted due to the very small efficiency of finding the GM.

the best price-performance ratio in local relaxations (see Fig. 2). The generation based GA is also compared running on up to 240 cores, which is the same amount as in the calculations using 5 pool subprocesses. It is clear that the sequential GA plateaus when using a large number of cores due to the imperfect DFT parallelisation, while a linear scale-up in the pool-GA case is evident, when using an optimum number of cores.

The resulting structures below 0.4 eV from the predicted GM, as obtained at the pwSCF/PBE level of theory, are shown in Fig. 10. Both implementations are able to find identical local minima when optimising a comparable number of structures. The evolutionary progress plot (Fig. 11) shows an example for the pool-GA case, where the GM is found after the optimisation of about 50 structures. This number, however, varies from run to run due to the stochastic nature of the GA, which originates from constructing the initial population by producing random structures. In any case, it shows how the current best (lowest energy) solution evolves towards the planar GM isomer **10-a** with D_{2h} symmetry.

The potential lowest energy isomers below 0.4 eV, as obtained at this level of theory, including the planar GM isomer **10-a** are in agreement with the previous findings of Götz *et al.*[47] However, the trigonal prism with both triangular faces and two rectangular faces capped, suggested by Choi *et al.*,[56] has been found to lie high in energy at this level of theory, as well as all other isomers found in these previous studies. A new planar isomer **10-g**, which has been described for the Au_{10}^- cluster,[57] and a 3D structure **10-e** were also found to lie below 0.4 eV. Nevertheless, it should be mentioned that the relative energies obtained at this level of theory, using loose convergence criteria, should always be treated with care. A reminimisation of the

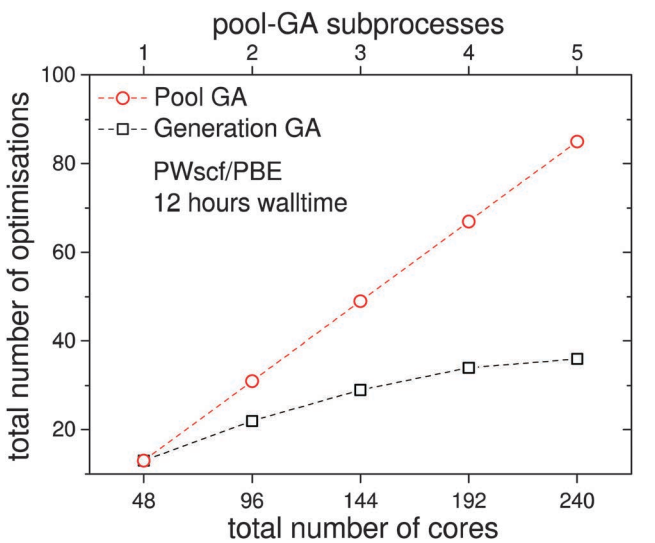

Fig. 9 Comparison of the total number of geometry optimisations from the pool-GA, with up to five subprocesses each running on 48 cores, to the generation based approach as obtained in 12 hours. A linear scale-up of the total number of optimisations is observed when several parallel working subprocesses are used on an optimum number of cores. The top horizontal axis, showing the number of subprocesses, only corresponds to the pool calculations.

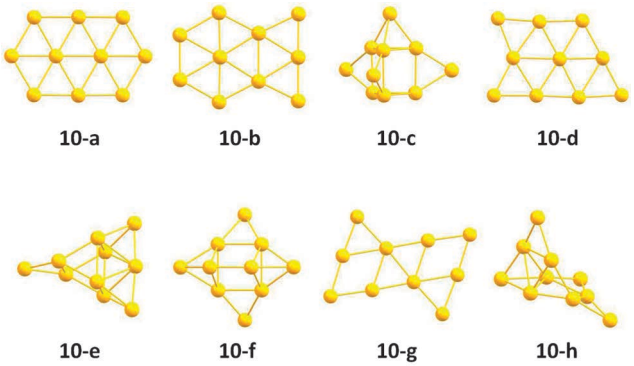

Fig. 10 Structures of Au_{10} below 0.4 eV from the predicted GM (**10-a**) as obtained from the DFT-based pool-GA global optimisation approach. The nomenclature of the individual isomers is sorted by increasing energy at the pwSCF/PBE level of theory.

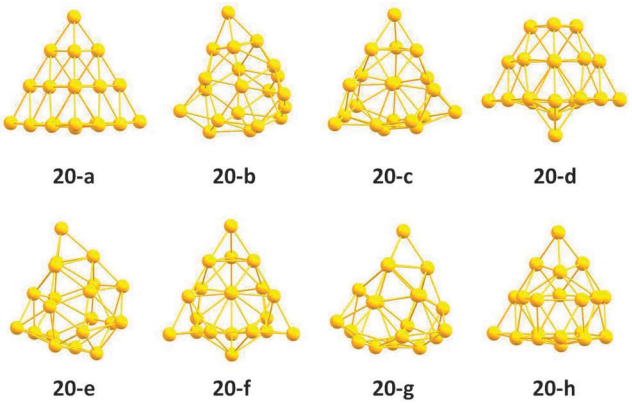

Fig. 12 Structures of Au_{20} below 0.5 eV from the predicted GM **20-a** as obtained from the generation based DFT-BCGA global optimisation approach. The nomenclature of the individual isomers is guided by the energy order at the pwSCF/PBE level of theory.

structures at a higher level of theory or the use of tighter convergence conditions can unpredictably change the energetic ordering, although **10-a** is expected to remain the GM.

The PES can be described by a sequence of local minima interconnected by transition states where monotonic sequences form funnels.[58] A given topology, once in a funnel, must eventually overcome several energy barriers in order to reach the GM or another specific local minimum as the PES is explored. This means that a given local optimisation within a GA optimisation task could potentially relax into a so-called metabasin with small geometrical deviation from the minimum. Therefore energetic discrepancies should not only be discussed as depending on the xc functional and pseudopotentials used, but should also be attributed to the cases where local optimisations end in metabasins near a local minimum, leading to an apparently wrong energy ordering.

However, this should not be interpreted as a problem. Genetic algorithms used in this manner can be thought of as a coarse grain filter. The idea is to reduce a large configuration space to a manageable size. The reduced configurational space

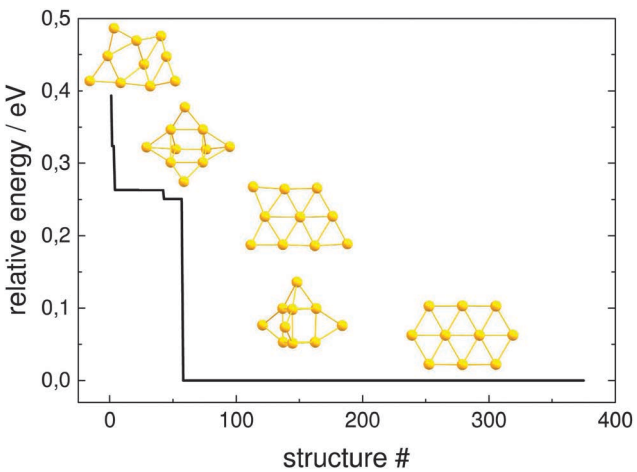

Fig. 11 Evolution of the globally lowest-lying isomer for Au_{10} with the number of optimised structures within a pool-GA run, relative to the energy E_0 of the GM isomer **10-a**. Each step represents a new global minimum depicted here within the pool-GA run.

then opens up the possibility of a more detailed description of only a few isomers at a higher level of theoretical complexity, often required for the description of binary clusters in combination with experiments.

3.2.2 Au_{20}. The ability of the pool-GA to scale linearly with the number of processors is shown in Fig. 9. This allows the global optimisation of cluster structures, directly at the pwSCF/PBE level, for clusters larger than previously possible with the sequential GA in a reasonable time. The pool-GA is used to perform a global optimisation on the Au_{20} cluster. Calculations were performed with a pool size of 10 and a mutation rate of 0.1. The tetrahedral structure (T_d) of Au_{20} is well known and has been shown previously by both theory,[38,39,48] and experiment.[36,37]

The structures of the putative pool-GA GM and minima lying below 0.5 eV are shown in Fig. 12. The pool-GA successfully finds the tetrahedral structure, **20-a**, as the GM. The tetrahedron is first found after the optimisation of only 56 structures. There is a large gap between the GM and the next lowest-lying structure, a distorted geometry with C_1 symmetry. Structures similar to **20-b** are seen in minima **20-e** and **20-g**, while structures **20-c**, **20-f** and **20-h** are C_1 geometries based on more subtle distortions of the tetrahedron.

4 Conclusions

We have demonstrated the efficiency of the new pool-based parallel implementation of the BCGA. The new implementation leads to a greater efficiency for the global optimisation of monoatomic or binary clusters. The change in implementation makes the approach efficient for an arbitrary numbers of parallel processes, as shown by the benchmark calculations. In addition, the pool-BCGA can also adapt to the given utilisation of a given high-performance computer, as it supports different numbers of processors in order to achieve maximum efficiency. Since processor speed is generally starting to plateau, it will be more and more appropriate to develop better parallel algorithms suitable for future computer architectures. The pool-BCGA is a

good example of how this can be done efficiently. Additionally, the use of distributed computing architectures (*e.g.* BOINC) would be now enabled where server could potentially manage the pool while optimisations can be run on an arbitrary number of clients. Since the amount of data transferred between server and clients is small, bandwidth requirements would be minimal.

By replacing the sequential working generation concept, serial bottlenecks are eliminated. A typical pool calculation can be started as a job array of several pool-GA subprocesses enabling the treatment of larger cluster sizes than previously studied or even opens up the possibility of using a higher level of theory. Alternatively, one can think about using wavefunction based methods in geometry relaxations for the global optimisation of small cluster systems as implemented in program packages such as CFOUR,[59] or NWChem v6.3,[54] which enable geometry optimisations based on coupled cluster methods. Such a pool implementation would emerge as the method of choice, especially in this sophisticated task of performing global optimisation using multi-electron wavefunctions to account for electron correlation with higher accuracy.

Also the very recently developed S-BCGA could be improved by using the flexible pool concept, which would allow the study of more complicated supported clusters, such as larger clusters and nanoalloys, and permit calculations at a higher level of theory.

A comparison of the results obtained by the generation- and pool-based BCGA show that the pool-GA is finally able to find all isomers predicted by the generation based implementation while both GAs give results in good agreement with existing global optimisation calculations reported in the literature.

Acknowledgements

The calculations reported here have been performed on the following HPC facilities: The University of Birmingham BlueBEAR facility (ref. 60); the MidPlus Regional Centre of Excellence for Computational Science, Engineering and Mathematics, funded under EPSRC grant EP/K000128/1 (R. L. J.); and *via* our membership of the UK's HPC Materials Chemistry Consortium funded under EPSRC grant EP/F067496 (R. L. J.). A. S. and R. S. acknowledge financial support by the DFG (grant SCHA 885/10-2) and the Merck'sche Gesellschaft für Kunst und Wissenschaft e.V. We are thankful to group members and collaborators, past and present, for their contributions to this research, particularly in the area of global optimisation. In terms of the development and testing of the DFT based BCGA code, special thanks are extended to Christopher Heard (Chalmers University, Gothenburg) and Sven Heiles (Justus-Liebig-Universität, Gießen).

References

1 W. A. de Heer, *Rev. Mod. Phys.*, 1993, **65**, 611–676.
2 F. Cleri and V. Rosato, *Phys. Rev. B: Condens. Matter Mater. Phys.*, 1991, **48**, 22–33.
3 A. P. Sutton and J. Chen, *Philos. Mag. Lett.*, 1990, **61**, 139–146.
4 J. N. Murrell and R. E. Mottram, *Mol. Phys.*, 1990, **69**, 571–585.
5 R. Ferrando, J. Jellinek and R. L. Johnston, *Chem. Rev.*, 2008, **108**, 845–910.
6 J. Jellinek and E. B. Krissinel, *Chem. Phys. Lett.*, 1996, **4**, 283–292.
7 R. Ferrando, A. Fortunelli and R. L. Johnston, *Phys. Chem. Chem. Phys.*, 2008, **10**, 640–649.
8 J. Jellinek and E. B. Krissinel, *Theory of Atomic and Molecular Clusters*, Springer, Berlin, 1999, p. 277.
9 R. L. Johnston, *Dalton Trans.*, 2003, 4193–4207.
10 S. Heiles, A. J. Logsdail, R. Schäfer and R. L. Johnston, *Nanoscale*, 2012, **4**, 1109–1115.
11 S. Heiles, R. L. Johnston and R. Schäfer, *J. Phys. Chem. A*, 2012, **116**, 7756–7764.
12 D. A. Götz, S. Heiles, R. L. Johnston and R. Schäfer, *J. Chem. Phys.*, 2012, **136**, 186101.
13 A. Bruma, R. Ismail, L. O. Paz-Borbón, H. Arslan, G. Barcaro, A. Fortunelli, Z. Y. Li and R. L. Johnston, *Nanoscale*, 2013, **5**, 646–652.
14 G. Kwon, G. A. Ferguson, C. J. Heard, E. C. Tyo, C. Yin, J. DeBartolo, S. Seifert, R. E. Winans, A. J. Kropf, J. Greeley, R. L. Johnston, L. A. Curtiss, M. J. Pellin and S. Vajda, *ACS Nano*, 2013, **7**, 5808–5817.
15 A. Shayeghi, C. J. Heard, R. L. Johnston and R. Schäfer, *J. Chem. Phys.*, 2014, **140**, 054312.
16 D. A. Götz, A. Shayeghi, R. L. Johnston, P. Schwerdtfeger and R. Schäfer, *J. Chem. Phys.*, 2014, **140**, 164313.
17 S. Heiles and R. L. Johnston, *Int. J. Quantum Chem.*, 2013, **113**, 2091–2109.
18 G. Rossi and R. Ferrando, *J. Phys.: Condens. Matter*, 2009, **21**, 084208.
19 B. Hartke, *J. Phys. Chem.*, 1993, **97**, 9973–9976.
20 Y. Xiao and D. E. Williams, *Chem. Phys. Lett.*, 1993, **215**, 17–24.
21 B. Hartke, *Chem. Phys. Lett.*, 1996, **258**, 144–148.
22 B. Hartke, H.-J. Flad and D. Michael, *Phys. Chem. Chem. Phys.*, 2001, **3**, 5121–5129.
23 B. Hartke, *Phys. Chem. Chem. Phys.*, 2003, **5**, 275–284.
24 Y. Zeiri, *Phys. Rev. E*, 1995, **51**, 2769.
25 D. M. Deaven and K. M. Ho, *Phys. Rev. Lett.*, 1995, **75**, 288–291.
26 D. J. Wales and J. P. K. Doye, *J. Phys. Chem. A*, 1997, **101**, 5111–5116.
27 J. M. Dieterich and B. Hartke, *Mol. Phys.*, 2010, **108**, 279–291.
28 M. Sierka, *Prog. Surf. Sci.*, 2010, **85**, 398–434.
29 K. Kwapien, M. Sierka, J. Döbler, J. Sauer, M. Haertelt, A. Fielicke and G. Meijer, *Angew. Chem.*, 2011, **50**, 1716–1719.
30 A. N. Alexandrova, A. I. Boldyrev, Y.-J. Fu, X. Yang, X.-B. Wang and L.-S. Wang, *J. Chem. Phys.*, 2004, **121**, 5709–5718.
31 A. N. Alexandrova and A. I. Boldyrev, *J. Chem. Theory Comput.*, 2005, **1**, 566–580.
32 C. J. Heard, S. Heiles, S. Vajda and R. L. Johnston, *Nanoscale*, 2014, 54–57.
33 L. B. Vilhelmsen and B. Hammer, *J. Chem. Phys.*, 2014, **141**, 044711.

34 F. Weigend, *J. Chem. Phys.*, 2014, **141**, 134103.
35 B. Bandow and B. Hartke, *J. Phys. Chem. A*, 2006, **110**, 5809–5822.
36 J. Li, X. Li, H.-J. Zhai and L.-S. Wang, *Science*, 2003, **299**, 864–867.
37 P. Gruene, D. M. Rayner, B. Redlich, A. F. G. van der Meer, J. T. Lyon, G. Meijer and A. Fielicke, *Science*, 2008, **321**, 674–676.
38 B. Assadollahzadeh and P. Schwerdtfeger, *J. Chem. Phys.*, 2009, **131**, 064306.
39 E. Aprá, R. Ferrando and A. Fortunelli, *Phys. Rev. B: Condens. Matter Mater. Phys.*, 2006, **73**, 205414.
40 Y. Ge and J. D. Head, *Chem. Phys. Lett.*, 2004, **398**, 107–112.
41 E. Cantu-Paz, *Efficient and Accurate Parallel Genetic Algorithms*, Kluwer Academic Publishers, Boston, 2001.
42 A. N. Alexandrova, *J. Phys. Chem. A*, 2010, **114**, 12591–12599.
43 K. Doll, J. C. Schön and M. Jansen, *J. Chem. Phys.*, 2010, **133**, 024107.
44 B. Hartke, *Wiley Interdiscip. Rev.: Comput. Mol. Sci.*, 2011, **1**, 879–887.
45 M. Chen, D. Kumar, C.-W. Yi and D. W. Goodman, *Science*, 2005, **310**, 291–293.
46 A. V. Walker, *J. Chem. Phys.*, 2005, **122**, 094310.
47 D. A. Götz, R. Schäfer and P. Schwerdtfeger, *J. Comput. Chem.*, 2013, **34**, 1–7.
48 J. Wang, G. Wang and J. Zhao, *Phys. Rev. B: Condens. Matter Mater. Phys.*, 2002, **66**, 035418.
49 R. Ismail and R. L. Johnston, *Phys. Chem. Chem. Phys.*, 2010, **12**, 8607–8619.
50 J. Perdew, K. Burke and M. Ernzerhof, *Phys. Rev. Lett.*, 1996, **77**, 3865–3868.
51 A. M. Rappe, K. M. Rabe, E. Kaxiras and J. D. Joannopoulos, *Phys. Rev. B: Condens. Matter Mater. Phys.*, 1990, **41**, 1227–1230.
52 M. Methfessel and A. T. Paxton, *Phys. Rev. B: Condens. Matter Mater. Phys.*, 1989, **40**, 3616–3621.
53 P. Giannozzi, S. Baroni, N. Bonini, M. Calandra, R. Car, C. Cavazzoni, D. Ceresoli, G. L. Chiarotti, M. Cococcioni, I. Dabo, A. Dal Corso, S. de Gironcoli, S. Fabris, G. Fratesi, R. Gebauer, U. Gerstmann, C. Gougoussis, A. Kokalj, M. Lazzeri, L. Martin-Samos, N. Marzari, F. Mauri, R. Mazzarello, S. Paolini, A. Pasquarello, L. Paulatto, C. Sbraccia, S. Scandolo, G. Sclauzero, A. P. Seitsonen, A. Smogunov, P. Umari and R. M. Wentzcovitch, *J. Phys.: Condens. Matter*, 2009, **21**, 395502.
54 M. Valiev, E. J. Bylaska, N. Govind, K. Kowalski, T. P. Straatsma, H. J. J. Van Dam, D. Wang, J. Nieplocha, E. Apra, T. L. Windus and W. A. de Jong, *Comput. Phys. Commun.*, 2010, **181**, 1477–1489.
55 S. Darby, T. V. Mortimer-Jones, R. L. Johnston and C. Roberts, *J. Chem. Phys.*, 2002, **116**, 1536–1550.
56 Y. C. Choi, W. Y. Kim, H. M. Lee and K. S. Kim, *J. Chem. Theory Comput.*, 2009, **5**, 1216–1223.
57 F. Furche, R. Ahlrichs, P. Weis, C. Jacob, S. Gilb, T. Bierweiler and M. M. Kappes, *J. Chem. Phys.*, 2002, **117**, 6982–6990.
58 R. E. Kunz and R. S. Berry, *J. Chem. Phys.*, 1995, **103**, 1904–1912.
59 M. E. Harding, T. Metzroth and J. Gauss, *J. Chem. Theory Comput.*, 2008, **4**, 64–74.
60 See http://www.bear.bham.ac.uk/bluebear for a description of the BlueBEAR HPC facility.

5.3 Publication 6

Title

The Birmingham Parallel Genetic Algorithm and its application to the direct DFT global optimisation of Ir_N $(N = 10 - 20)$ clusters.

Authors

Jack B. A. Davis, Armin Shayeghi, Sarah L Horswell and Roy L Johnston

Journal Nanoscale

Volume 7

Pages 14032-14038

DOI 10.1039/C5NR03774C

Submitted

8th June 2015

Accepted

17th July 2015

Nanoscale

PAPER

Cite this: *Nanoscale*, 2015, **7**, 14032

The Birmingham parallel genetic algorithm and its application to the direct DFT global optimisation of Ir_N (N = 10–20) clusters†

Jack B. A. Davis,*[a] Armin Shayeghi,[b] Sarah L. Horswell[a] and Roy L. Johnston*[a]

Received 8th June 2015,
Accepted 17th July 2015

DOI: 10.1039/c5nr03774c

www.rsc.org/nanoscale

A new open-source parallel genetic algorithm, the Birmingham parallel genetic algorithm, is introduced for the direct density functional theory global optimisation of metallic nanoparticles. The program utilises a pool genetic algorithm methodology for the efficient use of massively parallel computational resources. The scaling capability of the Birmingham parallel genetic algorithm is demonstrated through its application to the global optimisation of iridium clusters with 10 to 20 atoms, a catalytically important system with interesting size-specific effects. This is the first study of its type on Iridium clusters of this size and the parallel algorithm is shown to be capable of scaling beyond previous size restrictions and accurately characterising the structures of these larger system sizes. By globally optimising the system directly at the density functional level of theory, the code captures the cubic structures commonly found in sub-nanometre sized Ir clusters.

1. Introduction

Nanosized materials are currently being investigated for potential use in a variety of applications. This is because the nanosizing effects seen in such materials result in properties different from those of the bulk material. These properties can also be tuned, normally through altering the size and shape of the cluster.

Metallic nanoparticles are such materials, with potential optical, magnetic and catalytic applications.[1] Small Ir nanoparticles, in particular, are currently used as catalysts for a range of organic reactions, including olefin hydrogenation, oligomerisation, and ring-opening of cycloalkanes.[2] Ir has been shown both experimentally[3] and theoretically[4] to exhibit significant nanosize-induced hydrogen adsorption capacity. Larger Ir nanoparticles have been shown to be active in C–C bond hydrogenolysis.[5] Selective molecular recognition has also been seen in supported Ir cluster-based catalysts.[6]

A key step in rationalising properties, such as the catalytic activity of nanoparticles, is their structural characterisation. To achieve this it is necessary to sample comprehensively the potential energy landscape (PES) of the nanoparticle. A wide variety of methods is available for the exploration of the PES. These methods include statistical mechanical methods, such as the CBEV/FCEM method,[7,8] basin-hopping methods,[9] such as GMIN,[10] and genetic algorithms, such as the Birmingham cluster genetic algorithm (BCGA).[11] The choice of method largely depends on the size and complexity of the system.

It is necessary to decide the level of theory required to replicate accurately a particular PES of a system. For example, the electronic structure of larger nanoparticles is thought to resemble closely that of the bulk material. This means the use of empirical potentials, such as the Gupta potential,[12] is suitable for the accurate representation of the PES. Statistical mechanical methods, such as CBEV/FCEM, may be best suited to these larger systems.[8] However, for smaller, sub-nanometre clusters a much more computationally demanding quantum mechanical description of the cluster PES is necessary as quantum-size effects, such as spin–orbit coupling, tend to dominate.[13–15] A variety of methods has been developed to achieve this, many of which have been outlined by Heiles and Johnston.[16]

The cubic structures adopted by sub-nanometre Ir clusters have been previously shown up to the CCSD(T) level of theory,[17–24] differing from the *fcc* structure of the bulk material. It is therefore vital that any global optimisation of Ir_N (N = 10–20) structures is performed directly at the density functional theory (DFT) level of theory at least.

A quantum description of the PES greatly increases the cost of exploring it comprehensively, limiting the size of the cluster it is possible to investigate.[16] It is therefore necessary that

[a]*School of Chemistry, University of Birmingham, Birmingham, B15 2TT, UK. E-mail: jbad90@gmail.com, r.l.johnston@bham.ac.uk; Tel: +44 (0)1214 147477*
[b]*Eduard-Zintl-Institut, Technische Universität Darmstadt, Alarich-Weiss-Straße 8, 64287 Darmstadt, Germany. E-mail: shayeghi@cluster.pc.chemie.tu-darmstadt.de*
†Electronic supplementary information (ESI) available. See DOI: 10.1039/C5NR03774C

efficient parallel methodologies, with the ability to utilise greater computational resources, are developed. There have been several implementations of parallel schemes within genetic algorithms for both atomic and molecular clusters but few combine this parallelism with direct DFT global optimisation.[25–29]

This work presents the global optimisation of Ir_N (N = 10–20) clusters directly at the DFT level of theory. This is achieved using the Birmingham parallel genetic algorithm (BPGA), a new open-source genetic algorithm available *via* Bitbucket.[30] The BPGA utilises a pool genetic algorithm methodology combined with the evaluation of potential cluster geometries in parallel.[25] This combination ensures highly efficient scaling when compared with generation based genetic algorithms and allows the structural characterisation of larger and more complex systems. The pool methodology has been recently applied to metallic clusters[31] and was benchmarked and applied successfully to the global optimisation of the much studied Au_{10} and Au_{20} clusters.[31] Its predictions for Ag_{10}^{+} have also been shown to be accurate when compared with spectra from molecular beam experiments.[32] The BPGA incorporates this highly efficient algorithm within a flexible Python framework.

Due to the $5d^76s^2$ ground state and other low lying states originating from its $5d^86s^1$ configuration,[33] the spin of the Ir_N clusters must be considered in the calculations.[33] To account for this, spin-polarised DFT global optimisations are performed. The use of spin-polarised local minimisations effectively doubles the computational cost and can only now be performed due to the parallelism of the BPGA.

The BPGA is also capable of globally optimising bimetallic nanoalloys, whose PES is complicated by the presence of homotops.[34] It is hoped that this work demonstrates that scaling capability of the BPGA and its ability to utilise massively parallel architectures, which enable the program to predict accurately the geometries of metallic nanoparticles.

2. Methodology

2.1. Birmingham parallel genetic algorithm

The BPGA is a parallel genetic algorithm for the structural characterisation of nanoparticles. The program is written in object-oriented Python. This allows greater flexibility and the ability to utilise the large existing libraries of Python code, such as the atomic simulation environment.[35] Python is well suited to job submission, required by the DFT interface, on a large shared HPC resource, such as ARCHER.[36] The program is open-source and available *via* BitBucket.[30]

The BPGA utilises a pool methodology, shown in Fig. 1.[25,31] This differs from a generation-based code, where structures belong to and are evaluated generation by generation. When executed in parallel, multiple instances of the BPGA are started sequentially within a run. Each instance is a separate BPGA run with its own set of processes. The BPGA initially generates a fixed-size pool of n random geometries and places

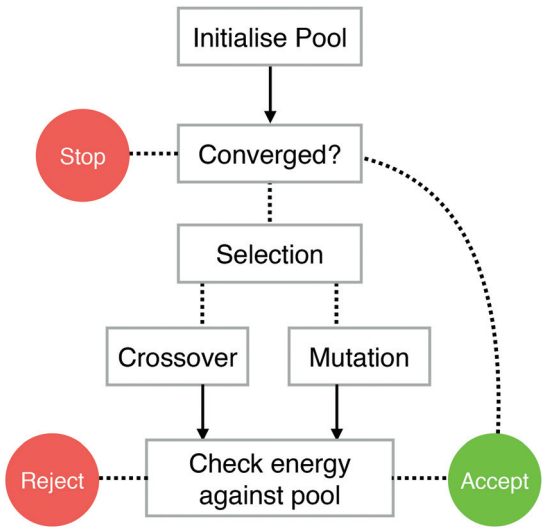

Fig. 1 The pool scheme used by the BPGA. Arrows represent DFT local minimisations.

them in a central database file which is available to the other instances of the program. In the present study the pool is set to n = 15 random geometries. These initial geometries are fixed so that no two atoms are overlapping.

In the local minimisation the energy of a structure is minimised with respect to its coordinates. This transforms the PES into a simpler stepped surface, greatly reducing the search space. If an instance becomes free and all structures in the pool are being or have been minimised the instance will continue to evaluate further random structures. If one of these new structures is lower in energy than the highest energy cluster in the pool, the new lower energy structure will replace it.

Once the initial pool of structures has been minimised, offspring and mutants are produced through crossover and mutation. The choice of producing either an offspring or mutant is based on the mutation rate, which is set to anywhere between 0–100% of the fixed pool size. In the present work the mutation rate is set to 10%.

Mutation is defined as the selection of a cluster at random from the pool and the displacement of two of its atoms by up to 1 Å. Other mutations schemes are available in the code, including generating a new random geometry or, for bimetallic systems, swapping unlike atoms.

Selection for crossover is carried out using the tournament method. Once selected, clusters undergo crossover according to the Deaven and Ho cut and splice method.[37] The cutting plane is weighted based on the fitness of each of the clusters selected. A higher fitness represents a lower energy.

A local minimisation of the offspring is performed and its energy is checked against those of the other structures in the pool. If the offspring's energy is lower than that of the highest energy structure in the pool, the offspring structure replaces it. Convergence is achieved when the energies of the structures in

the pool differ by no less than 10^{-3} eV. For larger clusters, convergence may not be achievable. In this case the lowest energy structure in the pool after a run of around 500 separate minimisations is taken as the putative global minimum.

The BPGA also has the ability to perform a DFT-level global optimisation of a cluster supported on a surface. This method, within a generation based code, has been demonstrated previously.[38]

2.2. DFT

Gamma-point, spin-polarised DFT calculations were performed with VASP.[39–43] Projected-augmented wave (PAW) pseudopotentials were used with the PBE exchange correlation functional.[44,45] A plane-wave basis set with a cut-off of 400 eV was used. Methfessel–Paxton smearing, with a sigma value of 0.01 eV, was utilised to improve metallic convergence.[46]

2.3. Energetics

The binding energies per atom were calculated using

$$E_b = \frac{1}{N}(E_{Ir_N} - NE_{Ir}), \quad (1)$$

where N is the total number of atoms, E_{Ir_N} is total energy of an N-atom Ir cluster and E_{Ir} is the energy of a spin-polarised Ir atom.

The stability of the clusters, relative to their $N+1$ and $N-1$ neighbours, is given by their second-order differences $\Delta^2 E$, calculated using

$$\Delta^2 E = 2E_{Ir_N} - (E_{Ir_{N+1}} + E_{Ir_{N-1}}). \quad (2)$$

3. Results

The BPGA calculations were performed on the UK's national supercomputer ARCHER.[36] Each was run in parallel with eight instances of the code operating on the pool. The theoretical scaling of this parallel pool methodology has been shown previously.[31] Around 500 structures were evaluated for each cluster size. Due to the high computational cost of the calculations multiple runs are not possible for each system size.

The parallelism within the code, and the scaling capabilities of VASP on ARCHER, allows for spin-polarised calculations to be carried out during the global optimisation. The binding energies E_b, point groups and spin multiplicities of the putative global minimum are given in Table 1. The coordinates of the global minima and the additional minima discussed are supplied in the ESI.†

Overall, the putative global minima from the BPGA searches are in good agreement with structures suggested in previous work on Ir clusters.[18,21–23] Some structures have been previously characterised and give a good indication of the ability of the BPGA to find the putative global minimum at a given level of theory. Other structures are reported here for the first time.

Table 1 Binding energies E_b, point groups and multiplicities ($2S+1$) for the putative global minimum of Ir_N (N = 10–20) clusters

Cluster	Point group	E_b/eV	$(2S+1)$
Ir_{10}	C_s	−4.914	3
Ir_{11}	C_1	−4.932	4
Ir_{12}	D_{4h}	−5.172	3
Ir_{13}	C_s	−5.139	4
Ir_{14}	C_s	−5.220	3
Ir_{15}	C_{2v}	−5.206	2
Ir_{16}	C_s	−5.301	3
Ir_{17}	C_s	−5.348	4
Ir_{18}	D_{4h}	−5.452	7
Ir_{19}	C_1	−5.416	2
Ir_{20}	C_1	−5.436	3

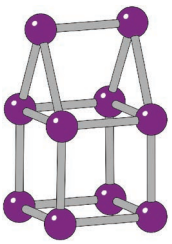

Ir_{10}

Fig. 2 The dimer-capped ("house") structure of Ir_{10}.

The BPGA successfully finds the C_{2v} dimer-capped ("house") structure, shown in Fig. 2, as the putative global minimum for Ir_{10} and scales successfully well beyond this previous 10-atom limit. The putative global minimum structures of Ir_N (N = 11–20) clusters are shown in Fig. 3.

The overall global minimum structure for Ir_{11} is a triangle-capped cube. This structure, together with a second highly competitive low lying minimum, an edge-bridged structure based on the Ir_{10} "house", are shown in Fig. 4. The two structures differ by 0.05 eV. The global minimum structure is a high spin structure with a spin multiplicity of 4, compared with the competitive minimum's multiplicity of 2. The spin polarised DFT global optimisation has allowed this lower energy putative global minimum to be reported for the first time.

The additional Ir in Ir_{12} now makes it possible to complete a third cubic face and the 3 × 2 × 2 D_{2h} cuboid structure becomes the global minimum. For Ir_{13} the extra Ir bridges an edge on one of the cubes.

It was thought that the global minimum structure for Ir_{13} may be a C_{4v} structure, with an Ir atom capping an end of the cuboid, and that the cubic bounding cell used to generate the initial random geometries may have biased the search against any elongated structures. Local minimisations were carried out on C_{2v} centre edge-bridged, C_s top edge-bridged and C_{4v} top-capped cuboid structures, shown in Fig. 5. The C_{2v} centre edge-bridged structure locally minimises into a face-capped C_s structure. The structures were found to lie 0.26, 0.33 and 0.97

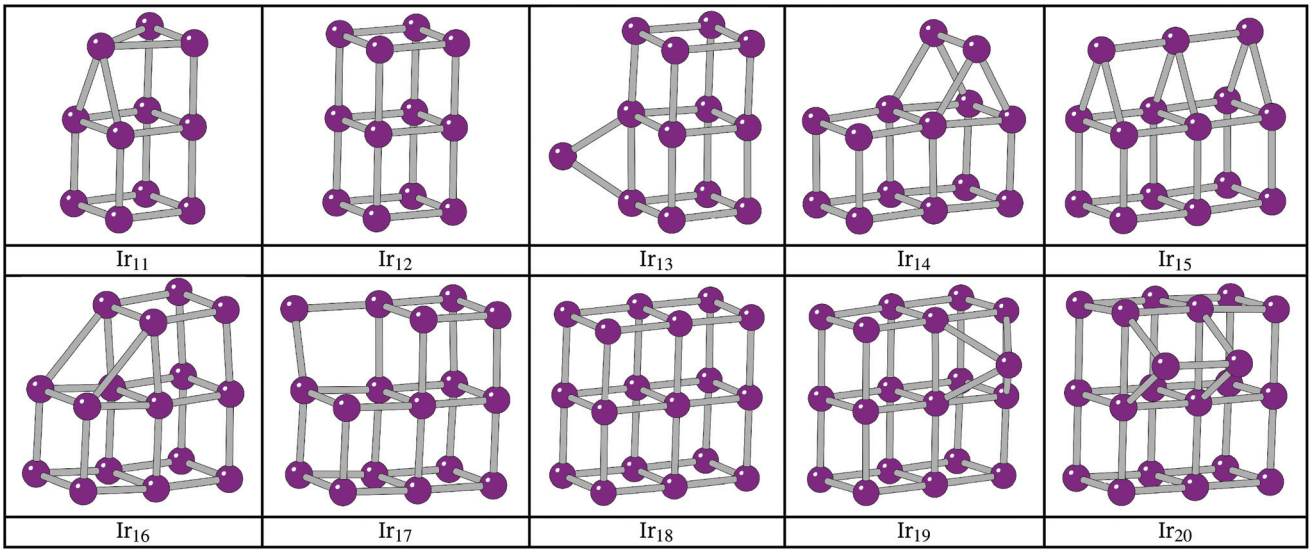

Fig. 3 Putative global minimum structures for Ir_N (N = 10–20) from the BPGA searches.

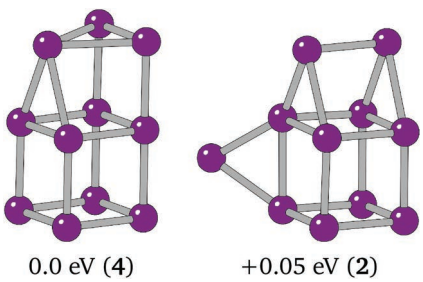

Fig. 4 Putative global minimum (left) and competitive low-lying minima (right). Relative energies and spin multiplicities (in brackets) are shown below.

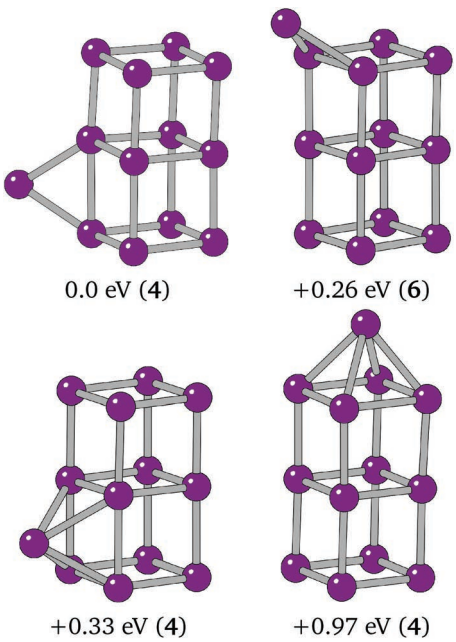

Fig. 5 Global minimum (top-left), top edge-bridged (top-right), centre edge-bridged (bottom-left) and top-capped (bottom-right) cubic structures assessed for Ir_{13}. The centre edge-bridged structure is shown after local minimisation to the face-capped cuboid structure.

eV higher in energy than the putative global minimum structure from the BPGA search, respectively. This structural preference is also confirmed by previous work on Ir_{13}.[19,20]

The structure of Ir_{14} is a dimer-capped 3 × 2 × 2 cuboid, analogous to the Ir_{10} structure with the dimer lying perpendicular to the long edges of the Ir_{12} cuboid structure. This structure has been previously shown.[21] Upon addition of an extra Ir, the structure of Ir_{15} becomes a trimer-capped cuboid, with the Ir_3 trimer lying parallel to the long sides of the rectangular face.

The preference of Ir_{16} is shown to be a slightly deformed L-shaped cubic structure, so that two elongated 3.1 Å bonds can form between two cubes of the structure. Cubic bounding may also have affected Ir_{16}, as it follows from the structure of Ir_8, a cube, and Ir_{12} that the global minimum could be a 4 × 1 × 1 cuboid. This structure was assessed alongside two other low-lying minima, T-capped and square-capped cuboid structures. The structures and relative energies of these minima are shown in Fig. 6, with the 4 × 1 × 1 cuboid found to lie 0.88 eV higher in energy than the BPGA global minimum.

The structure of Ir_{17} shows the additional Ir in between two cubes of the Ir_{16} cuboid, the start of a complete 3 × 3 × 2 cuboid. The additional Ir of Ir_{18} sits between two cubes of the L-shaped Ir_{17} cluster and forms the complete 3 × 3 × 2 cuboid.

The extra Ir in Ir_{19} caps a cubic face on the 3 × 3 × 2 cuboid. This putative global minimum was tested against an edge-bridged structure, which was believed to be the more likely global minimum structure following the trend seen in smaller

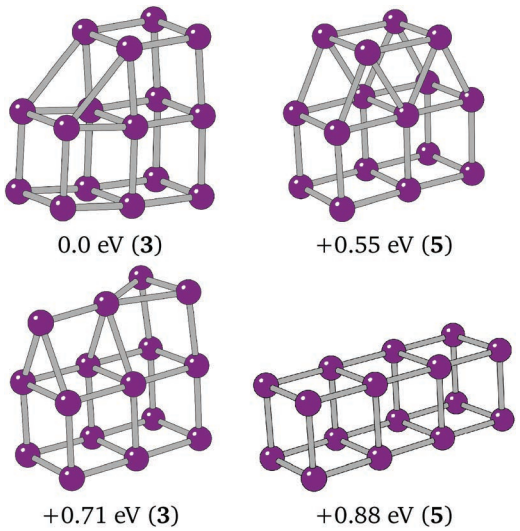

Fig. 6 Putative global minimum (top-left), 4 × 1 × 1 cuboid, T-capped and square capped 3 × 1 × 1 cubic structures assessed for Ir_{16}.

clusters. The C_1 edge-bridged structure, shown in Fig. 7, was found to have a spin multiplicity of 6 and to be just 0.008 eV lower in energy than the BPGA global minimum.

The energetic differences between the low lying minima of Ir_{11} and Ir_{19} are far smaller than that seen for the various Ir_{13} minima and smaller than the error in the current DFT calculations. To determine accurately the global minimum, higher level calculations, coupled with experiment, will be required in the future.

The structure of Ir_{20} is analogous to that of Ir_{13} with an Ir_2 dimer lying perpendicular to the long edges of the 3 × 3 × 2 cuboid structure.

The binding energies of the clusters give an indication of the relative stability of the clusters, with more negative values indicating greater stability. E_b values are shown in Fig. 8. Overall, E_b tends to decrease as N increases, with Ir_{18} having the lowest E_b.

For several N-atom clusters E_b is higher (less stable) than for the $N - 1$ cluster: in particular Ir_{13}, Ir_{15} and Ir_{19}. Ir_{20}, despite Ir forming a dimer capping a face, has a higher E_b than Ir_{18}. The increased stability displayed by the even numbered clusters is more clearly shown by their second-order difference plot shown in Fig. 9. Each odd numbered cluster clearly shows decreased stability, indicated by a positive Δ^2E, relative to its even numbered neighbours.

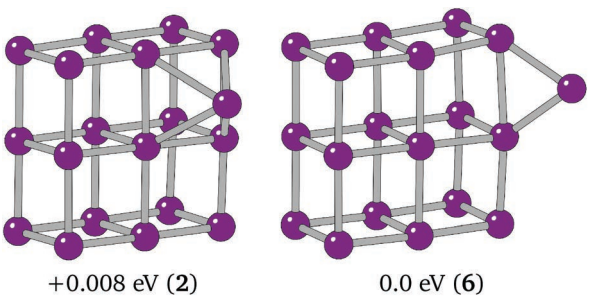

Fig. 7 Putative global minimum (left) and edge-bridged cuboid structure for Ir_{19}.

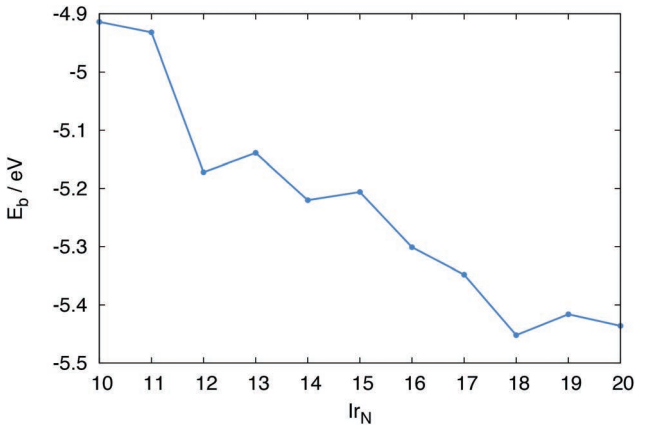

Fig. 8 Binding energies E_b, for Ir_N (N = 10–20) clusters.

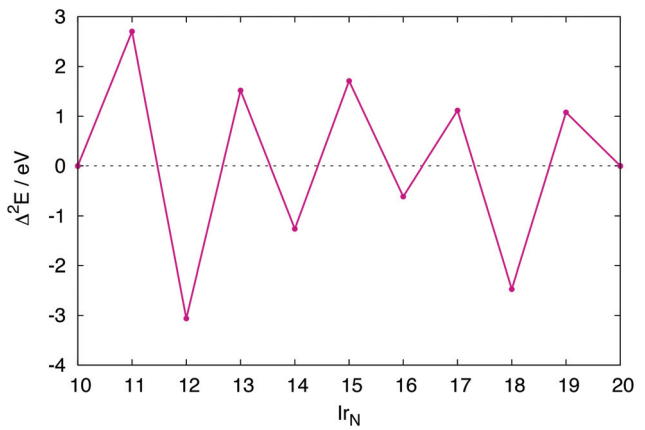

Fig. 9 Second-order differences Δ^2E, for Ir_N (N = 10–20) clusters.

The spin multiplicities of the clusters are given in Table 1. All global minima are found to have multiplicities of between 2 and 7. This is a clear indication of the importance of magnetic effects in these clusters. In particular, high spin structures are shown to be the global minimum structures of Ir_{11} and Ir_{19}. It is likely that these and other low energy minima would have been excluded from the searches if non-spin-polarized calculations had been carried out.

4. Conclusions

The BPGA has successfully coupled the computation resources of ARCHER[36] with the scaling capability of a pool genetic algorithm methodology. This has allowed the direct DFT global optimisation of Ir_N (N = 10–20) clusters, with some

global minimum structures being reported here for the first time.

The code has captured the cubic nature of the sub-nanometre Ir clusters with the putative global minima evaluated and compared with previous results. For Ir_{11} and Ir_{19} their spin has been shown to determine their global minimum structures, which would have otherwise been missed in a low-spin search. The use of spin polarized calculations has been made possible because of the BPGA's ability to utilise greater computational resources. The structural characterisation of a system is a vital first step in exploring its catalytic properties. The structures of the Ir_N clusters will form the basis of future studies of the catalytic properties of the system, including modelling their interaction with small molecules.

The cubic structures found here are in agreement with higher level CCSD(T) and CASSCF calculations on Ir_8, reported by Dixon *et al.*[18] In future work, we will investigate the effect of changing the functional in DFT calculations on Ir clusters; in particular we will explore the use of meta-GGA functionals.[47,48]

The development of the BPGA will continue. This will include the implementation of new features, such as the global optimisation of a system in the presence of a ligand or directly on a variety of surfaces. Further improvements to the efficiency of the parallel scheme will also be made. The code will be applied to a variety of new supported and ligated mono- and bimetallic cluster systems. The number of interfaces to common quantum chemistry programs within the BPGA will be expanded and applied to the global optimisation of systems at theory levels beyond DFT.

Acknowledgements

J.B.A.D. and R.L.J. acknowledge the Engineering and Physical Sciences Research Council, U.K. (EPSRC) for funding under Critical Mass Grant EP/J010804/1 "TOUCAN: Towards an Understanding of Catalysis on Nanoalloys".

A.S. acknowledges financial support by the DFG (grant SCHA885/10-2) and the Merck'sche Gesellschaft für Kunst und Wissenschaft e.V.

Calculations were performed *via* membership of the UK's HPC Materials Chemistry Consortium, which is funded by EPSRC (EP/L000202), this work made use of the facilities of ARCHER, the UK's national high-performance computing service, which is funded by the Office of Science and Technology through EPSRC's High End Computing Programme.

References

1 R. Ferrando, J. Jellinek and R. L. Johnston, *Chem. Rev.*, 2008, **108**, 845–910.
2 A. Uzun, D. A. Dixon and B. C. Gates, *ChemCatChem*, 2011, **3**, 95–107.
3 H. Kobayashi, M. Yamauchi and H. Kitagawa, *J. Am. Chem. Soc.*, 2012, **134**, 6893–6895.
4 J. B. A. Davis, S. L. Horswell, L. Piccolo and R. L. Johnston, *J. Organomet. Chem.*, 2015, DOI: 10.1016/j.jorganchem.2015.04.03.
5 L. Piccolo, S. Nassreddine, G. Toussaint and C. Geantet, *ChemSusChem*, 2012, **5**, 1717–1723.
6 A. Okrut, R. C. Runnebaum, X. Ouyang, J. Lu, C. Aydin, S.-J. Hwang, S. Zhang, O. A. Olatunji-Ojo, K. A. Durkin, D. A. Dixon, B. C. Gates and A. Katz, *Nat. Nanotechnol.*, 2014, **9**, 459–465.
7 M. Polak and L. Rubinovich, *Surf. Sci.*, 2005, **584**, 41–48.
8 J. B. A. Davis, R. L. Johnston, L. Rubinovich and M. Polak, *J. Chem. Phys.*, 2014, **141**, 224307.
9 D. Wales and J. P. K. Doye, *J. Phys. Chem. A*, 1997, **101**, 5111–5116.
10 http://www-wales.ch.cam.ac.uk/GMIN/.
11 R. L. Johnston, *Dalton Trans.*, 2003, 4193–4207.
12 F. Cleri and V. Rosato, *Phys. Rev. B: Condens. Matter*, 1993, **48**, 22–33.
13 S. Heiles, A. J. Logsdail, R. Schäfer and R. L. Johnston, *Nanoscale*, 2012, **4**, 1109–1115.
14 C. J. Heard and R. L. Johnston, *Eur. Phys. J. D*, 2013, **67**, 34.
15 P. C. Jennings and R. L. Johnston, *Comput. Theor. Chem.*, 2013, **1021**, 91–100.
16 S. Heiles and R. L. Johnston, *Int. J. Quantum Chem.*, 2013, **113**, 2091–2109.
17 Y. Chen, M. Huo, T. Chen, Q. Li, Z. Sun and L. Song, *Phys. Chem. Chem. Phys.*, 2015, **17**, 1680–1687.
18 M. Chen and D. A. Dixon, *J. Phys. Chem. A*, 2013, **117**, 3676–3688.
19 M. J. Piotrowski, P. Piquini, M. M. Odashima and J. L. Da Silva, *J. Chem. Phys.*, 2011, **134**, 134105.
20 M. Zhang and R. Fournier, *Phys. Rev. A*, 2009, **79**, 043203.
21 J. Du, X. Sun, J. Chen and G. Jiang, *J. Phys. Chem. A*, 2010, **114**, 12825–12833.
22 T. Pawluk, Y. Hirata and L. Wang, *J. Phys. Chem. B*, 2005, **109**, 20817–20823.
23 W. Zhang, L. Xiao, Y. Hirata, T. Pawluk and L. Wang, *Chem. Phys. Lett.*, 2004, **383**, 67–71.
24 G. Ping, Z. Ji-Ming, Z. Pei, Z. Lin-Lin and R. Zhao-Yu, *Chin. Phys. B*, 2010, **19**, 083601.
25 B. Bandow and B. Hartke, *J. Phys. Chem. A*, 2006, **110**, 5809–5822.
26 L. B. Vilhelmsen and B. Hammer, *J. Chem. Phys.*, 2014, **141**, 044711.
27 Y. Ge and J. D. Head, *J. Phys. Chem. B*, 2004, **108**, 6025–6034.
28 J. M. Dieterich and B. Hartke, *Mol. Phys.*, 2010, **108**, 279–291.
29 F. Weigend, *J. Chem. Phys.*, 2014, **141**, 134103.
30 https://bitbucket.org/JBADavis/bpga/.
31 A. Shayeghi, D. Götz, J. B. A. Davis, R. Schäfer and R. L. Johnston, *Phys. Chem. Chem. Phys.*, 2015, **17**, 2104–2112.
32 A. Shayeghi, R. L. Johnston and R. Schäfer, *J. Chem. Phys.*, 2014, **141**, 181104.
33 J. E. Sansonetti and W. C. Martin, *J. Phys. Chem. Ref. Data*, 2005, **34**, 1777–1781.
34 J. Jellinek and E. B. Krissinel, *Chem. Phys. Lett.*, 1996, **258**, 283–292.

35 https://wiki.fysik.dtu.dk/ase/.
36 http://www.archer.ac.uk.
37 D. M. Deaven and K. M. Ho, *Phys. Rev. Lett.*, 1995, **75**, 288–291.
38 C. J. Heard, S. Heiles, S. Vajda and R. L. Johnston, *Nanoscale*, 2014, **6**, 11777–11788.
39 G. Kresse and J. Hafner, *Phys. Rev. B: Condens. Matter*, 1993, **47**, 558–561.
40 G. Kresse and J. Hafner, *Phys. Rev. B: Condens. Matter*, 1994, **49**, 14251–14269.
41 G. Kresse and J. Furthmüller, *Comput. Mater. Sci.*, 1996, **6**, 15–50.
42 G. Kresse and J. Furthmüller, *Phys. Rev. B: Condens. Matter*, 1996, **54**, 11169–11186.
43 H. J. Monkhorst and J. D. Pack, *Phys. Rev. B: Solid State*, 1976, **13**, 5188–5192.
44 J. Perdew, K. Burke and Y. Wang, *Phys. Rev. B: Condens. Matter*, 1996, **54**, 533–539.
45 G. Kresse and D. Joubert, *Phys. Rev. B: Condens. Matter*, 1999, **59**, 1758–1775.
46 M. Methfessel and A. T. Paxton, *Phys. Rev. B: Condens. Matter*, 1989, **40**, 3616–3621.
47 L. A. Constantin, E. Fabiano and F. Della Sala, *J. Chem. Theory Comput.*, 2013, **9**, 2256–2263.
48 P. Hao, J. Sun, B. Xiao, A. Ruzsinszky, G. I. Csonka, J. Tao, S. Glindmeyer and J. P. Perdew, *J. Chem. Theory Comput.*, 2013, **9**, 355–363.

5.4 Draft Publication 7

Title

The Application of a Parallel Genetic Algorithm to the Global Optimisation of Gas-Phase and Supported Gold-Iridium Nanoalloys

Authors

Jack B. A. Davis, Sarah L. Horswell and Roy L Johnston

The Application of a Parallel Genetic Algorithm to the Global Optimisation of Gas-Phase and Supported Gold-Iridium Nanoalloys

Jack B. A. Davis, Sarah L. Horswell, and Roy L. Johnston*

School of Chemistry, University of Birmingham

E-mail: r.l.johnston@bham.ac.uk

Abstract

The direct density functional theory global optimisation of MgO(100)-supported AuIr nanoalloys is performed using the Birmingham Parallel Genetic Algorithm (BPGA). The BPGA is a pool genetic algorithm for the structural characterisation of nanoalloys. The parallel pool methodology utilised within the BPGA allows the code to characterise the structures of $N = 4 - 6$ Au_nIr_{N-n} clusters in the presence of the MgO(100) surface. The use of density functional theory allows the code to capture quantum size effects in the system which determine their structures. The searches reveal significant differences in structure and chemical ordering between the surface-supported and gas-phase global minimum structures.

Introduction

Nanoalloys (NAs) are a class of nanomaterial composed of multiple metallic elements. The combination of metals results in properties which are not only dependent on the size and shape of the cluster but on the composition and ordering of elements.[1] NAs have potential optical, magnetic and catalytic applications.[2]

AuIr NAs have been investigated previously both theoretically and experimentally,[3–5] particularity for CO oxidation catalysis. The activity of monometallic Au CO oxidation catalysts was found to decrease over time, either because of sintering or poisoning.[6] The addition of Ir to the catalyst has been shown to prevent sintering and improve the overall catalytic activity of the system through the formation of nanoalloy particles.[3,5] In the studies of both the mono- and bimetallic Au systems, the support was shown to play an important role in the activity of the catalyst.[7,8]

The structural characterisation of NAs is a vital first step toward rationalising their catalytic properties. In the present study the structures of $N = 4 - 6$ Au_nIr_{N-n} NAs are characterised using direct DFT global optimisation. This is performed both in the gas-phase and in the presence of an MgO(100) slab to better understand the effect of a surface on the

structures of AuIr NAs. The use of direct DFT global optimisation is necessary to reveal any quantum size effects, commonly seen for Au and Ir, in the NA structures.[9]

Both the gas-phase and MgO(100)-supported global optimisations of the AuIr clusters are performed using the Birmingham Parallel Genetic Algorithm (BPGA).[10] The BPGA is a pool-based genetic algorithm, capable of performing multiple DFT calculations in parallel.[11] This parallelism is of particular importance for the surface-supported calculations. While numerous methods for the direct DFT global optimisation of surface-supported clusters have been developed,[12,13] the inclusion of a surface slab within a local minimisation increases the cost of the underlying DFT calculations and therefore greatly increases the overall cost of the global optimisation.

Methodology

DFT

Gamma-point, spin-polarised DFT calculations were performed with VASP.[14–18] Projected-augmented wave (PAW) pseudopotentials were used with the PBE exchange correlation functional.[19,20] A plane-wave basis set with a cut-off of 400 eV was used. Methfessel-Paxton smearing, with a sigma value of 0.01 eV, was utilised to improve metallic convergence.[21]

BPGA

The BPGA is an open-source genetic algorithm for the direct DFT global optimisation of nanoalloys.[22] The program utilises a pool methodology which allows the evaluation of multiple potential cluster geometries in parallel.[11,23] Calculations are performed in parallel with between 2 and 4 instances of the BPGA operating on shared pools, depending on the size of the cluster. Depending on access to computational resources, the number of instances could be far larger.

An initial pool of 10 random structures is generated and evaluated by local minimisation

within VASP. These initial structures are prepared so that no two atoms are overlapping. Once the initial pool has been minimised, crossover and mutation operations are carried out. For crossover, pairs of clusters are selected from the pool through tournament selection. Offspring are then produced through single-point, weighted crossover, carried out according to the Deaven and Ho cut and splice method.[24] The mutation rate is set to 10% of the pool size.

For the supported clusters the local minimisation of the cluster geometry is performed in the presence of an MgO(100) slab, which is not relaxed during the calculation due to the high computational cost of doing so. The slab unit cell used in the present study is 6×6×2 atoms with a 14.7 Å vacuum spacing, to ensure there is no interaction between the cluster and the periodic cell. The use of two layers of MgO(100) has previously been shown to be capable of replicating the behaviour of the surface and its effect on the properties of a cluster.[25–28] The height of the cluster is fixed so that the lowest lying atom is 1.5 Å above the surface, as is shown in figure 1.

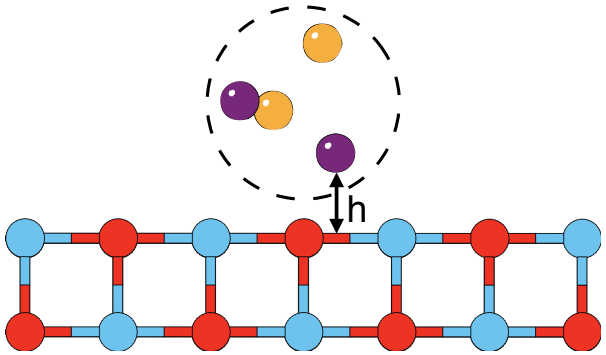

Figure 1: An initial random geometry is generated and placed at a fixed height, $h = 1.5$ Å, above the MgO(100) slab.

The mutation operator for the surface-supported clusters is a random rotation of the cluster with respect to the fixed slab. For the gas-phase clusters, the mutation operators are a random perturbation (up to a 1 Å displacement of 20% of the cluster atoms) for monometallic clusters and a homotop-swap for bimetallic clusters.

Crossover and mutation operations are performed until the highest and lowest energies

of the pool differ by no more than 10^{-3} eV. If complete convergence cannot be obtained the lowest energy structure is selected from a run of around 150 local minimisations. Due to the high computational cost, only one run is carried out per composition.

Energetics

The binding energies, E_{b}, were calculated using the following expression

$$E_{\mathrm{b}} = \frac{E_{\mathrm{Au}_n\mathrm{Ir}_m} - (nE_{\mathrm{Au}} + mE_{\mathrm{Ir}})}{N} \tag{1}$$

where $E_{\mathrm{Au}_n\mathrm{Ir}_m}$ is the total energy of cluster $\mathrm{Au}_n\mathrm{Ir}_m$, E_{Au} and E_{Ir} are the energies of single, spin-polarised Au and Ir atoms and N is the total number of atoms ($N = n + m$).

The excess energies, Δ,[29] of the clusters was calculated using

$$\Delta = E_{\mathrm{Au}_n\mathrm{Ir}_m} - n\left(\frac{E_{\mathrm{Au}_N}}{N}\right) - m\left(\frac{E_{\mathrm{Ir}_N}}{N}\right) \tag{2}$$

where E_{Au_N} and E_{Ir_N} are the energies of the monometallic Au and Ir clusters with the same total number of atoms as $\mathrm{Au}_n\mathrm{Ir}_m$.

The adsorption energies E_{ads} of the surface -supported clusters were calculated as follows

$$E_{\mathrm{ads}} = E_{\mathrm{slab+Au}_n\mathrm{Ir}_m} - (E_{\mathrm{slab}} + E_{\mathrm{Au}_n\mathrm{Ir}_m}) \tag{3}$$

where E_{slab} is the energy of the MgO(100) slab and $E_{\mathrm{Au}_n\mathrm{Ir}_m}$ is the energy of the $\mathrm{Au}_n\mathrm{Ir}_m$ cluster, locally minimised in the gas-phase.

Results

The putative global minimum structures of the gas-phase $N = 4 - 6$ $\mathrm{Au}_n\mathrm{Ir}_{N-n}$ clusters are shown in figures 2, 3 and 4. Global minimum structures for the MgO(100)-supported $N = 4 - 6$ $\mathrm{Au}_n\mathrm{Ir}_{N-n}$ clusters are shown in figures 5, 6 and 7.

Table 1: Binding energies E_b (gas-phase only), adsorption energies E_ads (surface-supported only), excess energies Δ and spin-multiplicities $2S+1$ for the $N=4-6$ $\mathbf{Au}_n\mathbf{Ir}_{N-n}$ clusters.

	Gas-Phase			Surface-Supported		
	E_b / eV	Δ / eV	$2S+1$	E_ads / eV	Δ / eV	$2S+1$
Au_4	-1.546	0	1	-1.951	0	1
Au_3Ir	-1.840	0.948	3	-2.342	0.890	3
Au_2Ir_2	-2.397	0.845	5	-3.251	0.332	3
$AuIr_3$	-2.928	0.843	5	-3.434	0.459	1
Ir_4	-3.670	0	9	-2.933	0	3
Au_5	-1.692	0	2	-1.973	0	2
Au_4Ir	-1.975	0.784	4	-2.341	0.317	2
Au_3Ir_2	-2.458	0.565	4	-2.963	0.132	2
Au_2Ir_3	-2.892	0.593	6	-2.784	0.371	4
$AuIr_4$	-3.478	-0.137	4	-3.083	-0.307	2
Ir_5	-3.890	0	8	-3.325	0	4
Au_6	-1.929	0	1	-1.592	0	1
Au_5Ir	-2.117	1.113	3	-2.465	1.356	1
Au_4Ir_2	-2.500	1.060	5	-3.621	0.830	3
Au_3Ir_3	-2.913	0.829	7	-3.559	0.574	1
Au_2Ir_4	-3.382	0.255	7	-3.211	0.847	3
$AuIr_5$	-3.730	0.415	7	-3.043	1.083	5
Ir_6	-4.173	0	5	-3.494	0	5

Global minima for the gas-phase and supported Au_nIr_{4-n} clusters are all found to be planar. The surface-supported global minimum structures are all found to be normal to the plane of the surface as a result of the 'metal-on-top effect' commonly seen in such subnanometre size clusters.[30] Ir_4 is found to be a square, as seen in previous studies of gas-phase Ir clusters,[31] and Au_4 is found to favour a rhombus structure. Differences between the gas-phase and adsorbed clusters are subtle. On the surface the structure of Au_4 is elongated so that two Au atoms can bond to two O atoms, increasing the Au-Au distance from 2.68 Å to 3.76 Å. The adsorbed structure of Ir_4 is the same as the gas-phase structure, with the square standing upright and bound to two O atoms.

All surface-supported bimetallic structures favour the stronger Ir-O interactions over Au-O. The structures of Au_3Ir, Au_2Ir_2 and $AuIr_3$ all differ from the gas-phase structures. The structures of Au_3Ir and Au_2Ir_2 are both Y-shaped in the gas-phase. On the surface the preferred structure is a rhombus, with Au_2Ir_2 having an elongated Au-Au bond. The gas-phase structure of $AuIr_3$ is a distorted rhombus. On the surface, the three Ir atoms form a linear chain with the Au atom bridging an Ir-Ir bond. In doing so $AuIr_3$ is able to maximise the number of Ir-O interactions.

The structure of the surface-supported Au_5 is similar to that of Au_4, with the structure again having an elongated Au-Au bond so as to bond across two O atoms. The structure of gas-phase Ir_5 is an edge-bridged square, with the bridging atom lifting out of the square-plane. The supported structure is a square-based pyramid structure with the basal plane lying parallel to the surface, forming four Ir-O bonds.

The supported and gas-phase structures of Au_4Ir are both tetrahedral structures. The supported structure is similar to that of supported Au_5 but the structure is now inverted and a single Ir-O bond is formed. The supported Au_3Ir_2, Au_2Ir_3 and $AuIr_4$ structures are all edge-bridged squares. The differences between these supported clusters and the corresponding gas-phase global minima vary. For Au_3Ir_2 the difference is simply a homotop swap maximising Ir-O bonds, whereas for Au_2Ir_3 there is a larger structural difference, with

a tetrahedral structure being preferred in the gas-phase.

$AuIr_4$ is found to have the same surface and the gas-phase structures; however the supported structure now only forms two Ir-O bonds, compared to the four Ir-O bonds of Ir_5. This may be due to an unfavourable interaction between the edge-bridging Au atom and the MgO(100) slab, had the Ir square remained four-coordinate, but it should be noted that the Ir4 square cluster also sits perpendicular to the surface, so it may just reflect the competition between the metal-on-top effect and localised Ir-O bonding effects.

The gas-phase structure of Ir_6 is a slightly bent double-square structure, with a 154° angle between squares. On the MgO(100)-support the structure is a 3D trigonal prism bound to the surface by four Ir-O bonds. The planar-triangular structure of Au_6 is found in both the gas-phase and on the surface. Au_4Ir and Au_5Ir have similar gas-phase and supported structures, with the extra Au in Au_5Ir capping a Au-Ir bond in the tetrahedral structure. On the surface, the structure of Au_5Ir is still based on the tetrahedral structure but the Au atom now caps a face.

Both Au_4Ir_2 and Au_3Ir_3 have the same planar-triangular structure on the surface and in the gas-phase. There are, however, differences in the homotop of each structure as they try to maximise Ir-O bonding. The Ir atoms in each surface-supported structure sit at the bottom of the structure, forming a dimer and trimer, for Au_4Ir_2 and Au_3Ir_3, respectively. Au_2Ir_4 has a planar bi-edge-bridged square structure in both the gas-phase and the surface, with the two bridging Au atoms adopting *cis* positions in the gas-phase GM and *trans* positions in the GM of the supported cluster. The gas-phase structure of $AuIr_5$ is similar to that of Au_2Ir_4 except that the bridging Ir sits out of plane of the square. The lowest energy $AuIr_5$ structure on the MgO(100) surface is an Ir_5 square pyramid (as for the Ir_5 cluster) with one of the edges on the square face bridged by Au. In contrast to Ir5, however, the square pyramid lies on its side on the MgO surface (with only 3 Ir atoms in contact with the surface) which may be due to an unfavourable interaction of the Au atom with the surface if the cluster sits with the square face on the surface.

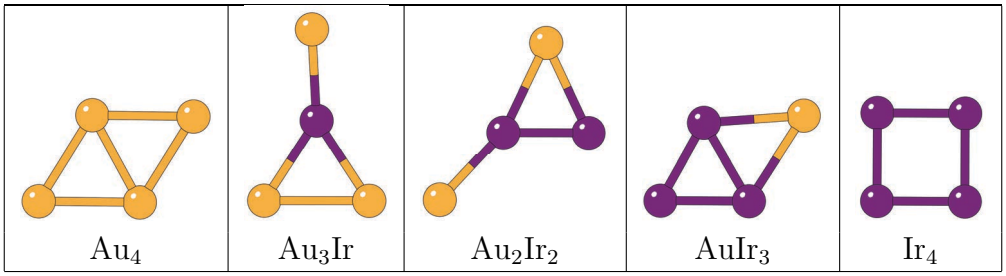

Figure 2: Putative global minimum structures of gas-phase Au_nIr_{4-n} clusters. Au and Ir are shown in gold and purple, respectively.

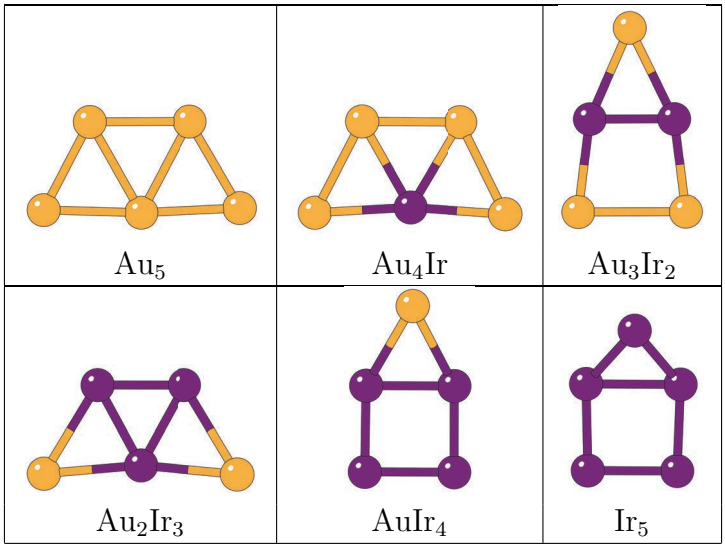

Figure 3: Putative global minimum structures of gas-phase Au_nIr_{4-n} clusters.

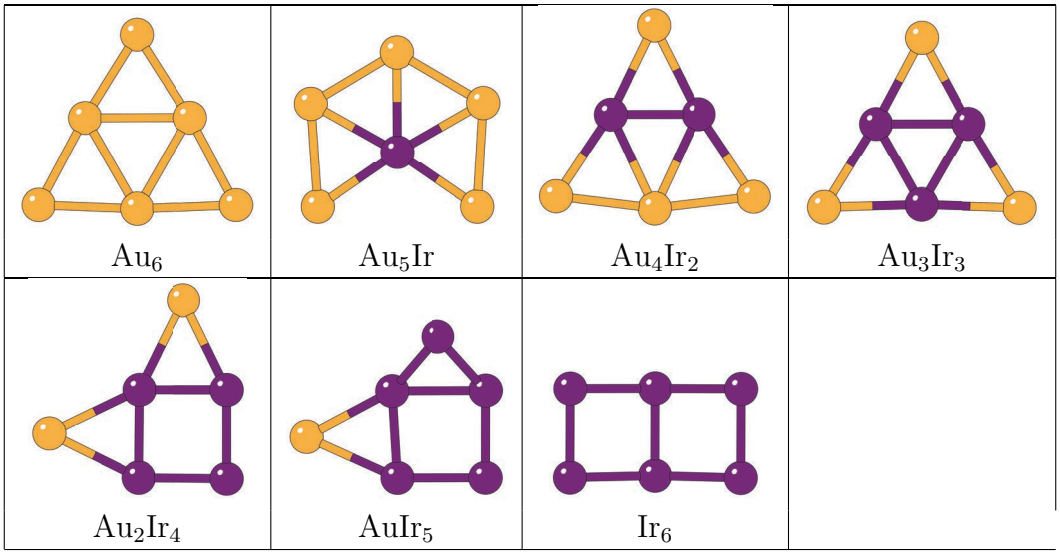

Figure 4: Putative global minimum structures of gas-phase Au_nIr_{6-n} clusters.

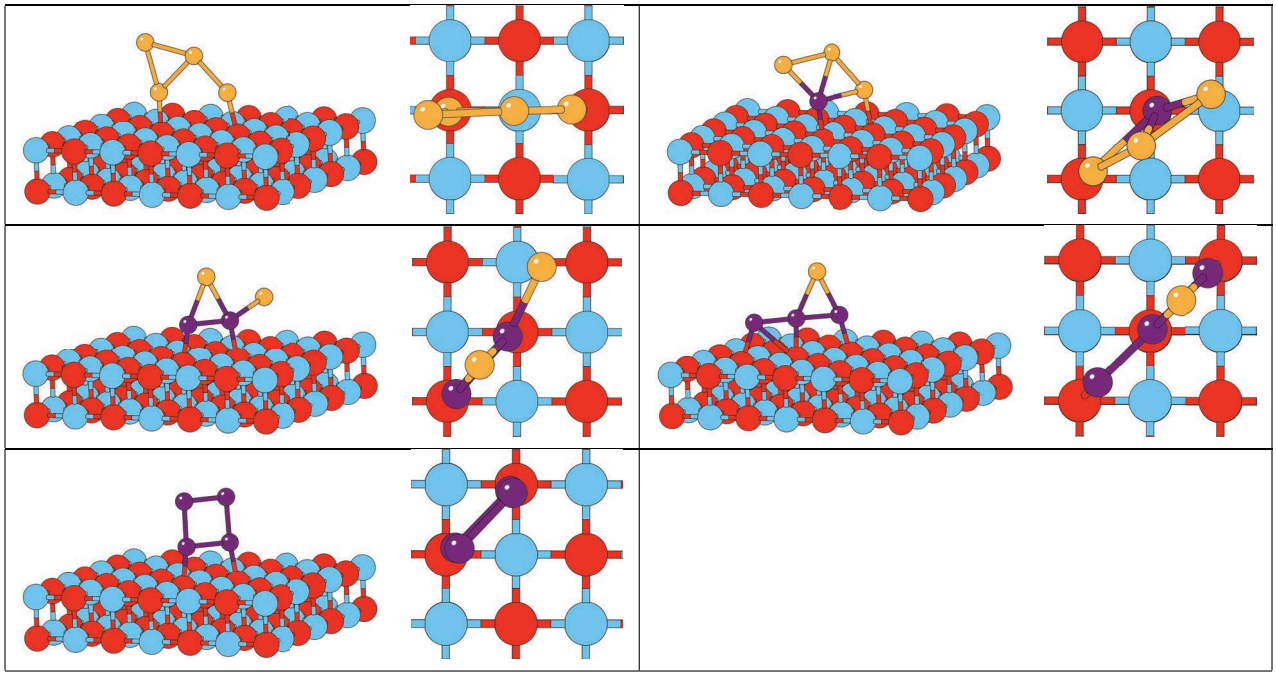

Figure 5: Putative global minimum structures of MgO(100)-supported Au_nIr_{4-n} clusters. Au, Ir, Mg and O are shown in gold, purple, red and blue, respectively.

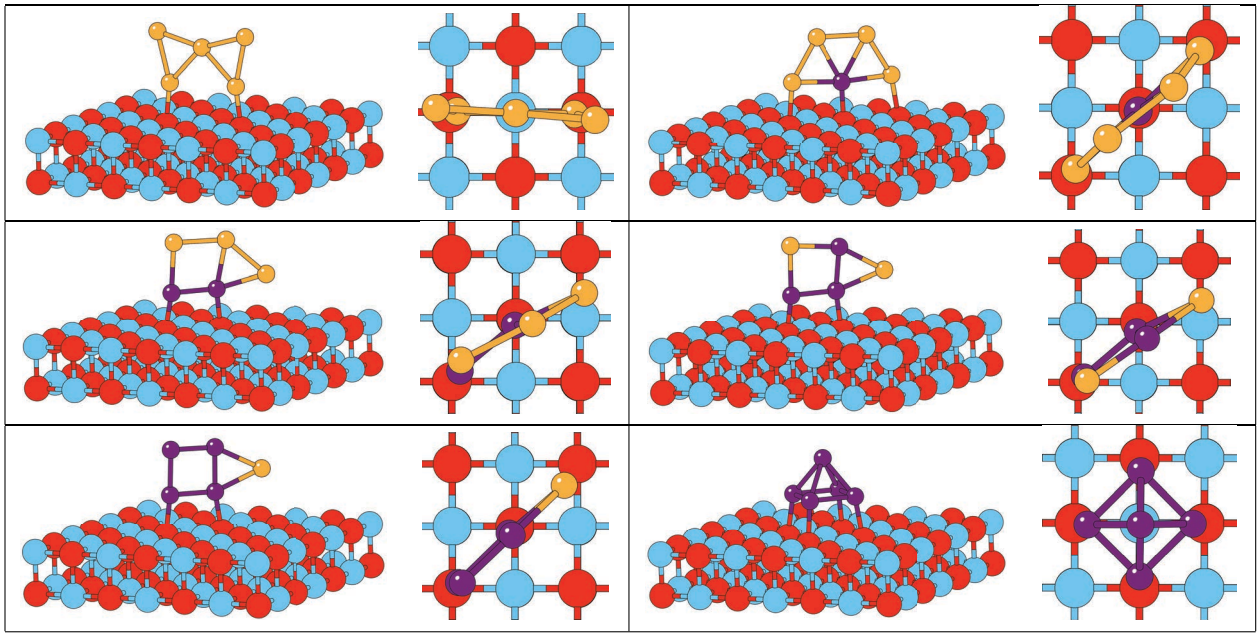

Figure 6: Putative global minimum structures of MgO(100)-supported Au_nIr_{5-n} clusters.

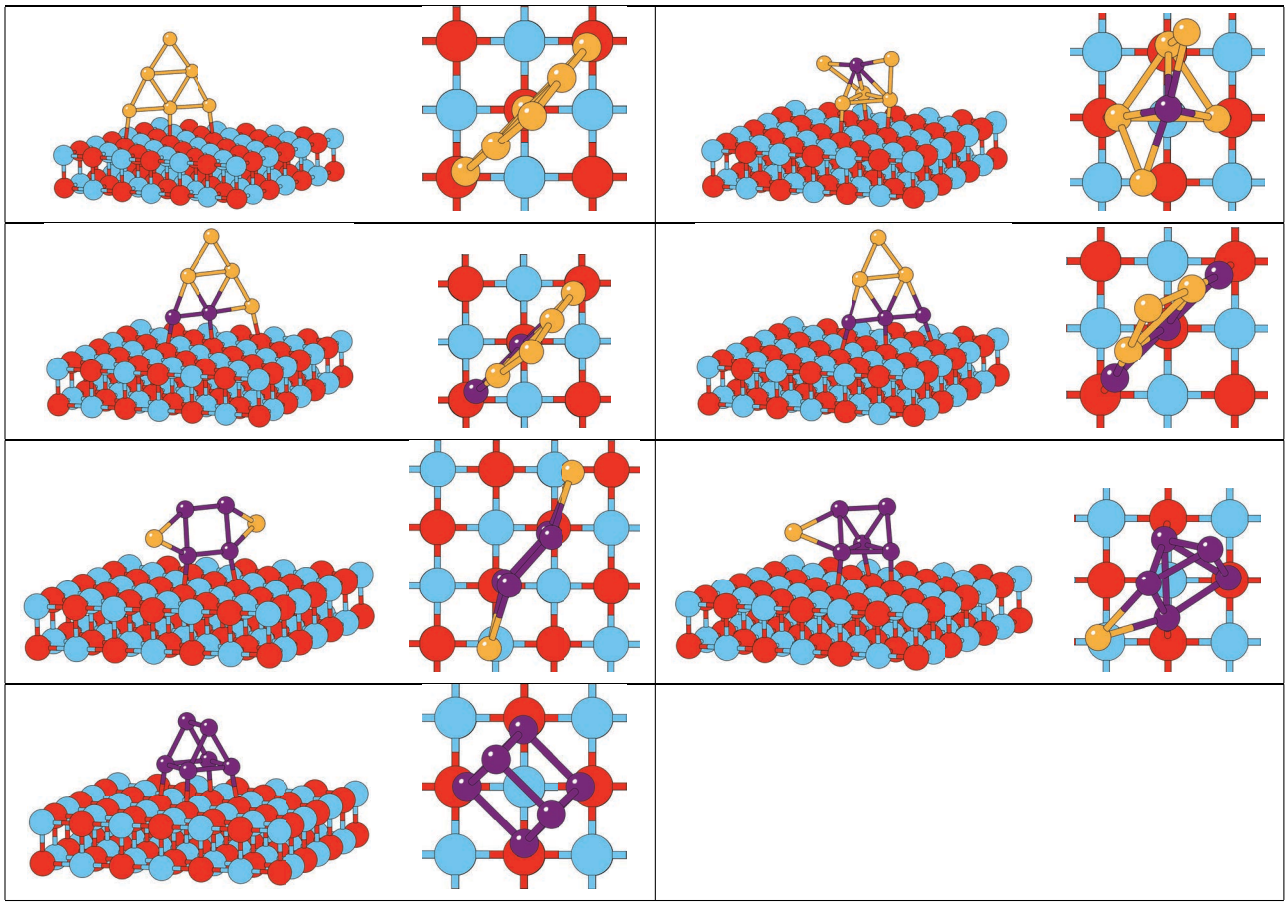

Figure 7: Putative global minimum structures of MgO(100)-supported Au_nIr_{6-n} clusters.

The results from our global optimisations, which are performed directly in the presence of an MgO(100) slab, can be compared with those from other studies. In many studies structures generated in the gas-phase are deposited on the surface, with very little change in the cluster structure. For example, our surface-supported results for Ir_4 and Ir_6 clearly differ from those reported in a recent study because of a difference in methodology utilised in their study.[32]

The spin multiplicities of the gas-phase and supported clusters are listed in table 1 and are plotted in figure 8. The Ir and Ir-rich clusters are generally found to possess higher spins than the Au and Au-rich clusters. The presence of the MgO(100) surface partially quenches the spins of the supported clusters, with clusters having lower-spin configurations. This is may be in part due to the Ir-O interactions which are favoured in these clusters, resulting in some of the unpaired Ir electrons being involved in Ir-O bonding.

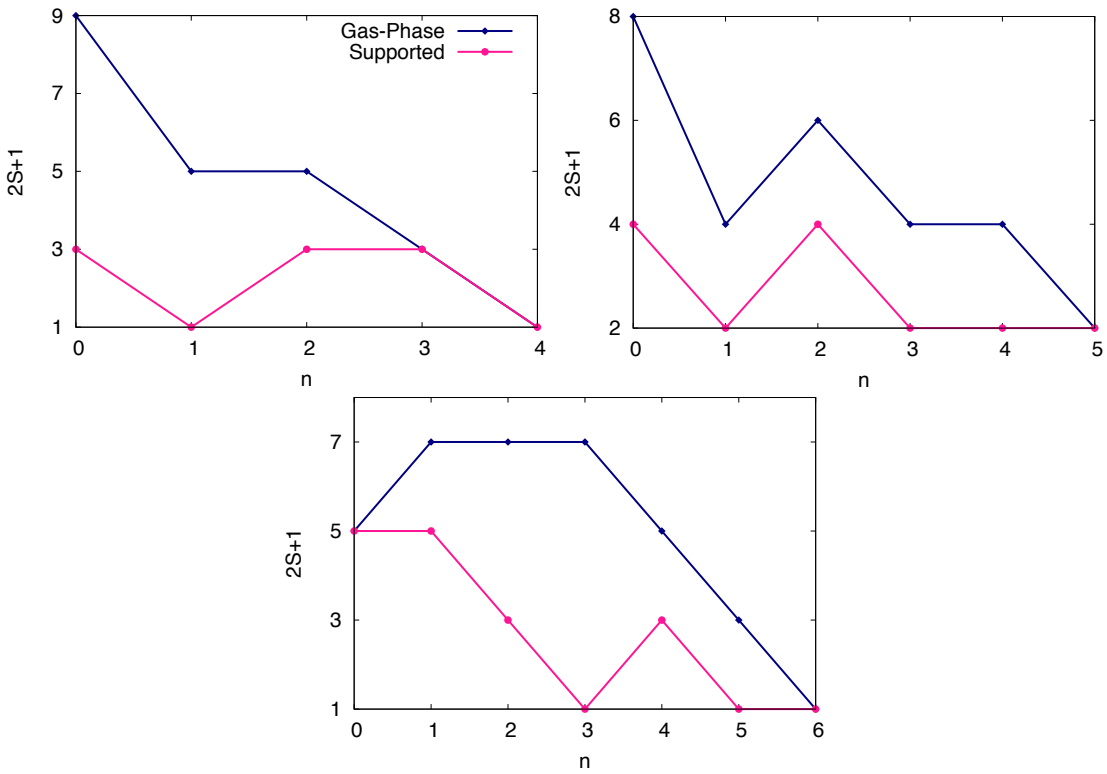

Figure 8: Spin multiplicities $2S+1$ of the $N = 4-6$ Au_nIr_{N-n} gas-phase and MgO(100)-supported putative global minimum structures.

The adsorption energies E_{ads} of the supported clusters are listed in table 1 and are plotted

in figure 9. There are differences between energies of supported clusters and the energies of the supported clusters with the slab removed, in particular the Au and Au-rich clusters are found to have the lowest E_{ads}, which then increases until the composition reaches around 50/50.

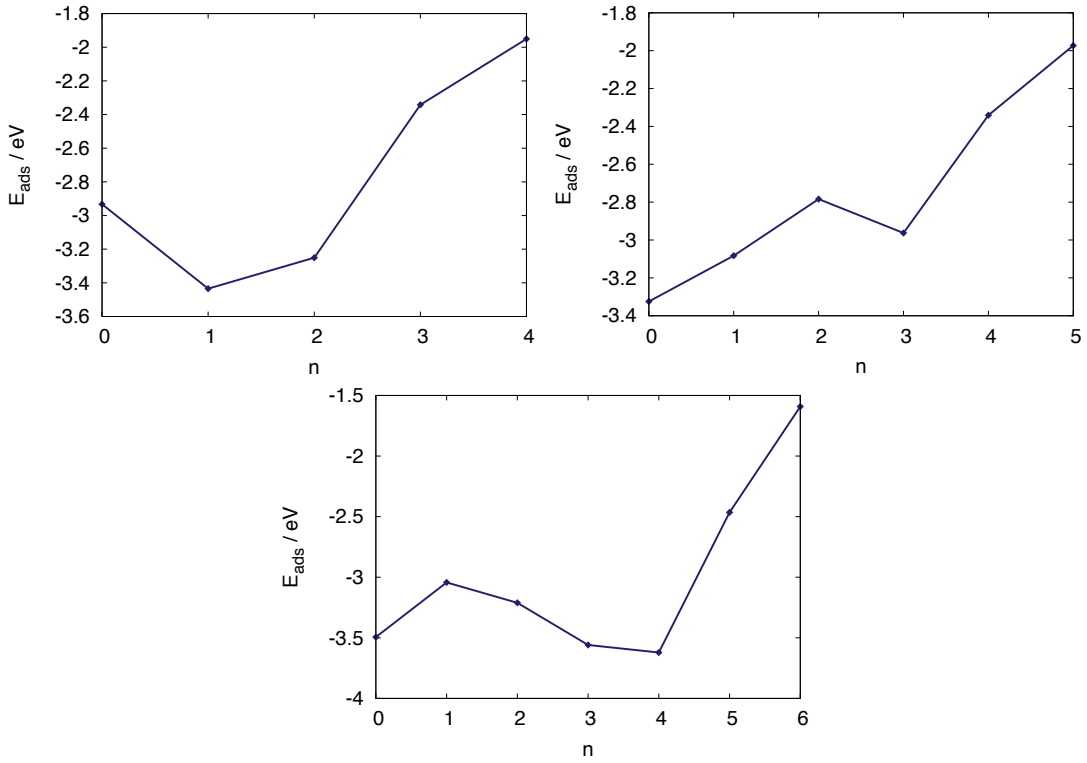

Figure 9: Adsorption energies E_{ads} of the MgO(100)-supported $N = 4-6$ $\mathrm{Au}_n\mathrm{Ir}_{N-n}$ clusters.

The excess energies plotted in figure 10, reveal the energetic preference for the alloying of the constituent elements in the nanoalloy. AuIr is found to be a strongly demixing system, with positive Δ values found for almost all gas-phase and supported clusters sizes and compositions. The only negative values are found for AuIr_4, where from Ir_5 there is a 3D to 2D transition. The excess energies for the surface-supported clusters, particularly for 4 and 5-atoms, are found to have lower excess energies. In these cases the surface could be acting to promote alloying in the system. This trend, however, is not continued for the 6-atom clusters, with the gas-phase structures sometimes being less positive than those that are surface-supported.

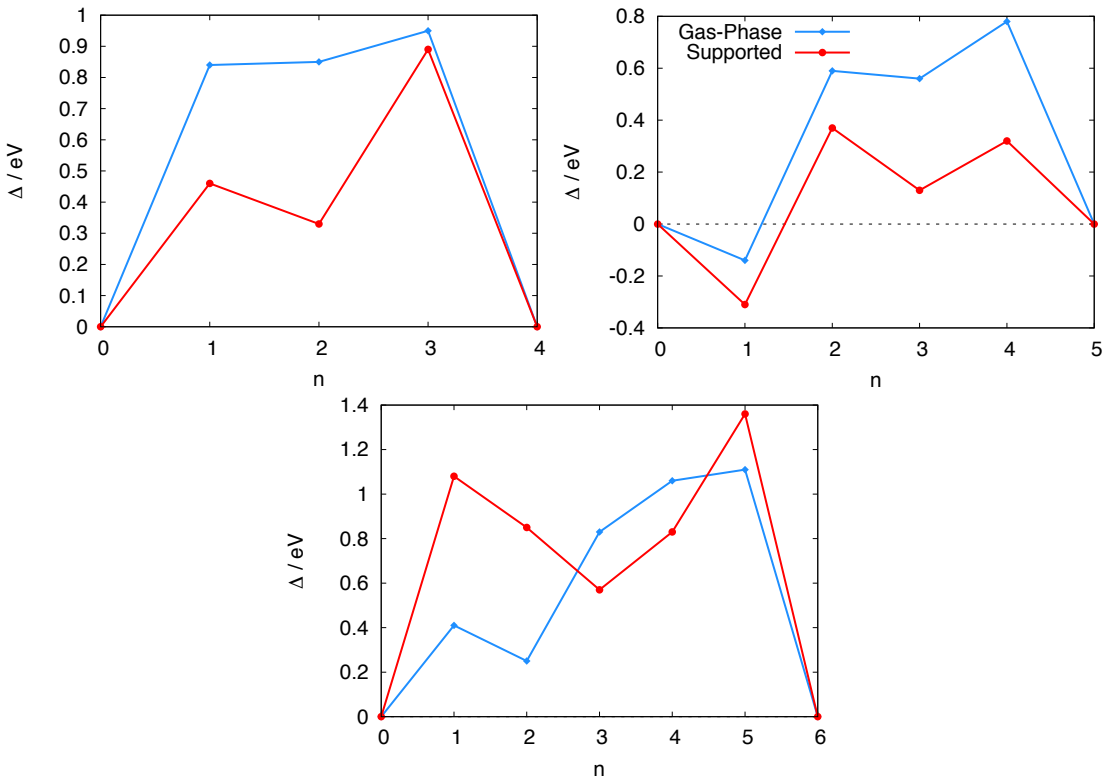

Figure 10: Excess energies E_Δ of the gas-phase and MgO(100)-supported $N = 4{-}6$ Au_nIr_{N-n} clusters.

Conclusions and Future Work

The BPGA has been successfully applied to the global optimisation of both gas-phase and MgO(100)-supported $N = 4 - 6$ Au_nIr_{N-n} clusters. The direct global optimisation in the presence of an MgO slab has revealed significant differences in gas-phase and surface-supported global minimum structures, with those on MgO(100) maximising the number of Ir-O bonds. The MgO(100) surface not only affects the structures and atomic ordering of the AuIr clusters, but the surface is also observed to suppress the spin of the clusters.

Future work will include expanding the BPGA's library of surface generators. In particular to include rutile, which has been shown to play an active role in increasing the catalytic performance of AuIr.[3] The larger number of surface sites on rutile will require greater computational effort and mutation schemes capable of exploring these sites completely during a search.

Acknowledgement

This study was built upon the initial studies of AuIr performed by Chuheng Li and Anastasija Jevgrafova.

J.B.A.D. and R.L.J. acknowledge the Engineering and Physical Sciences Research Council, U.K. (EPSRC) for funding under Critical Mass Grant EP/J010804/1 "TOUCAN: Towards an Understanding of Catalysis on Nanoalloys". Calculations were performed via membership of the UK's HPC Materials Chemistry Consortium, which is funded by EPSRC (EP/L000202), this work made use of the facilities of ARCHER, the UK's national high-performance computing service, which is funded by the Office of Science and Technology through EPSRC's High End Computing Programme.

References

(1) Johnston, R. L. *Atomic and Molecular Clusters*; Taylor and Francis: London, 2002.

(2) Ferrando, R.; Jellinek, J.; Johnston, R. L. Nanoalloys: From Theory to Applications of Alloy Clusters and Nanoparticles. *Chem. Rev.* **2008**, *108*, 845–910.

(3) Bokhimi, X.; Zanella, R.; Angeles-Chavez, C. Rutile-supported Ir, Au, and Ir-Au catalysts for CO oxidation. *J. Phys. Chem. C* **2010**, *114*, 14101–14109.

(4) Jiménez-Díaz, L. M.; Pérez, L. A. Structural and Electronic Properties of AuIr Nanoalloys. *Eur. Phys. J. D* **2013**, *67*, 15.

(5) Gómez-Cortés, A.; Díaz, G.; Zanella, R.; Ramírez, H.; Santiago, P.; Saniger, J. M. Au-Ir/TiO_2 Prepared by Deposition Precipitation with Urea: Improved Activity and Stability in CO Oxidation. *J. Phys. Chem. C* **2009**, *113*, 9710–9720.

(6) Choudhary, T. V.; Goodman, D. W. Methane Activation on Ruthenium: The Nature of the Surface Intermediates. *Top. Catal.* **2002**, *20*, 35–42.

(7) Schubert, M. M.; Hackenberg, S.; van Veen, A. C.; Muhler, M.; Plzak, V.; Behm, R. J. CO Oxidation over Supported Gold CatalystsInert and Active Support Materials and Their Role for the Oxygen Supply during Reaction. *J. Catal.* **2001**, *197*, 113–122.

(8) Okumura, M.; Akita, T.; Haruta, M.; Wang, X.; Kajikawa, O.; Okada, O. Multi-Component Noble Metal Catalysts Prepared by Sequential Deposition Precipitation for Low Temperature Decomposition of Dioxin. *Appl. Catal. B* **2003**, *41*, 43–52.

(9) Heiles, S.; Johnston, R. L. Global Optimization of Clusters using Electronic Structure Methods. *Int. J. Quantum Chem.* **2013**, *113*, 2091–2109.

(10) Davis, J. B. A.; Shayeghi, A.; Horswell, S. L.; Johnston, R. L. The Birmingham Parallel Genetic algorithm and its Application to the Direct DFT Global Optimisation of Ir_N (N = 10-20) Clusters. *Nanoscale* **2015**, *7*, 14032–14038.

(11) Bandow, B.; Hartke, B. Larger Water Clusters with Edges and Corners on their way to Ice: Structural Trends Elucidated with an Improved Parallel Evolutionary Algorithm. *J. Phys. Chem. A* **2006**, *110*, 5809–5822.

(12) Vilhelmsen, L. B.; Hammer, B. A Genetic Algorithm for First Principles Global Structure Optimization of Supported Nano Structures. *J. Chem. Phys.* **2014**, *141*, 044711.

(13) Heard, C. J.; Heiles, S.; Vajda, S.; Johnston, R. L. $Pd_nAg_{(4-n)}$ and $Pd_nPt_{(4-n)}$ clusters on MgO (100): a density functional surface genetic algorithm investigation. *Nanoscale* **2014**, *6*, 11777–11788.

(14) Kresse, G.; Hafner, J. Ab Initio Molecular Dynamics for Liquid Metals. *Phys. Rev. B* **1993**, *47*, 558–561.

(15) Kresse, G.; Hafner, J. Ab Initio Molecular-Dynamics Simulation of the Liquid-Metal-Amorphous-Semiconductor Transition in Germanium. *Phys. Rev. B* **1994**, *49*, 14251–14269.

(16) Kresse, G.; Furthmüller, J. Efficiency of Ab-Initio Total Energy Calculations for Metals and Semiconductors using a Plane-Wave Basis Set. *Comput. Mater. Sci.* **1996**, *6*, 15–50.

(17) Kresse, G.; Furthmüller, J. Efficient iterative schemes for ab initio total-energy calculations using a plane-wave basis set. *Physical Review. B* **1996**, *54*, 11169–11186.

(18) Monkhorst, H. J.; Pack, J. D. Special points for Brillouin-zone integrations. *Phys. Rev. B* **1976**, *13*, 5188–5192.

(19) Perdew, J.; Burke, K.; Wang, Y. Generalized Gradient approximation for the Exchange-Correlation Hole of a Many-Electron System. *Phys. Rev. B* **1996**, *54*, 533–539.

(20) Kresse, G.; Joubert, D. From Ultrasoft Pseudopotentials to the Projector Augmented-Wave Method. *Phys. Rev. B* **1999**, *59*, 1758 – 1775.

(21) Methfessel, M.; Paxton, A. T. High-precision Sampling for Brillouin-Zone Integration in Metals. *Phys. Rev. B* **1989**, *40*, 3616–3621.

(22) https://bitbucket.org/JBADavis/bpga/.

(23) Shayeghi, A.; Götz, D.; Davis, J. B. A.; Schäfer, R.; Johnston, R. L. Pool-BCGA: a Parallelised Generation-Free Genetic Algorithm for the Ab Initio Global Optimisation of Nanoalloy Clusters. *Phys. Chem. Chem. Phys.* **2015**, *17*, 2104–2112.

(24) Deaven, D. M.; Ho, K. M. Molecular Geometry Optimization with a Genetic Algorithm. *Phys. Rev. Lett.* **1995**, *75*, 288–291.

(25) Gro, H.; Broqvist, P. CO-Induced Modification of the Metal/MgO(100) Interaction. *J. Phys. Chem. B* **2003**, *107*, 12239–12243.

(26) Grönbeck, H.; Broqvist, P. Pt and Pt_2 on MgO(100) and BaO(100): Structure, Bonding, and Chemical Properties. *J. Chem. Phys.* **2003**, *119*, 3896–3904.

(27) Ferrando, R.; Fortunelli, A. Diffusion of Adatoms and Small Clusters on Magnesium Oxide Surfaces. *J. Phys.: Condens. Matter* **2009**, *21*, 264001.

(28) Ismail, R.; Ferrando, R.; Johnston, R. L. Theoretical Study of the Structures and Chemical Ordering of Palladium-Gold Nanoalloys Supported on MgO(100). *J. Phys. Chem. C* **2013**, *117*, 293–301.

(29) Ferrando, R.; Fortunelli, A.; Rossi, G. Quantum effects on the structure of pure and binary metallic nanoclusters. *Phys. Rev. B* **2005**, *72*, 085449.

(30) Barcaro, G.; Fortunelli, A. The Interaction of Coinage Metal Clusters with the MgO(100) Surface. *J. Chem. Theory Comput.* **2005**, *1*, 972–985.

(31) Pawluk, T.; Hirata, Y.; Wang, L. Studies of Iridium Nanoparticles Using Density Functional Theory Calculations. *J. Phys. Chem. B* **2005**, *109*, 20817–20823.

(32) Chen, Y.; Huo, M.; Chen, T.; Li, Q.; Sun, Z.; Song, L. The Properties of Ir_n (n = 2-10) Clusters and their Nucleation on γ-Al_2O_3 and MgO Surfaces: from Ab Initio Studies. *Phys. Chem. Chem. Phys.* **2015**, *17*, 1680–1687.

6 | Conclusions and Outlook

This thesis has presented publications dedicated to the initial stages of understanding the catalytic properties of NAs, their structural characterisation and their subsequent interactions with small molecules. Publications have also explored the applicability of dispersion corrected DFT and the development of novel methods for their structural characterisation, in both the gas-phase and supported on a MgO(100) surface.

PdIr NAs, in particular, have been studied because of their promising catalytic properties. In Chapter 3 their structural characterisation, for a range of PdIr NA sizes, was performed with a variety of methods, including BCGA-Gupta, BCGA-DFT and FCEM.

The use of direct DFT global optimisation, using the BCGA-DFT method, was shown to be necessary for the structural characterisation of the system, with the NA structures displaying significant quantum size effects. Cubic global minimum structures were revealed for both monometallic Ir clusters and for the first time in bimetallic PdIr clusters. Structures were found to prefer high spin configurations and be strongly demixing, mirroring the behaviour of the bulk alloy.

The FCEM statistical mechanical method was shown to be capable of accurately characterising chemical ordering, particularly in larger NAs, when compared to the BCGA-Gupta method through direct DFT comparison. The FCEM method was found to offer significant advantages over the BCGA approach, as FCEM calculations require significantly less computational effort and can be performed on considerably larger, and catalytically relevant, NAs. Statistical mechanical methods

are less commonly used in studies of compositional ordering and it is hoped that this comparative study will promote their further development and application.

In Chapter 4 the interaction of metallic NPs and NAs with small molecules was probed. The interaction of PdIr NAs with benzene and hydrogen was modelled using a combined DFT and random search approach. The effect of dispersion corrections, at a range of theory levels, was also established through the study of the adsorption of CO on a range of metallic NPs.

The predicted lowest energy homotops for PdIr NAs from the FCEM method provided ideal candidates for which to study the effect of composition on NA adsorption properties. The interactions of two molecules, hydrogen and benzene, were modeled in order to better understand the catalytic activity of PdIr in tetralin hydroconversion and the preferential oxidation of CO. Significant nanosize effects were seen in the adsorption hydrogen onto Ir, with hydrogen binding dissociatively to the surface of the NP. Both benzene and hydrogen were found to prefer the Ir (100) facet of the bimetallic structures, with energetic preferences mirroring those displayed on the corresponding bulk surfaces.

The effect of a range of dispersion corrections on the site preference for CO on Pt, Au, Ir and Pd NPs were then determined. Previous studies on the effects of the corrections are limited and this work was intended to show the effect of the corrections at a range of theory levels. The corrections were found to have an effect on both the site preferences and energetic ordering of sites. Particularly significant effects were seen in the Pt and Au NPs. The study provides an initial insight in the applicability of dispersion corrected DFT to the study of metallic nanoparticles.

Chapter 5 outlined the development of parallel methodologies, with the ability to utilise massively parallel computational computational resources, for the structural characterisation of metallics NPs and NAs. Initially the parallel pool methodology was implemented with the BCGA and applied to the DFT global optimisation of Au_10 and Au_20. These are NP whose structures have been well studied by both experiment and theory. The method was shown to successfully characterise their

structures whilst efficiently utilising greater computational resources.

This methodology was then implemented within the new open-source BPGA program and applied to both Ir and AuIr NPs and NAs. The BPGA successfully revealed the structures of Ir NPs significantly larger than previously possible. The spin-unrestricted global optimisations revealed the importance of spin in the system, with high-spin global minima being preferred for a number of sizes. Finally, the BPGA was applied to the global optimisation of gas-phase and MgO(100)-supported AuIr NAs. The inclusion of the surface significantly increases the overall cost of these calculations and this study benefited from the parallel methodology. Significant structural differences were found between the gas-phase and surface-supported global minima structures. The surface was also found to influence both the excess energies and the spin of the clusters.

Future studies on the PdIr system must include close collaboration with experimental groups in order to develop a more complete understand of their catalytic properties. Theoretical studies must move beyond the structural characterisation of PdIr and their interaction with small molecules to calculations of the barriers present in the system. Collaboration should also extend to the assessment of predictions made by the BPGA, both for gas-phase and supported NAs.

Bibliography

[1] R. L. Johnston and J. P. Wilcoxon, *Frontiers of Nanoscience (Vol. 3)*, 2012.

[2] R. L. Johnston, *Atomic and Molecular Clusters*, Taylor and Francis, London, 2002.

[3] J. Jortner, *Z. Chem. D*, 1992, **24**, 247–275.

[4] R. L. Johnston, *Phil. Trans. R. Soc. A*, 1998, **356**, 211–230.

[5] W. A. de Heer, *Rev. Mod. Phys.*, 1993, **65**, 611–676.

[6] F. Baletto and R. Ferrando, *Rev. Mod. Phys.*, 2005, **77**, 371.

[7] R. Ferrando, J. Jellinek and R. L. Johnston, *Chem. Rev.*, 2008, **108**, 845–910.

[8] R. Ferrando, J. Jellinek and R. L. Johnston, *Faraday Discuss.*, 2008, **138**, 1–442.

[9] J. Jellinek and E. B. Krissinel, *Chem. Phys. Lett.*, 1996, **258**, 283–292.

[10] D. Wales and J. P. K. Doye, *J. Phys. Chem. A*, 1997, **101**, 5111–5116.

[11] R. L. Johnston, *Dalton Trans.*, 2003, 4193–4207.

[12] M. Polak and L. Rubinovich, *Surf. Sci.*, 2005, **584**, 41–48.

[13] M. Mitchell, *An Introduction to Genetic Algorithms*, MIT Press, 1998.

[14] J. H. Holland, *Adaptation in natural and artificial systems*, University of Michigan Press, 1975.

[15] D. E. Goldberg, *Genetic Algorithms in Search, Optimization and Machine Learning*, Addison -Wesley, Boston, 1989.

[16] Y. Xiao and D. E. Williams, *Chem. Phys. Lett.*, 1993, **215**, 17–24.

[17] B. Hartke, *J. Phys. Chem.*, 1993, **97**, 9973–9976.

[18] Y. Zeiri, *Phys. Rev. E*, 1995, **51**, 2769–2772.

[19] Y. Zeiri, *Comput. Phys. Commun.*, 1997, **103**, 28–42.

[20] Y. Zeiri, *J. Phys. Chem. A*, 1998, **102**, 2785–2791.

[21] D. M. Deaven and K. M. Ho, *Phys. Rev. Lett.*, 1995, **75**, 288–291.

[22] J. E. Jones, *Proc. R. Soc. A*, 1924, **106**, 441.

[23] M. Born and J. E. Mayer, *Z. Phys.*, 1932, **75**, 1–18.

[24] A. P. Sutton and J. Chen, *Philos. Mag. Lett.*, 1990, **61**, 139–146.

[25] J. N. Murrell and R. E. Mottram, *Mol. Phys.*, 1990, **69**, 571–585.

[26] S. Heiles and R. L. Johnston, *Int. J. Quant. Chem.*, 2013, **113**, 2091–2109.

[27] P. Gruene, D. M. Rayner, B. Redlich, A. F. G. van der Meer, J. T. Lyon, G. Meijer and A. Fielicke, *Science*, 2008, **321**, 674–676.

[28] M. Chen and D. A. Dixon, *J. Phys. Chem. A*, 2013, **117**, 3676–3688.

[29] A. Shayeghi, D. Götz, J. B. A. Davis, R. Schäfer and R. L. Johnston, *Phys. Chem. Chem. Phys.*, 2015, **17**, 2104–2112.

[30] L. B. Vilhelmsen and B. Hammer, *J. Chem. Phys.*, 2014, **141**, 044711.

[31] A. N. Alexandrova and A. I. Boldyrev, *J. Chem. Theory Comput.*, 2005, **1**, 566–580.

[32] E. Oger, N. R. M. Crawford, R. Kelting, P. Weis, M. M. Kappes and R. Ahlrichs, *Angew. Chem. Int. Ed.*, 2007, **46**, 8503–8506.

[33] B. Assadollahzadeh, C. Thierfelder and P. Schwerdtfeger, *Phys. Rev. B*, 2008, **78**, 245423.

[34] R. Kelting, A. Baldes, U. Schwarz, T. Rapps, D. Schooss, P. Weis, C. Neiss, F. Weigend and M. M. Kappes, *J. Chem. Phys.*, 2012, **136**, 154309.

[35] V. Habibpour, C. Yin, G. Kwon, S. Vajda and R. E. Palmer, *J. Exp. Nanosci.*, 2013, **8**, 993–1003.

[36] G. Kwon, G. A. Ferguson, C. J. Heard, E. C. Tyo, C. Yin, J. DeBartolo, S. Seifert, R. E. Winans, A. J. Kropf, J. Greeley, R. L. Johnston, L. A. Curtiss, M. J. Pellin and S. Vajda, *ACS Nano*, 2013, **7**, 5808–5817.

[37] F. Mehmood, J. Greeley and L. A. Curtiss, *J. Phys. Chem. C*, 2009, **113**, 21789–21796.

[38] S. Lee, B. Lee, F. Mehmood, S. Seifert, J. A. Libera, J. W. Elam, J. Greeley, P. Zapol, L. A. Curtiss, M. J. Pellin, P. C. Stair, R. E. Winans and S. Vajda, *J. Phys. Chem. C*, 2010, **114**, 10342–10348.

[39] M. Moseler, M. Walter, B. Yoon, U. Landman, V. Habibpour, C. Harding, S. Kunz and U. Heiz, *J. Am. Chem. Soc.*, 2012, **134**, 7690–7699.

[40] W. E. Kaden, W. A. Kunkel, F. S. Roberts, M. Kane and S. L. Anderson, *J. Chem. Phys.*, 2012, **136**, 204705.

[41] A. Uzun, D. A. Dixon and B. C. Gates, *ChemCatChem*, 2010, **3**, 95–107.

[42] L. Piccolo, S. Nassreddine, G. Toussaint and C. Geantet, *ChemSusChem*, 2012, **5**, 1717–1723.

[43] A. Okrut, R. C. Runnebaum, X. Ouyang, J. Lu, C. Aydin, S.-J. Hwang, S. Zhang, O. A. Olatunji-Ojo, K. A. Durkin, D. A. Dixon, B. C. Gates and A. Katz, *Nat. Nanotechnol.*, 2014, **9**, 459–465.

[44] J. H. Sinfelt, *Bimetallic catalysts: Discoveries, concepts, and applications.*, Wiley, 1983.

[45] V. Ponec and G. C. Bond, *Studies in Surface Science and Catalysis; Catalysis by Metals and Alloys*, Elsevier, 1995.

[46] *Reprinted from the Journal of Catalysis, 292, Laurent Piccolo, Salim Nassreddine, Mimoun Aouine, Corinne Ulhaq, Christophe Geantet, Supported Ir-Pd nanoalloys: 'Size-composition correlation and consequences on tetralin hydroconversion properties', 173-180.*

[47] S. N. Tripathi, S. R. Bharadwaj and M. S. Chandrasekharaiah, *J. Phase Equilib.*, 1991, **12**, 603–605.

[48] P. E. A. Turchi, V. Drchal and J. Kudrnovský, *Phys. Rev. B*, 2006, **74**, 064202.

[49] B. Kolb, S. Müller, D. B. Botts and G. L. W. Hart, *Phys. Rev. B*, 2006, **74**, 144206.

[50] T. H. Andriamiharintsoa, a. Rakotomahevitra, L. Piccolo and C. Goyhenex, *J. Nanopart. Res.*, 2015, **17**, 1–14.

[51] J. B. A. Davis, R. L. Johnston, L. Rubinovich and M. Polak, *J. Chem. Phys.*, 2014, **141**, 224307.

[52] J. B. A. Davis, S. L. Horswell and R. L. Johnston, *J. Phys. Chem. A*, 2014, **118**, 208–214.

[53] C. Zlotea, F. Morfin, T. S. Nguyen, N. T. Nguyen, J. Nelayah, C. Ricolleau, M. Latroche and L. Piccolo, *Nanoscale*, 2014, **6**, 9955–9959.

[54] F. Morfin, S. Nassreddine, J. L. Rousset and L. Piccolo, *ACS Catal.*, 2012, **2**, 2161–2168.

[55] L. Piccolo, S. Nassreddine, M. Aouine, C. Ulhaq and C. Geantet, *J. Catal.*, 2012, **292**, 173–180.

[56] Y. M. López-De Jesús, C. E. Johnson, J. R. Monnier and C. T. Williams, *Top. Catal.*, 2010, **53**, 1132–1137.

[57] S. Shen, T. Zhao and J. Xu, *Electrochim. Acta*, 2010, **55**, 9179–9184.

[58] A. Rocha, E. Moreno, G. da Silva, J. Zotin and A. Faro, *Catal. Today*, 2008, **133-135**, 394–399.

[59] T. S. Nguyen, F. Morfin, M. Aouine, F. Bosselet, J. L. Rousset and L. Piccolo, *Catal. Today*, 2015, **253**, 106–114.

[60] T. Yang, Y. Ma, Q. Huang, G. Cao, S. Wan, N. Li, H. Zhao, X. Sun and F. Yin, *Electrochem. Commun.*, 2015, **59**, 95–99.

[61] S. Nassreddine, L. Massin, M. Aouine, C. Geantet and L. Piccolo, *J. Catal.*, 2011, **278**, 253–265.

[62] D. J. Wales, *Energy Landscapes*, Cambridge University Press, 2003.

[63] S. Heiles, A. J. Logsdail, R. Schäfer and R. L. Johnston, *Nanoscale*, 2012, **4**, 1109–1115.

[64] C. J. Heard and R. L. Johnston, *Eur. Phys. J. D*, 2013, **67**, 34.

[65] P. C. Jennings and R. L. Johnston, *Comp. Theor. Chem.*, 2013, **1021**, 91–100.

[66] R. H. Byrd, P. Lu, J. Nocedal and C. Zhu, *SIAM J. Sci. Comput.*, 1995, **16**, 1190.

[67] F. Cleri and V. Rosato, *Phys. Rev. B*, 1993, **48**, 22–33.

[68] C. Kittel, *Introduction to Solid State Physics*, John Wiley & Sons, New York, 1986.

[69] P. Hohenberg and W. Kohn, *Phys. Rev.*, 1964, **136**, 864–871.

[70] W. Kohn and L. J. Sham, *Phys. Rev.*, 1965, **140**, 1133–1138.

[71] S. Grimme, *J. Comput. Chem.*, 2006, **27**, 1787–1799.

[72] A. Tkatchenko and M. Scheffler, *Phys. Rev. Lett.*, 2009, **102**, 073005.

[73] A. D. Becke and E. R. Johnson, *J. Chem. Phys.*, 2006, **124**, 221101.

[74] S. Grimme, J. Antony, S. Ehrlich and H. Krieg, *J. Chem. Phys.*, 2010, **132**, 154104.

[75] K. Lee, E. D. Murray, L. Kong, B. I. Lundqvist and D. C. Langreth, *Phys. Rev. B*, 2010, **82**, 081101.

[76] T. Thonhauser, V. R. Cooper, S. Li, A. Puzder, P. Hyldgaard and D. C. Langreth, *Phys. Rev. B*, 2007, **76**, 125112.

[77] J. Klimeš, D. R. Bowler and A. Michaelides, *J. Phys.: Condens. Matter*, 2010, **22**, 022201.

[78] J. Klimeš, D. R. Bowler and A. Michaelides, *Phys. Rev. B*, 2011, **83**, 195131.

[79] L. Rubinovich, M. Haftel, N. Bernstein and M. Polak, *Phys. Rev. B*, 2006, **74**, 035405.

[80] D. Wales, *Energy Landscapes: Applications to Clusters, Biomolecules and Glasses*, Cambridge University Press, Cambridge, 2004.

[81] L. Rubinovich and M. Polak, *Phys. Rev. B*, 2004, **69**, 155405.

[82] L. Rubinovich and M. Polak, *Phys. Rev. B*, 2009, **80**, 045404.

[83] R. Ferrando, A. Fortunelli and G. Rossi, *Phys. Rev. B*, 2005, **72**, 085449.

[84] L. O. Paz-Borbón, R. L. Johnston, G. Barcaro and A. Fortunelli, *J. Chem. Phys.*, 2008, **128**, 134517.

[85] J. M. Montejano-Carrizales and J. L. Morán-López, *Surf. Sci.*, 1990, **239**, 169–177.

[86] J. M. Montejano-Carrizales and J. L. Moran-Lopez, *Surf. Sci.*, 1990, **239**, 178–188.

[87] M. Polak and L. Rubinovich, *Int. J. Nanotechnol.*, 2011, **8**, 898–906.

[88] V. Fiorentini and M. Methfessel, *J. Phys.: Condens. Matter*, 1996, **8**, 6525–6529.

[89] R. Vardi, L. Rubinovich and M. Polak, *Surf. Sci.*, 2008, **602**, 1040–1044.

[90] C. J. Pickard and R. J. Needs, *J. Phys.: Condens. Matter*, 2011, **23**, 053201.

[91] *https://bitbucket.org/JBADavis/ligand_randomsearch.*

[92] A. Tkatchenko, *Adv. Funct. Mater.*, 2015, **25**, 2054–2061.

[93] L. Kronik and A. Tkatchenko, *Acc. Chem. Res.*, 2014, **47**, 3208–3216.

[94] L. Schimka, J. Harl, A. Stroppa, A. Grüneis, M. Marsman, F. Mittendorfer and G. Kresse, *Nat Mater*, 2010, **9**, 741–744.

[95] X. Ren, P. Rinke and M. Scheffler, *Phys. Rev. B*, 2009, **80**, 045402.

[96] S. Grimme, *J. Comput. Chem.*, 2004, **25**, 1463–1473.

[97] M. Dion, H. Rydberg, E. Schröder, D. C. Langreth and B. I. Lundqvist, *Phys. Rev. Lett.*, 2004, **92**, 246401.

[98] J. Klimeš and A. Michaelides, *J. Chem. Phys.*, 2012, **137**, 120901.

[99] *https://bitbucket.org/JBADavis/bpga/*.

[100] G. Kresse and J. Furthmüller, *Phys. Rev. B*, 1996, **54**, 11169–11186.

[101] G. Kresse and J. Furthmüller, *Comput. Mater. Sci.*, 1996, **6**, 15–50.

[102] G. Kresse and J. Hafner, *Phys. Rev. B*, 1993, **47**, 558–561.

[103] G. Kresse and J. Hafner, *Phys. Rev. B*, 1994, **49**, 14251–14269.

[104] A. Uzun, D. A. Dixon and B. C. Gates, *ChemCatChem*, 2011, **3**, 95–107.

[105] T. Pawluk, Y. Hirata and L. Wang, *J. Phys. Chem. B*, 2005, **109**, 20817–20823.

[106] G. Ping, Z. Ji-Ming, Z. Pei, Z. Lin-Lin and R. Zhao-Yu, *Chin. Phys. B*, 2010, **19**, 083601.

[107] W. Zhang, L. Xiao, Y. Hirata, T. Pawluk and L. Wang, *Chem. Phys. Lett.*, 2004, **383**, 67–71.